nature chemistry

Supplementary information

https://doi.org/10.1038/s41557-026-02235-1

Secondary-sphere hydrogen bonding promotes catalytic nitrate reduction at iron

In the format provided by the authors and unedited

Table of Figures

Table of Tables

Experimental Procedures

General Considerations

All air- and moisture-sensitive manipulations were performed using standard Schlenk techniques or in an inert atmosphere glovebox with an atmosphere of purified nitrogen. The glovebox was equipped with a cold well designed for low temperature experiments as well as a −30 °C freezer for cooling samples and crystallizations. Solvents were purified using a Glass Contour solvent purification system through percolation through Q1-Cu catalyst beads and X13-molecular sieves (Benzene, Pentane, Toluene) or through alumina beads (THF, Et_2O, MeCN, CH_2Cl_2, DMF). Solvents were then stored over sodium and/or molecular sieves as appropriate. Deuterated solvents (other than d_3-MeCN) were purchased from Cambridge Isotope Laboratories, dried, distilled, and freeze-pump-thaw cycled three times. d_3-MeCN was purchased from Sigma Aldrich as a sealed ampoule stored under argon and used as received.

Iron(II) trifluoromethanesulfonate, zinc(II) trifluoromethanesulfonate, tetrabutyl ammonium nitrate, 1,2-diphenylhydrazine ($Ph_2N_2H_2$), diethyl 2,6-dimethyl-1,4-dihydropyridine-3,5-dicarboxylate (HEH_2), 2,6-dimethylpyridine or Lutidine (Lut), and 2,4,6-trimethylpyridine or Collidine (Col) were purchased from commercial vendors and dried under vacuum (for solids) or free-pump-thawed (for liquids) before transferring to a nitrogen glovebox. Collidinium triflate ([ColH][OTf]), anilinium triflate ([$PhNH_3$][OTf]), diphenylammonium triflate ([Ph_2NH_2][OTf]), and [DMF-H][OTf] were synthesized following literature procedures.[1-4] Tris(6-phenylamino-2-pyridylmethyl)-amine (L^H),[5] 6-((bis((6-((4-methoxyphenyl)amino)pyridin-2-yl)methyl)amino)methyl)-N-(4-methoxyphenyl)pyridin-2-amine (L^{OMe}),[5] 6-((bis((6-((4-(trifluoromethyl)phenyl)amino)pyridin-2-yl)methyl)amino)methyl)-N-(4-(trifluoromethyl)phenyl)pyridin-2-amine (L^{CF3}),[5] 6-((bis((6-((3,5-di-tert-butylphenyl)amino)pyridin-2-yl)methyl)amino)methyl)-N-(3,5-di-tert-butylphenyl)pyridin-2-amine (L^{tBu2}),[6] 6-((bis((6-((3,5-bis(trifluoromethyl)phenyl)amino)pyridin-2-yl)methyl)amino)methyl)-N-(3,5-bis(trifluoromethyl)phenyl) pyridin-2-amine ($L^{(CF3)2}$),[6] tris((6-methylpyridin-2-yl)methyl)amine (6-Me_3TPA),[7] and tris(2-pyridylmethyl)amine (TPA)[7]were synthesized according to literature procedures. Fe-complexes: **I-OTf**, **$I^{(tBu2)}$-OTf**,[6] **$I^{(CF3)2}$-OTf**,[6] **II-OTf**,[6] **VII-OTf**,[6] **III**,[8] **IV**,[9] and **VI**[8] were synthesized following literature procedures. Cobalt (II) tetraphenylporphyrin (CoTPP) was synthesized according to a previously reported procedure.[10,11]

NMR spectra were acquired on Varian MR400, Varian Vnmrs 500, 600, 700 spectrometers and Bruker Advance Neo 500 MHz spectrometer as indicated below. ^{1}H, ^{13}C, ^{19}F, and ^{15}N NMR chemical shifts are reported in parts per million (ppm) relative to tetramethylsilane and referenced internally to the residual solvent peak(s). Multiplicities are reported as follows: singlet (s), doublet (d), triplet (t), quartet (q), multiplet (m). The ^{1}H NMR spectra for paramagnetic molecules were obtained by using an acquisition time of 0.5 s and a relaxation delay of 0.05 s.

IR spectra were recorded on a Nicolet iS10 FT-IR spectrometer KBr pellets. Mass spectra were recorded on an Agilent 6230 ESI-MS TOF mass spectrometer with a liquid phase of 95% acetonitrile, 5% water, 0.1% formic acid. GC-MS analyses were performed with a Shimadzu QP-2010 gas-chromatograph mass spectrometer. This instrument uses a 30-meter-long DB-5 column with a 0.25 mm I.D. column with H_2 as the carrier gas. Electronic absorption spectra were recorded with a Varian Cary-50 spectrophotometer in sealed 1 cm^2 quart cuvettes equipped with a J-Young valve or Teflon stoppered high vacuum valve to maintain inert conditions.

Electronic absorption spectra were recorded at ambient temperature in custom made 1 cm path-length quartz cuvettes with a Varian Cary-50 spectrophotometer (resolution: <1.5 nm) equipped with a UNISOKU CoolSpeKCryostat USP-203. Temperature deviations during reactions were no more than $\pm$0.1 ˚C. Custom cuvettes were purchased from Starna Cells with a quartz-to-glass gradient tube and then modified to have a 4 mm high vacuum valve with associated Teflon stopper and a 14/20 female ground glass joint at approximately a 30˚ angle to the valve. The cuvettes are at least 140 mm tall with inner volumes of 8.7 to 9.5 mL.[8]

Cyclic voltammograms were recorded with a Pine Electronics WaveNow inside of an N_2-filled glovebox. Unless otherwise specified, all measurements were recorded in 0.1 M $[Bu_4N][OTf]$ in MeCN, with a platinum working electrode, a silver wire counter electrode, and a silver wire pseudo reference electrode. After data collection, a small amount of ferrocene was added to the cell as an external reference.

Single-crystal data for compounds **V** and **Zn(MeCNH)(OTf)L^H** were collected using a Rigaku AFC10K Saturn 944+ CCD-based X-ray diffractometer equipped with a low temperature device and a Micromax-007HF Cu-target microfocus rotating anode (λ = 1.54187 Å) operated at 1.2 kW power (40 kV, 30 mA). The data was collected using CrystalClear 2.016 software. The X-ray intensities were measured at 85 (2) K with the detector placed at a distance 42.00 mm from the crystal. Rigaku d*trek images were exported to *CrysAlisPro* 1.171.40.53 for processing and corrected for absorption. Reflections were merged by SHELXL and the structure solved using the Olex2 refinement program.

Single-crystal data for compounds **I-Zn-$(NO_3)_2$**, **II-Zn-(NO_3)**, and **II-NO_3** were collected using a XtaLAB Synergy, Dualflex, HyPix-Arc 150 diffractometer. The crystal was kept at a steady T = 100.00(10) K during data collection. The structure was solved with the ShelXT 2018/2 (Sheldrick, 2018) solution program using dual methods and by using Olex2 1.5 (Dolomanov et al., 2009) as the graphical interface. The model was refined with ShelXL 2019/3 (Sheldrick, 2015) using full matrix least squares minimization on |F| 2. Hydrogen atom positions were calculated geometrically and refined using the riding model.

Computational studies began with distorted and unrealistic starting geometries of **I-Zn**, **II-Zn**, **I-Zn$(NO_3)_2$**, **I-Zn(NO_3)**, **II-Zn(NO_3)**, and **II-Zn$(NO_3)_2$** and initially optimized using semi-empirical methods and conformational sampling (xTB2/CREST) to probe potential binding modes of the TPA^R, NO_3^- and OTf^- ligands. Afterwards, the minimum energy geometries were subjected to further geometry optimization and frequency analysis using Orca 6.0.1[12,13] with DFT methods (TPSSh[14,15] functional and ma-def2-tzvp basis[16] set), including Grimme's D3 dispersion corrections[17] with Beck-Johnson damping functions,[18] and the resolution of the identity approximation.[19] Local geometry minima were confirmed by the absence of imaginary (negative) frequencies greater than -10 cm^{-1}. Gas-phase free energies were refined and converted to solvated free energies through single point calculations with the conductor-like-polarizable continuum model (acetonitrile). Molecular orbitals, NBO charges, and WBI parameters were generated using NBO 7.0[20] in Orca 6.0.1.

Non-covalent interaction analyses based on promolecular density and molecular electrostatic potential maps were generated with multiwfn[21] and visualized in VMD (commands used in multiwfn described below).[22]

NCI isosurfaces (RDG vs sign(λ^2)ρ): multiwfn option 20 → option 2

Electron density isosurface: multiwfn option 5 → option 1.

Electrostatic potential: option 5 → option 12.

Color maps of the electrostatic potential on the electron density isosurfaces had their respective trajectory ranges altered to assign the most positive potential as blue and the most negative potential as red.

Isotherms were fit using the open source software, Suprafit.[23,24] Data from the titration studies were extracted as $\Delta\delta_i = \delta_i - \delta_0$, where δ_i is the chemical shift of the selected resonance for each titration point *i*, and δ_0 is the resonance's initial δ value before NO_3^- addition. Columns for [Host], [Guest], and $\Delta\delta_i$, (concentrations corrected for dilution) were exported as a plain-text ascii file (.txt file format) without column headers, then loaded into suprafit. Isotherms from replicate titrations were fit simultaneously to a global 2:1/1:1/1:2 model.

Synthesis of Compounds

Synthesis of [Fe(OTf)$_2$L^{OMe} + Fe(MeCNH)(OTf)L^{OMe}] (I^{OMe}-OTf): Inside a glove box, in a 20 mL scintillation vial, Fe(OTf)$_2$ (70.8 mg, 0.2 mmol) was taken in 5 mL MeCN and was stirred at 25 °C. To this, a 5 mL MeCN solution of L^{OMe} (132 mg, 0.202 mmol) was added dropwise over 5 minutes at 25 °C. The reaction mixture was allowed to stir at 25 °C for 48 h. The resulting pale yellow solution was filtered and dried. The resulting pale yellow oil was triturated with Et_2O (10 mL) to get a colorless solid residue. This mixture was allowed to stir for 16 h. The resulting mixture was decanted and further washed with Et_2O (3 x 5 mL) and decanted to get a yellow solid which was dried under vacuo to give the desired compound containing a mixture of Fe(OTf)$_2$L^{OMe} + Fe(MeCNH)(OTf)L^{OMe} (170 mg, 84%) (similar observation to that of complex **I-OTf**). **^{1}H NMR** (400 MHz, MeCN, 25 °C) δ δ 90.10, 65.40, 60.54, 60.39, 54.43, 42.98, 35.19, 30.28, 19.24, 18.11, 16.09, 14.22, 12.00, 10.53, -0.20, -3.43, -3.82, -6.09 ppm. **^{19}F NMR** (376 MHz, MeCN, 25 °C) δ No signal **Selected IR data** (ATR) ν =3368, 3279, 1611, 1580, 1512, 1456, 1315, 1235, 1166, 1027, 1001, 830, 793, 629 cm^{-1}. **HRMS (ESI-TOF)** m/z: [M – OTf]$^+$ Calcd. for $C_{41}H_{39}F_6FeN_7O_9S_2$ [M – OTf]$^+$: Calc. 858.1978, Found 858.1979.

Synthesis of Fe(OTf)$_2$L^{CF3} (I^{CF3}-OTf): Inside a glove box, in a 20 mL scintillation vial, Fe(OTf)$_2$ (70.8 mg, 0.2 mmol) was taken in 5 mL MeCN and was stirred at 25 °C. To this, a 5 mL MeCN solution of L^{CF3} (155 mg, 0.202 mmol) was added dropwise over 5 minutes at 25 °C. The reaction mixture was allowed to stir at 25 °C for 48 h. The resulting pale yellow solution was filtered and dried. The resulting pale yellow oil was triturated with Et_2O (10 mL) to get a colorless solid residue. This mixture was allowed to stir for 16 h. The resulting mixture was decanted and further washed with Et_2O (3 x 5 mL) and decanted to get a colorless solid which was dried under vacuo to give the desired compound (180 mg, 80%). **^{1}H NMR** (400 MHz, MeCN, 25 °C) δ 6^{1}H NMR (400 MHz, cd$_3$cn) δ 68.77, 65.62, 61.60, 44.82, 42.49, 8.40, 3.85, 2.94, -3.32, -4.06, -56.14, -74.28.**^{19}F NMR** (376 MHz, MeCN, 25 °C) δ-63.67, -64.26 ppm. **Selected IR data** (ATR) ν = 3535.4, 3476.1, 3362.8, 3278.4, 1607.4, 1579,9, 1530.2, 1466.6, 1324.4, 1237.1, 1201.9, 1164.8, 1114.7, 1069.8, 1024.0, 1001.3, 841.3, 791.6, 633.5 cm^{-1}. **HRMS (ESI-TOF)** m/z: [M – OTf]$^+$ Calcd. for $C_{41}H_{39}F_6FeN_7O_9S_2$ [M – OTf]$^+$: Calc. 972.1283, Found 972.1279.

Synthesis of I-Zn(NO$_3$)$_2$: Inside a glove box, in a 20 mL scintillation vial, Zn(OTf)$_2$ (10 mg, 0.0275 mmol, 1.0 equiv.) and L^H (15 mg, 0.0275 mmol, 1.0 equiv.) was taken in 2 mL MeCN and the reaction mixture was allowed to stir at 25 °C for 30 min. To it, [Bu$_4$N][NO$_3$] (65 mg, 0.22 mmol, 8.0 equiv) was added and the reaction mixture was allowed to stir at 25 °C for 30 min. The resulting pale yellow solution was triturated

with Et_2O (10 mL) to get a colorless solid residue. This mixture was allowed to stir at 25 °C for 30 min. The solvent from the resulting mixture was decanted and further washed with Et_2O (3 x 5 mL) and decanted each time to get a colorless solid which was dried under vacuo to give the desired product, $[Zn(NO_3)_2L^H]$. A single crystal suitable for x-ray crystallography was grown from slow solvent evaporation (at room temperature) of a d_3-MeCN solution (from the NMR titration studies below) after several days and chosen for crystal diffraction studies. **^{1}H NMR** (400 MHz, MeCN, 25 °C) δ 6 8.64, 7.58, 7.57, 7.56, 7.54, 7.23, 7.22, 7.21, 7.19, 7.19, 7.07, 7.05, 6.94, 6.94, 6.92, 6.92, 6.90, 6.70, 6.68, 4.18. **Selected IR data (ATR)** ν = 3318, 1614, 1593, 1575, 1497, 1471, 1451, 1333, 1297, 1283, 1164, 1028, 993, 785, 747, 700, 635 cm^{-1}. **HRMS (ESI-TOF)** m/z: $[M - NO_3]^+$ Calcd. for: 689.1967, Found 689.1961

Synthesis of II-Zn(NO_3): Inside a glove box, in a 20 mL scintillation vial, $Zn(OTf)_2$ (15 mg, 0.04 mmol, 1.0 equiv.) and $6Me_3TPA$ (13.7 mg, 0.04 mmol, 1.0 equiv.) was taken in 2 mL MeCN and the reaction mixture was allowed to stir at 25 °C for 30 min. To it, $[Bu_4N][NO_3]$ (63 mg, 0.2 mmol, 5.0 equiv) was added and the reaction mixture was allowed to stir at 25 °C for 2 h. The resulting colorless solution was layered with Et_2O (5 mL) and the vial was sealed and kept in a -35 °C freezer for overnight. Colorless crystals were found and the solvent from the resulting mixture was decanted and further washed with Et_2O (3 x 5 mL) and decanted each time to get a colorless solid which was dried under vacuo to give the desired product, $[Zn(NO_3)(6Me_3TPA)](NO_3)$. A single crystal suitable for x-ray crystallography was chosen for crystal diffraction studies. **^{1}H NMR** (400 MHz, d_3-MeCN, 25 °C) δ δ 7.84, 7.83, 7.82, 7.36, 7.35, 7.29, 7.28, 4.42, 2.77. **HRMS (ESI-TOF)** *m/z*: $[M]^+$ Calcd. for $C_{21}H_{24}N_5O_3Zn^+$ 458.1171, Found 458.1161

Synthesis of V: Inside an N_2-filled glovebox, a 20 mL scintillation vial was charged with Fe(OTf) (70 mg, 0.2 mmol), TPA^{NHPh}(112.7 mg, 0.2 mmol), $NaNO_2$ (41.3 mg, 0.6 mmol), a Teflon-coated stirbar, and 4 mL of MeCN. The reaction was stirred for 3 days at ambient temperature. The MeCN was removed *in vacuo,* affording a red/brown sludge. The sample was dissolved in minimal DCM (~2-3 mL), then filtered through a glass microfibre plug to remove excess $NaNO_2$ and any NaOTf byproducts. The DCM was removed *in vacuo,* then the sample was triturated with 3 mL of a 1:1 Et_2O:pentane mixture, washed with 2x3 mL Et_2O, then dried *in vacuo*, affording 60 mg of a red-brown powder. The crude product was recrystallized from CH_2Cl_2/Et_2O, affording 20 mg of red crystals (corresponding to **IV**), and a brown supernatant. The brown supernatant was decanted and dried in vacuo, affording a fine brown powder (40 mg, 0.02 mmol, 10% yield). Single crystals suitable for X-ray crystallography were grown from $MeCN/Et_2O$ vapor diffusion followed by slow evaporation over 1 month, affording dark red/black crystals. **^{1}H NMR** (400 MHz, MeCN, solvent suppressed, 25 °C) δ (ppm) 56.32, 52.93, 37.40, 33.96, 32.76, 32.09, 28.96, 28.18, 24.31, 23.19, 22.34, 20.88, 20.10, 14.71, 8.66, 8.32, 7.91, 7.68, 7.59, 7.38, 7.31, 7.13, 6.76, 6.72, 6.42, 6.34, 6.15, 3.61, 3.48, 3.36, 2.11, 1.97, 1.80, 1.20, 0.82, -2.38, -3.11, -5.34, -6.36, -8.33, -10.83, -11.97, -12.86, -13.70, -15.36, -24.68, -29.77, -30.32, -43.17, -48.65. **HRMS (ESI-TOF)** *m/z*: $[M - (OTf)_2]^{2+}$ Calcd. for $C_{72}H_{68}Fe_2N_{14}O_3^{2+}$: 644.2147, Found: 644.2144 **UV-Vis** (MeCN): λ max = 590 nm, ε = 0.47 $mM^{-1}cm^{-1}$.

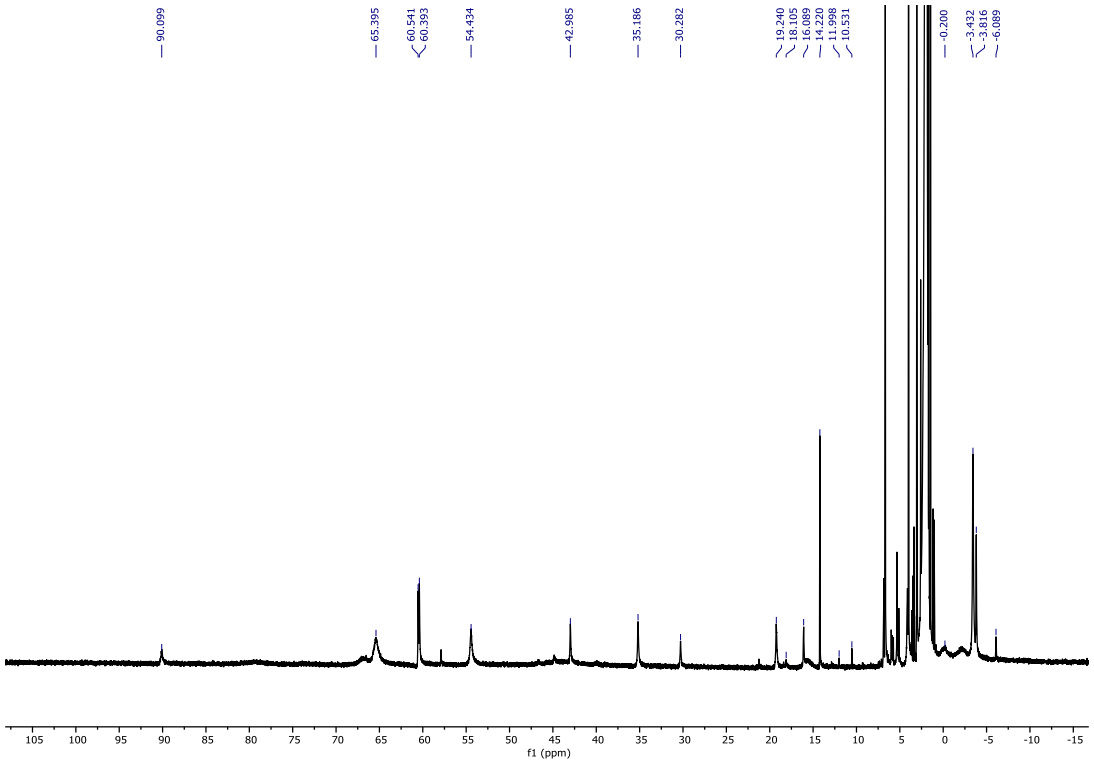

Supplementary Figure 1: ^{1}H NMR spectrum (400 MHz, MeCN, 25 °C) of **I^{OMe}-OTf**.

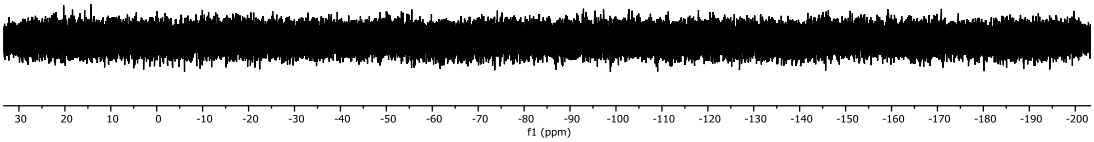

Supplementary Figure 2: ^{19}F NMR spectrum (376 MHz, MeCN, 25 °C) of **I^{OMe}-OTf**.

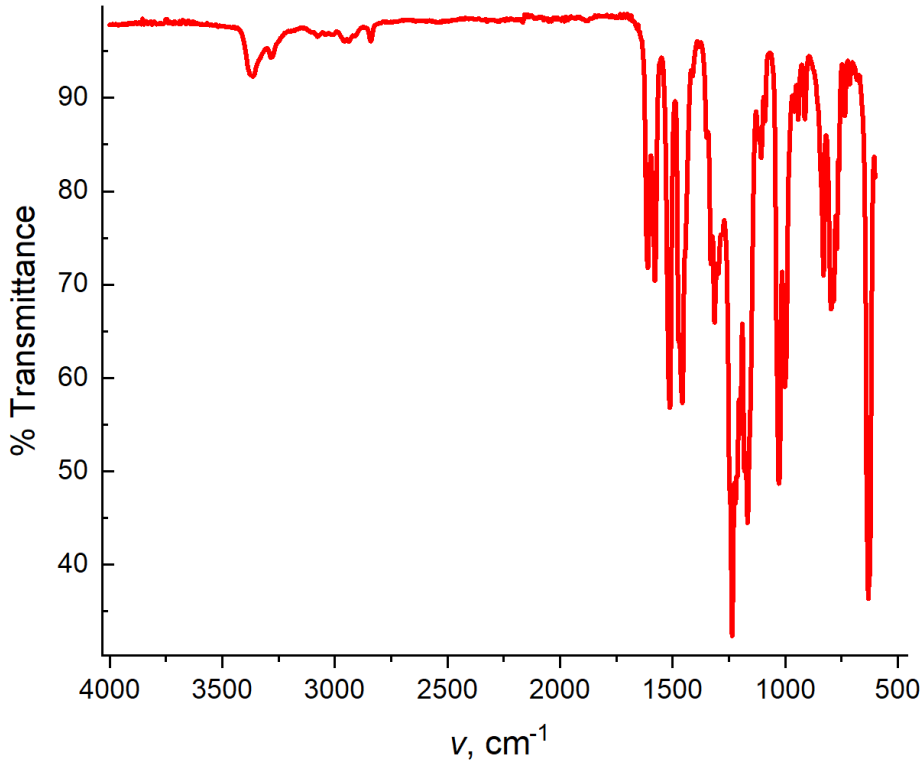

Supplementary Figure 3: FT-IR (ATR) spectrum of **I^{OMe}-OTf**.

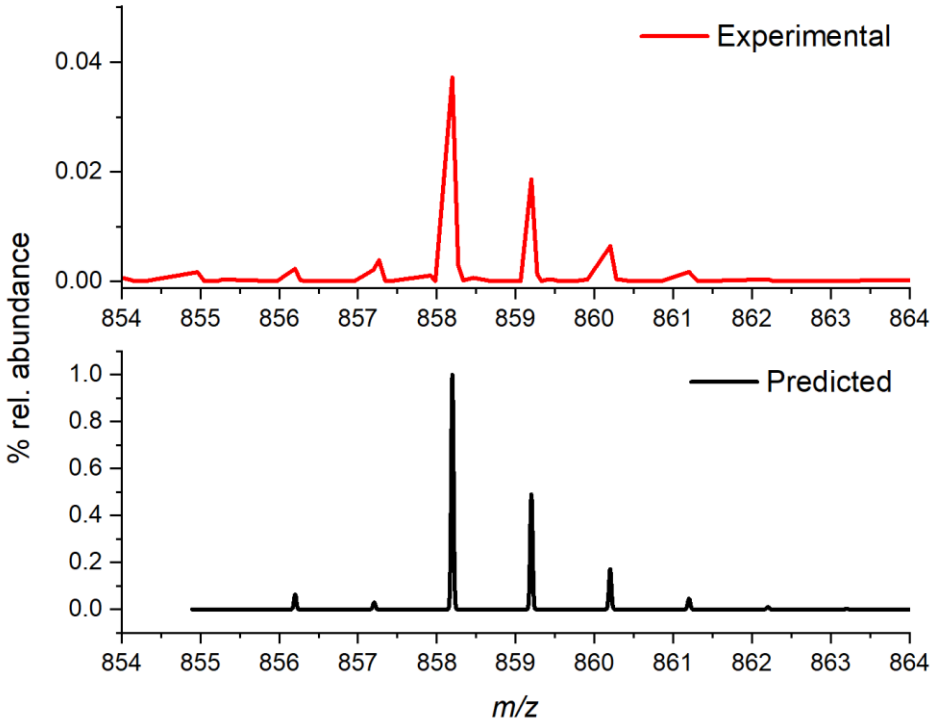

Supplementary Figure 4: HRMS (ESI) of **I^{OMe}-OTf** stacked with its expected isotope distribution.

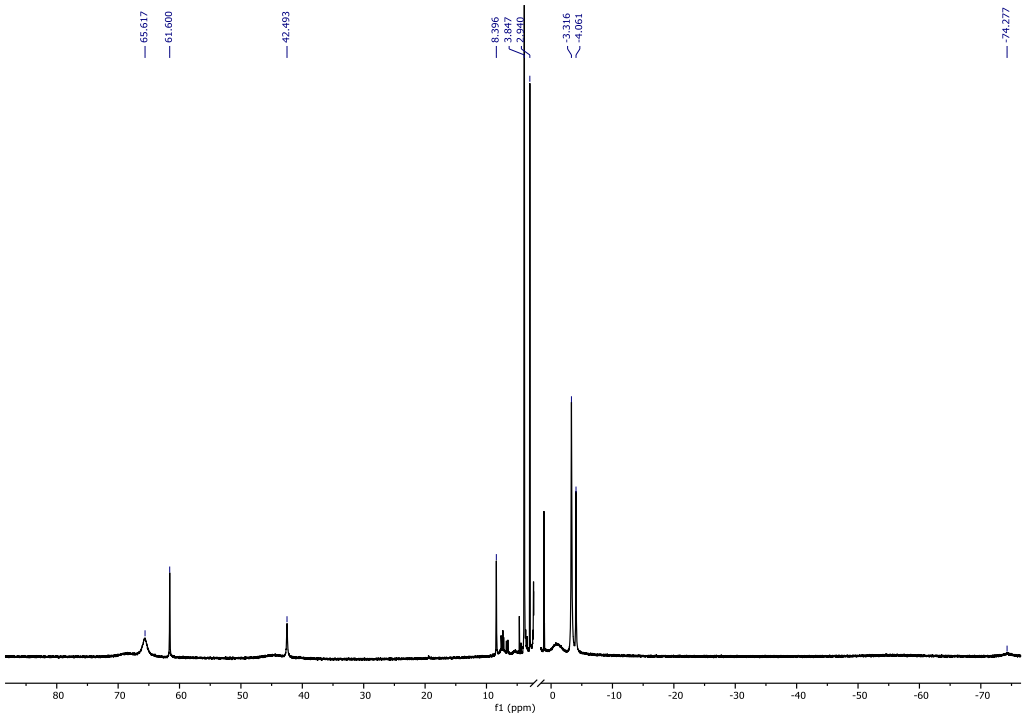

Supplementary Figure 5: ^{1}H NMR spectrum (400 MHz, MeCN, 25 °C) of **I^{CF3}-OTf** (solvent suppressed MeCN signal omitted for clarity).

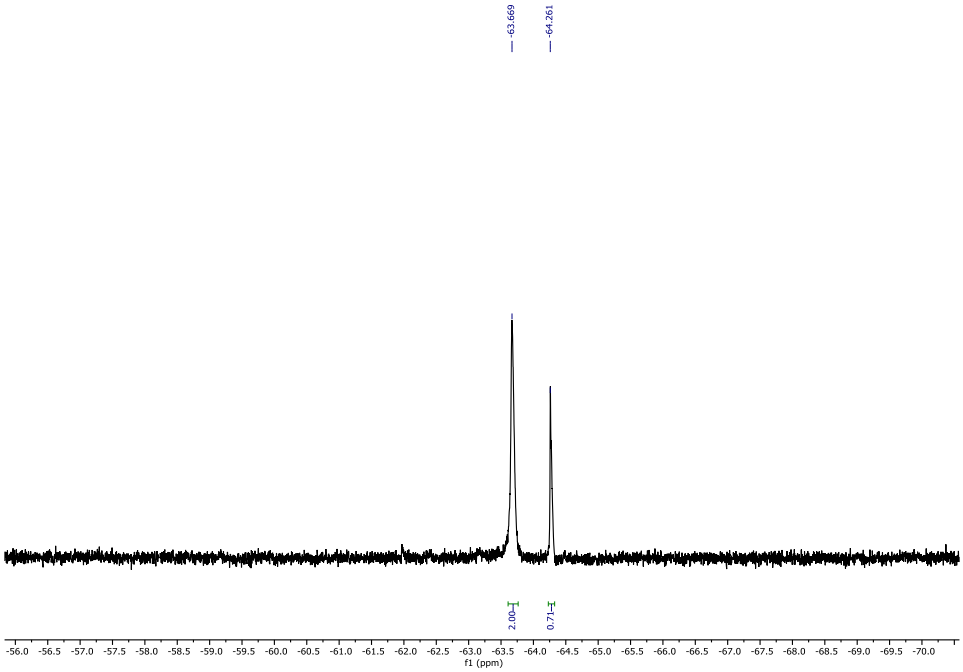

Supplementary Figure 6: ^{19}F NMR (376 MHz, MeCN, 25 °C) of **I^{CF3}-OTf**.

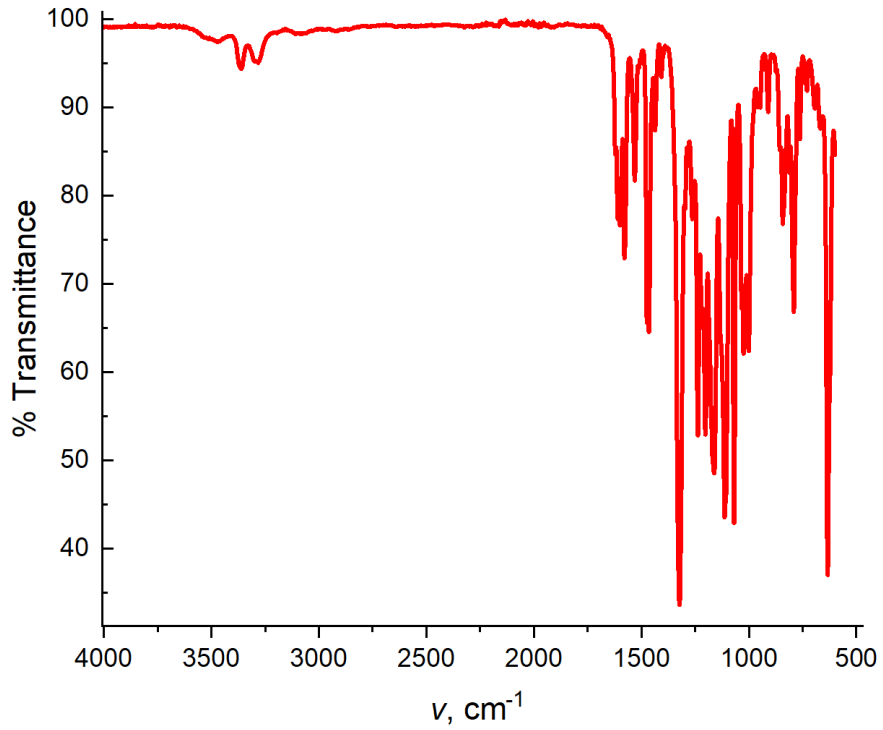

Supplementary Figure 7: FT-IR (ATR) spectrum of **I^{CF_3}-OTf**.

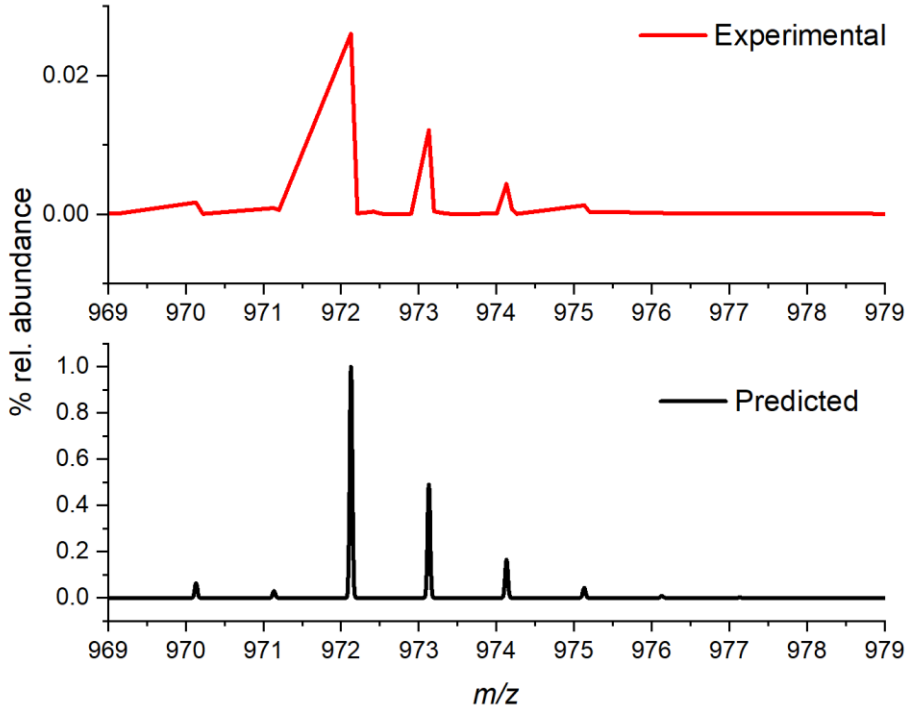

Supplementary Figure 8: HRMS (ESI) of **I^{CF_3}-OTf** stacked with its expected isotope distribution.

Preparation of I-Zn and NMR Titration with NO_3^-

Procedure: Inside an N_2-filled glovebox, a 2.00 mL volumetric flask was charged with TPA^{NHPh} (15 mg, 0.027 mmol) and $Zn(OTf)_2$ (9.7 mg, 0.027 mmol) and then dissolved in d_3-MeCN, added to the mark. A stirbar was added and then stirred for 30 minutes. A 1 mL volumetric flask was charged with enough $[Bu_4N][NO_3]$ to make either a 0.1 M or 0.2 M stock solution, then diluted to the mark with d_3-MeCN. A 0.75 mL aliquot of the in-situ metalated Zn solution was transferred to an NMR tube and sealed with a 2 mL vial cap with a Teflon septa, then the cap was wrapped tightly with electrical tape. A ^{1}H-NMR spectrum was recorded after each addition of titrant (using a Hamilton syringe) in varying aliquot sizes (between 1 to 50 µL) then followed by a thorough shaking (3 full shakes at a minimum). During each titration, at least one spectrum was recorded a second time after waiting for 15 minutes to ensure the reaction had reached equilibrium shortly after aliquot addition.

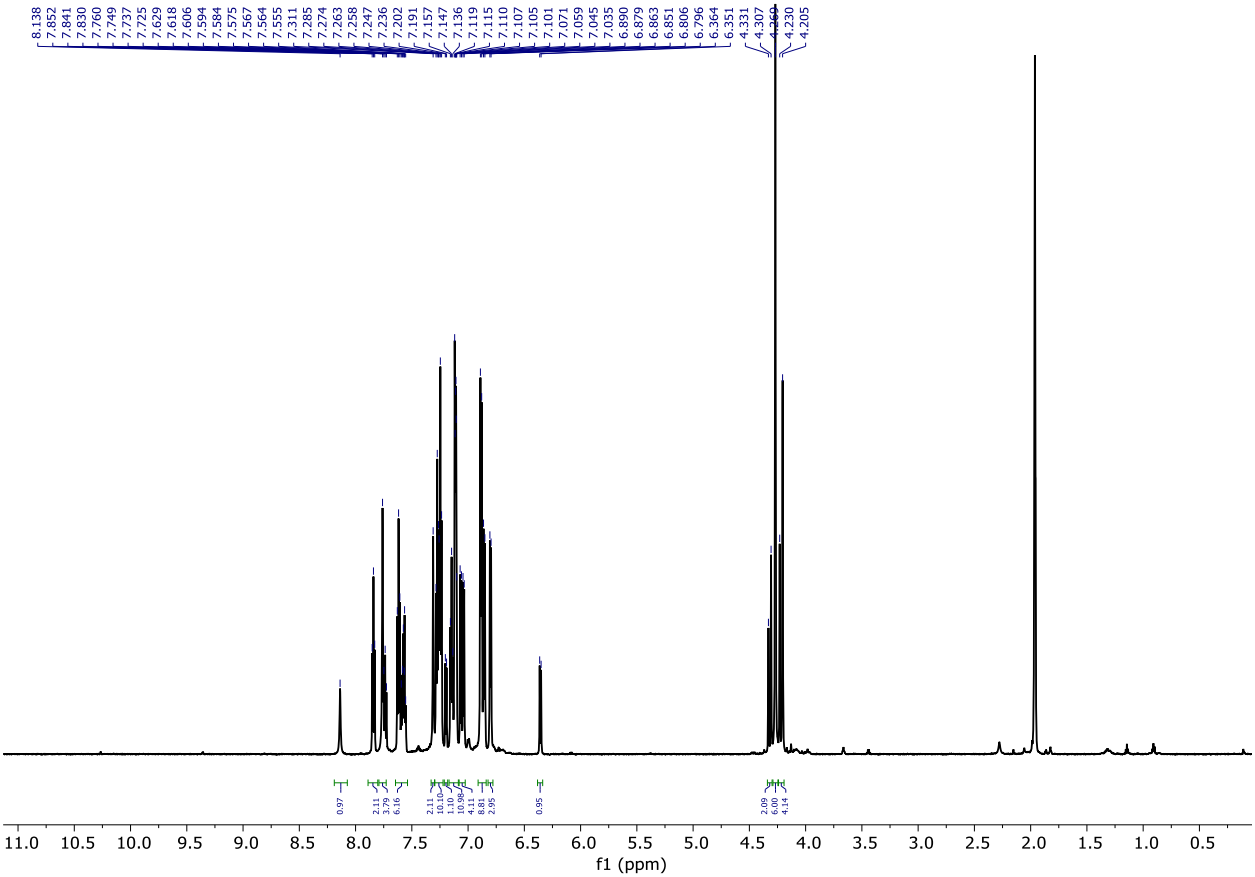

Supplementary Figure 9: ^{1}H NMR spectrum (700 MHz, d_3-MeCN, 25 °C) of **I-Zn** (metalated *in situ*).

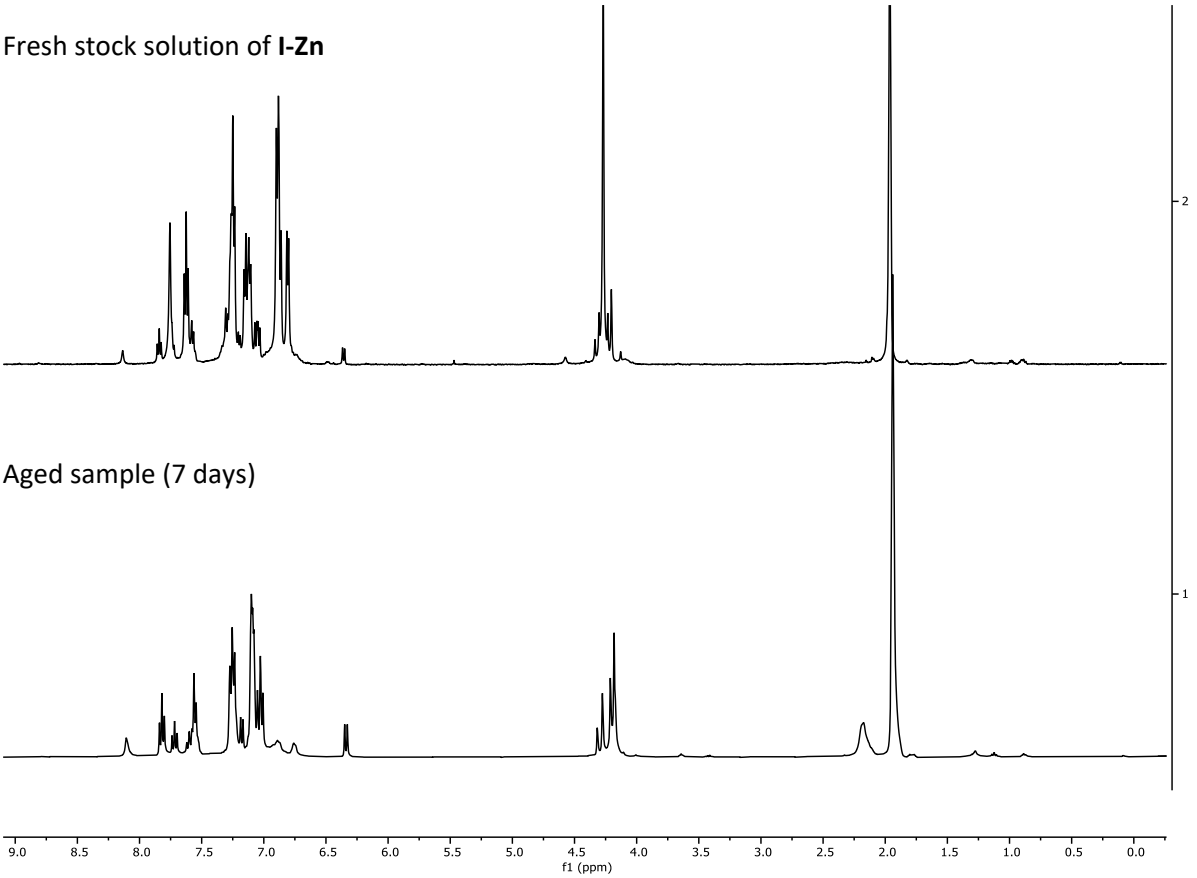

Supplementary Figure 10: ^{1}H NMR spectra (700 MHz, d_3-MeCN, 25 °C) of fresh **I-Zn** stacked with an aged sample (7 days).

There are two sets of resonances present in the spectrum, which we propose is slow exchange between the following three species. We attempted to crystallize **I-Zn** for structural analysis, however, the XRD experiment instead afforded the structure of **I-Zn(MeCNH)**$^{2+}$, see Supplementary Figure 109. The longer the stock solution of **I-Zn** aged, the further it converted to this second species, see Supplementary Scheme S1 (below) and Supplementary **Error! Reference source not found.** (above).

Supplementary Scheme 1: Proposed solution equilibria of **I-Zn** with OTf^{-}, MeCN, and an MeCN-derived amidine ligand.

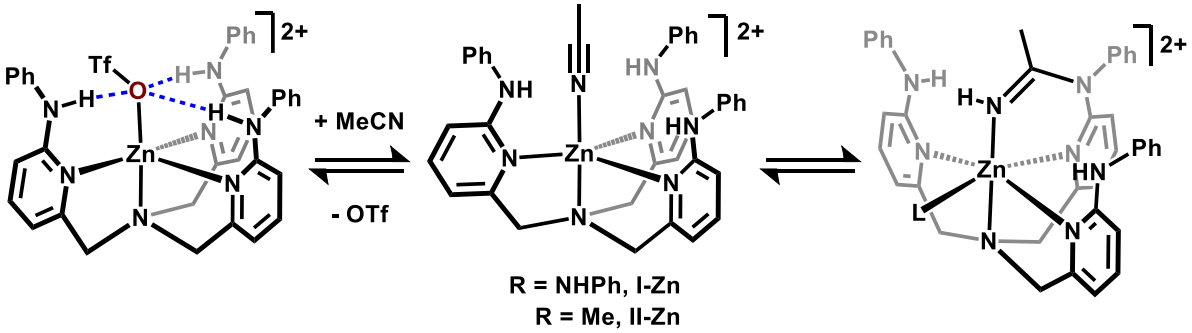

Our previous report showed that the amidine adduct with Fe (instead of Zn) could exchange the amidine ligand for chloride.[6] By analogy, we propose that the second species also exchanges with NO_3^- (in the slow exchange regime) thereby converting into **I-Zn(NO_3)**, which then shifts into the fast exchange regime. We note the peak at 8.15 ppm 6.35 ppm (among others) that broaden out as one peak disappears and another reappears, consistent with slow exchange. After this transition occurs, all resonances adopt fast exchange.

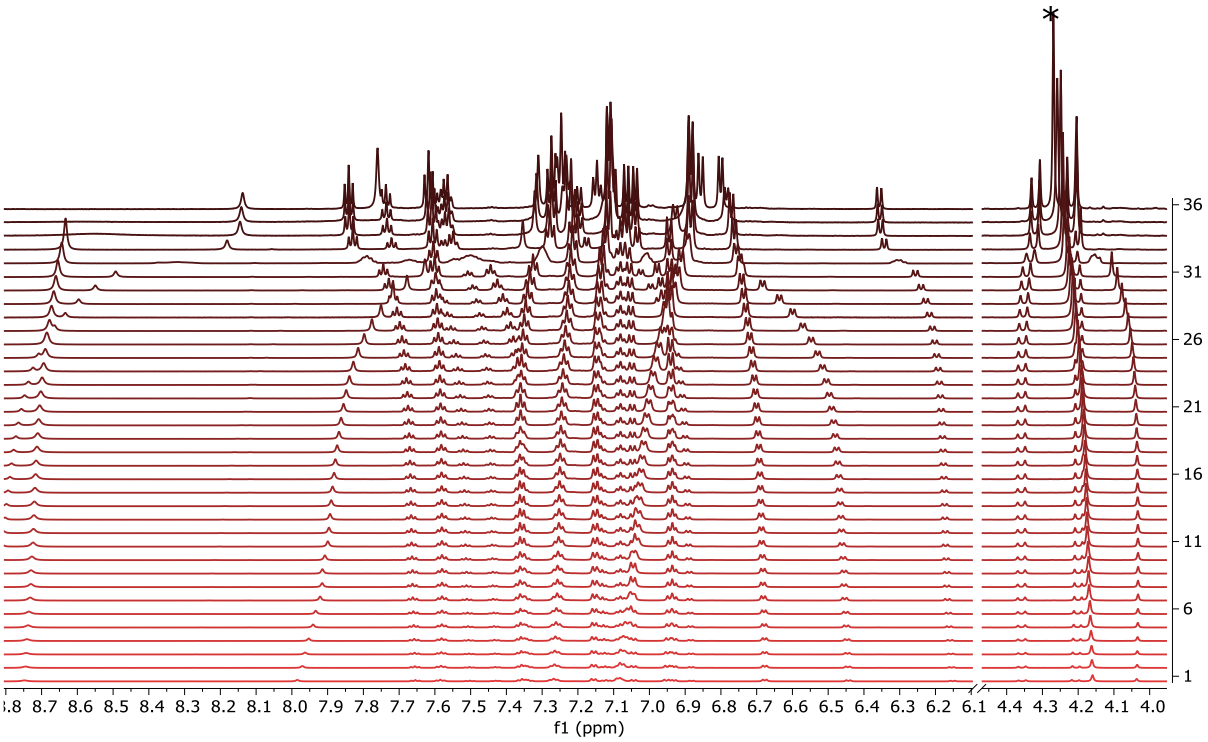

Supplementary Figure 11: Representative stacked ^{1}H NMR spectra (700 MHz, d_3-MeCN, 25 °C) for the titration of **I-Zn** with [Bu_4N][NO_3], starting from 0 equiv (top) to 8 equiv (bottom).

The resonance at 4.2 ppm marked by a * is the selected $(CH_2)_3$ resonance of **I-Zn**, plotted below.

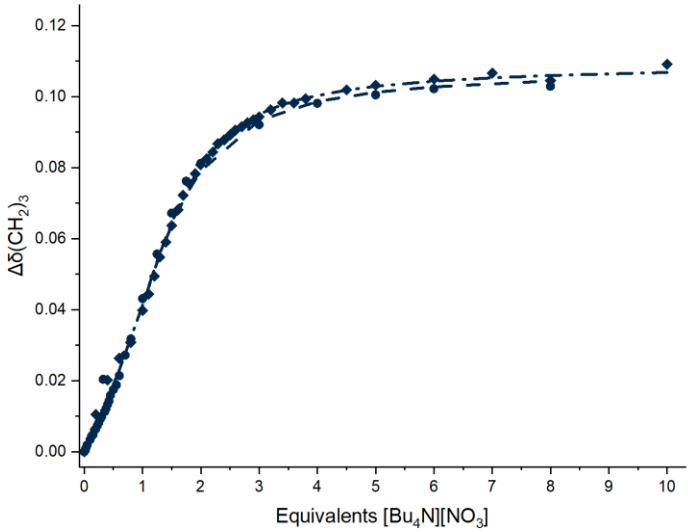

Supplementary Figure 12: Binding isotherm for **I-Zn**. Dotted line is calculated model (2:1/1:1/1:2 with full cooperativity).[23,24]

Supplementary Table 1: Calculated association constants from binding isotherm in Supplementary **Error! Reference source not found.**

$K_{2:1}$, M^{-1}	$K_{1:1}$, M^{-1}	$K_{1:2}$, M^{-1}
61 ± 2	(3.2 ± 0.3)•10^{6}	(2.5 ± 0.2)•10^{-1}

The 95% confidence intervals were generated from cross-validation leave-3-out statistical analysis (p-value of 0.05).[25]

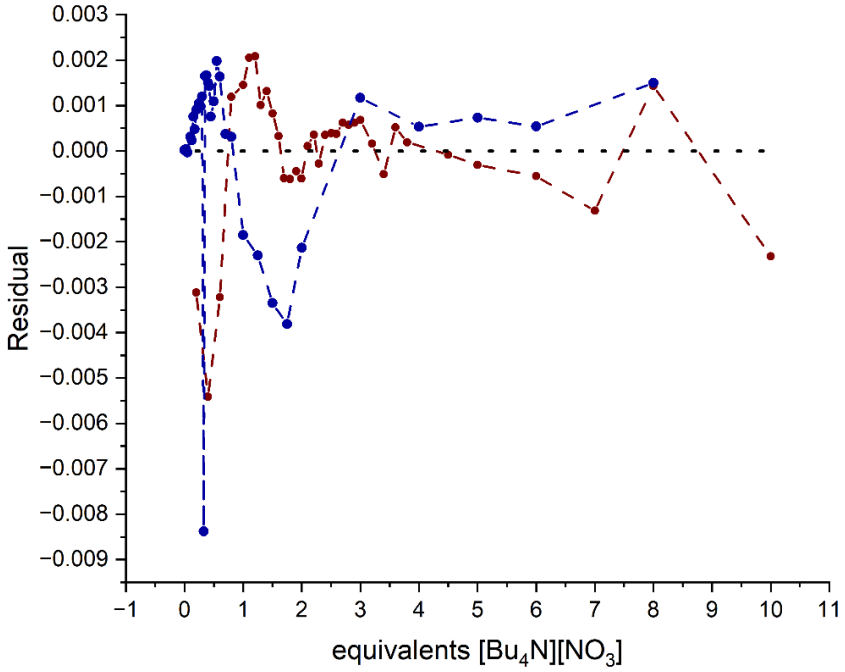

Supplementary Figure 13: Residuals of the calculated model for the isotherm of **I-Zn** (colors denote different titrations).

Using the other available binding models in Suprafit (1:1, 1:1/1:2, or 2:1/1:1) produced significantly less random residuals that exhibited noticeable sinusoidal patterns, unrealistic Δδ values, and unrealistic %errors on K_{eq} values (>100%).

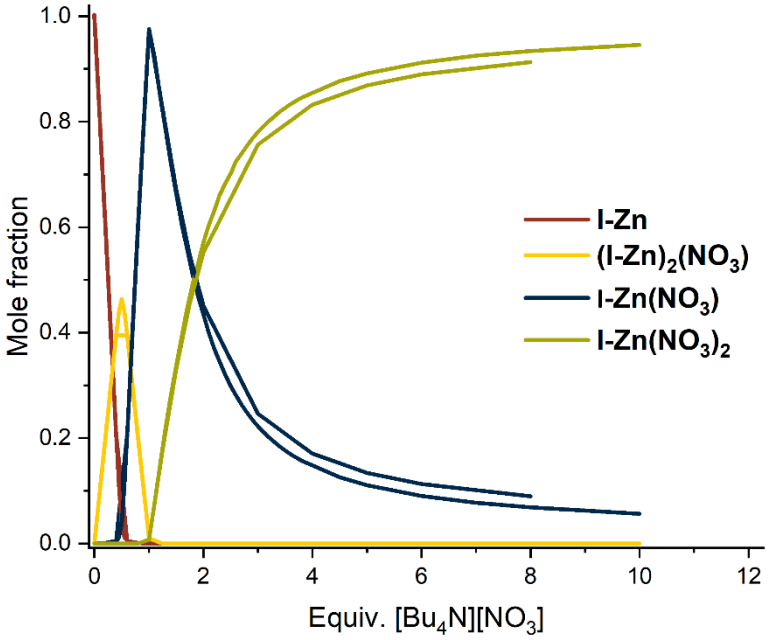

Supplementary Figure 14: Simulated mole fractions of **I-Zn** and its NO_3^- adducts.

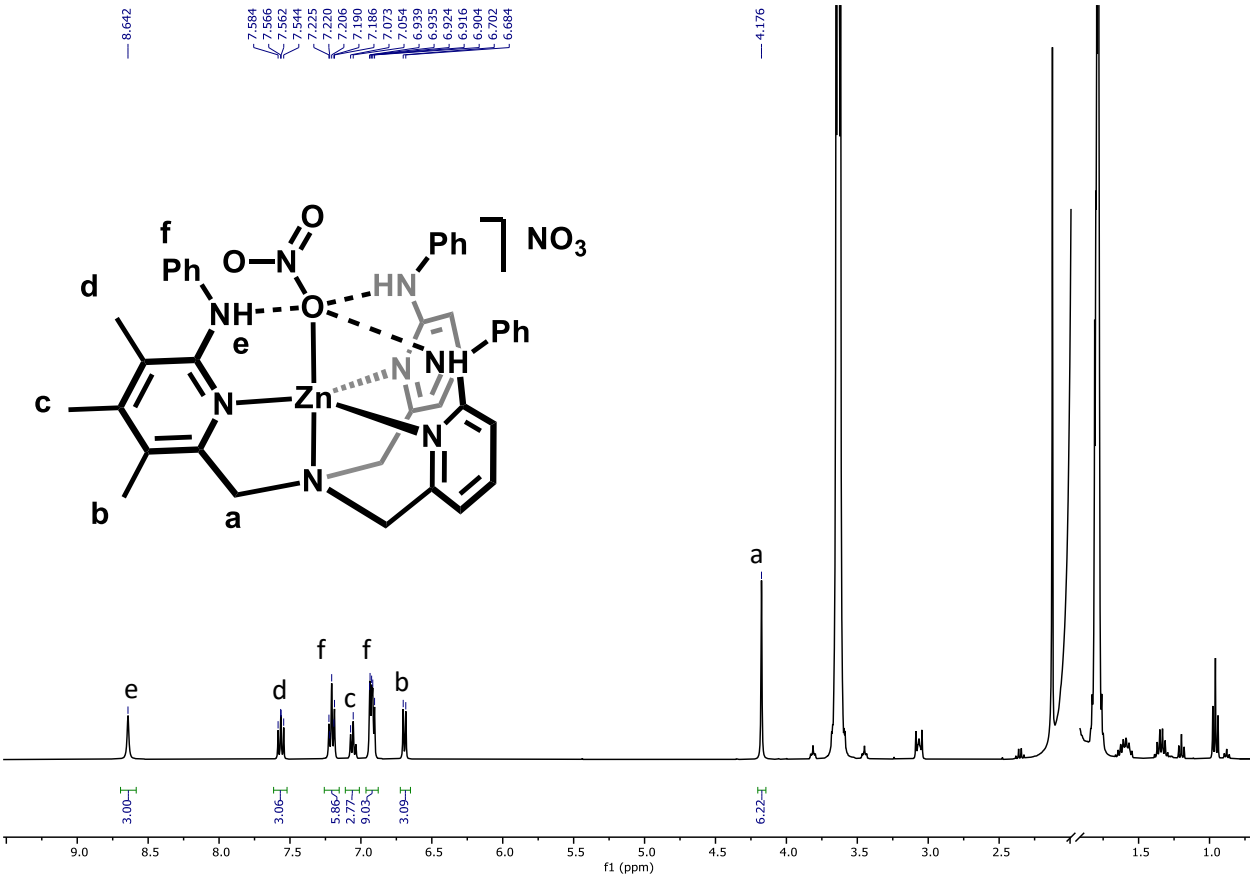

Supplementary Figure 15: ^{1}H-NMR spectrum (400 MHz, MeCN, 25 °C) of isolated crystals of **I-Zn(NO$_3$)$_2$** from the titration experiment.

Some residual [Bu$_4$N][NO$_3$] remains despite washing the crystalline sample with MeCN. The mole fraction plot derived from the simulated titration concentrations (Supplementary **Error! Reference source not found.**) suggests that **I-Zn** in presence of 2 equiv. NO_3^- forms a 50:50 mixture of **I-Zn(NO$_3$)** and **I-Zn(NO$_3$)$_2$**.

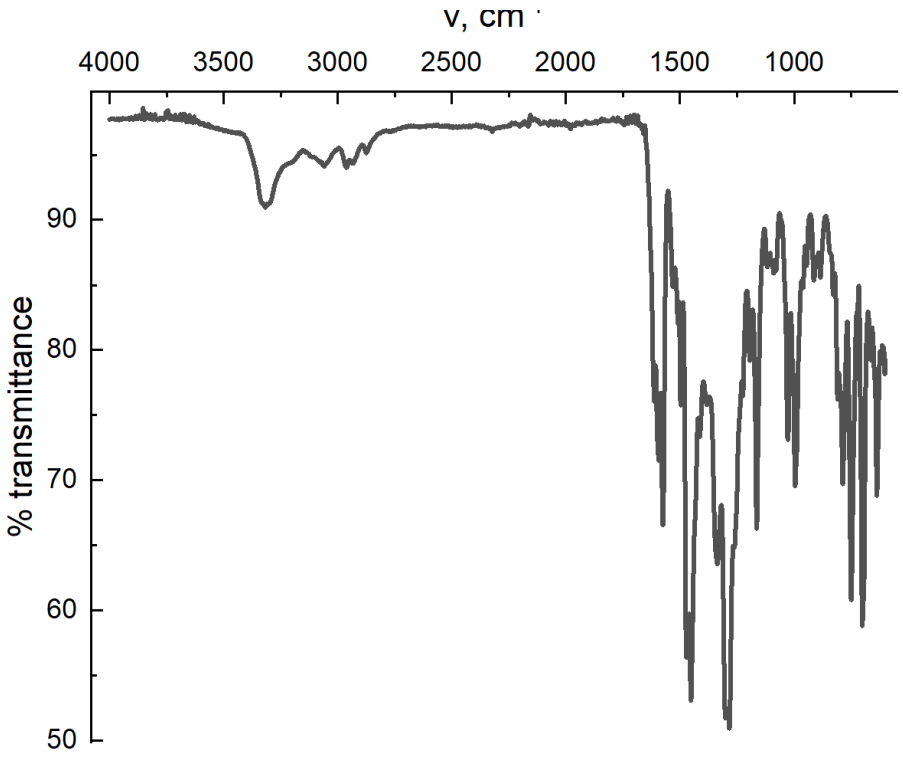

Supplementary Figure 16: FT-IR (ATR) spectrum of **I-Zn(NO$_3$)$_2$**.

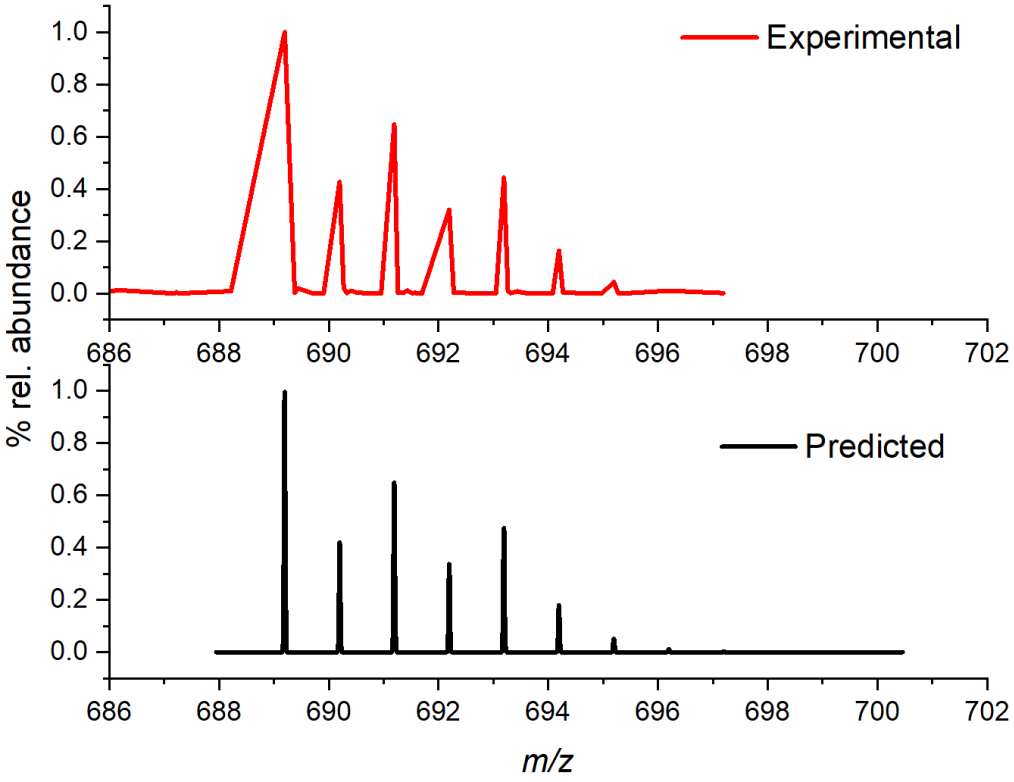

Supplementary Figure 17: ESI-MS of **I-Zn(NO$_3$)$_2$** stacked with its theoretical isotope envelope.

Preparation of II-Zn and NMR Titration with NO_3^-

Executed analogously to the titrations with **I-Zn** but initially metalated with TPA^{Me} instead of TPA^{NHPh}.

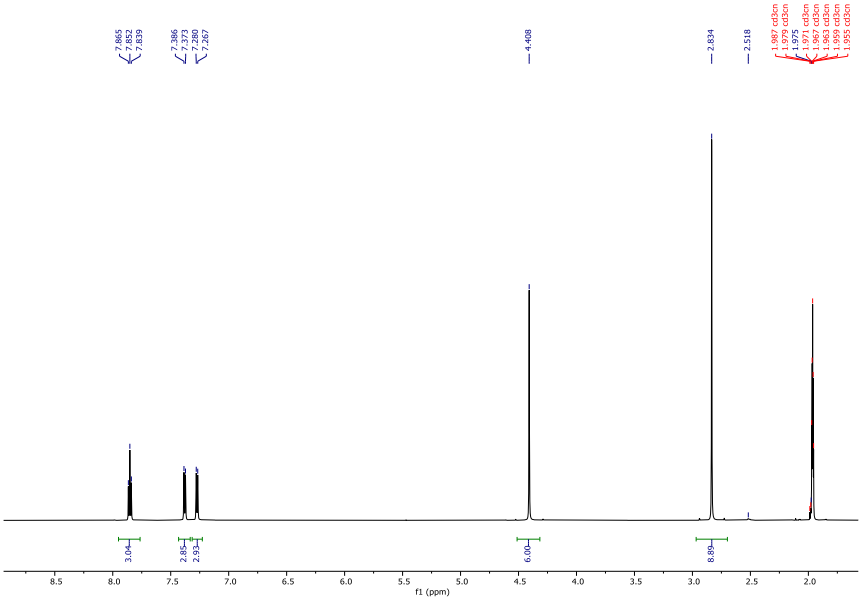

Supplementary Figure 18: ^{1}H-NMR spectrum (700 MHz, d_3-MeCN, 25 °C) of II-Zn (metalated *in situ*).

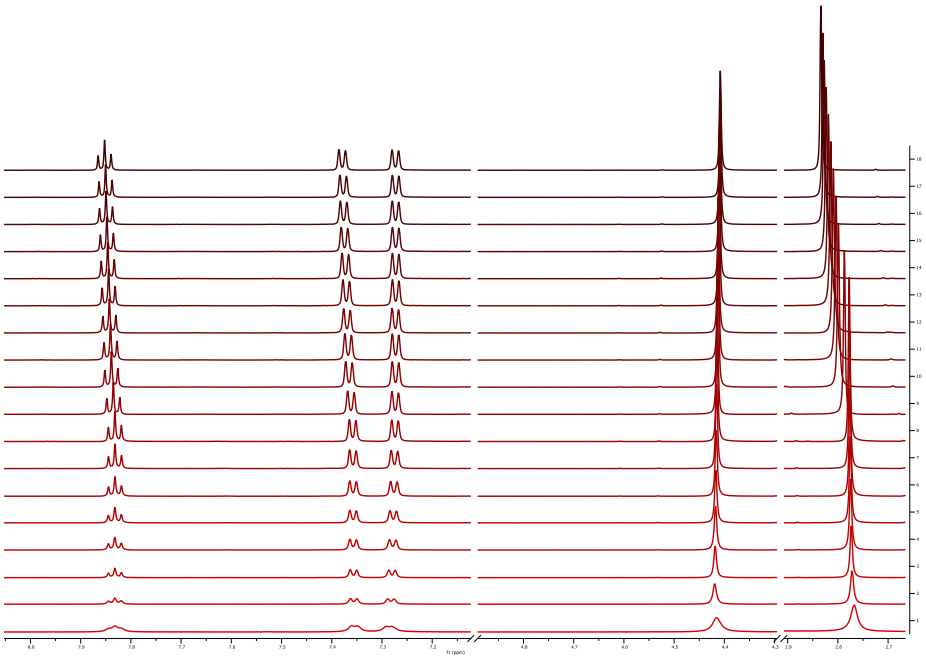

Supplementary Figure 19: Representative stacked ^{1}H-NMR spectra (700 MHz, d_3-MeCN, 25 °C) of a titration of **II-Zn** with $[Bu_4N][NO_3]$, starting from 0 equiv. (top) to 8 equiv. (bottom).

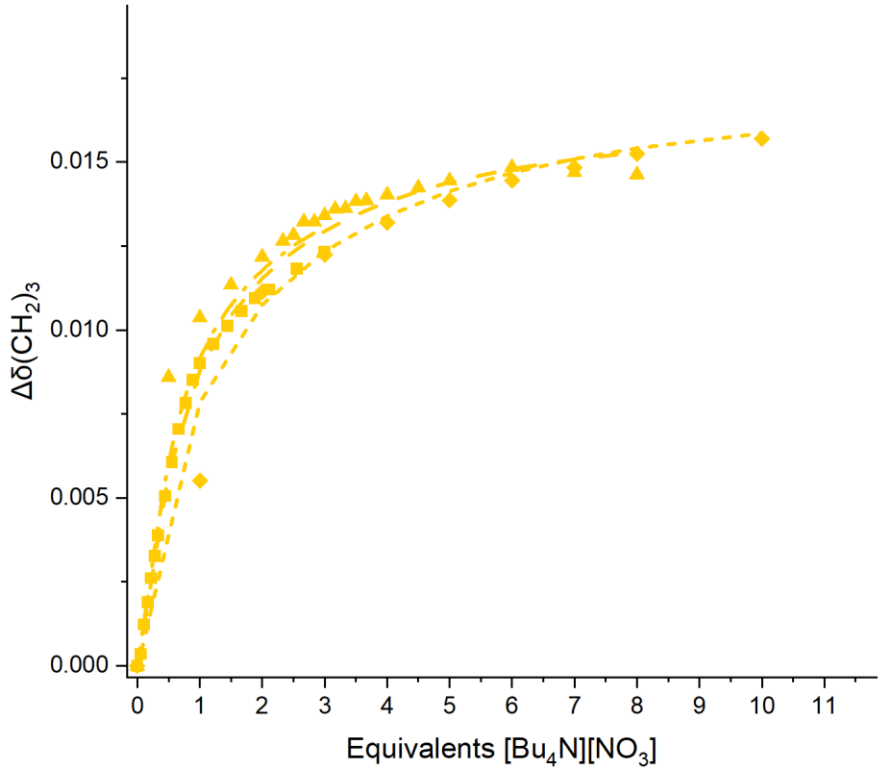

Supplementary Figure 20: Binding isotherm for **II-Zn**. Dotted line is calculated model (2:1/1:1/1:2 with full cooperativity).[23,24]

Supplementary Table 2: Calculated association constants from binding isotherm in Supplementary Error! Reference source not found.

$K_{2:1}$, M^{-1}	$K_{1:1}$, M^{-1}	$K_{1:2}$, M^{-1}
0.72 ± 0.14	0.34 ± 0.03	$(3.6 \pm 0.08) \bullet 10^{-3}$

The 95% confidence intervals were generated from cross-validation leave-3-out statistical analysis (p-value of 0.05).[25]

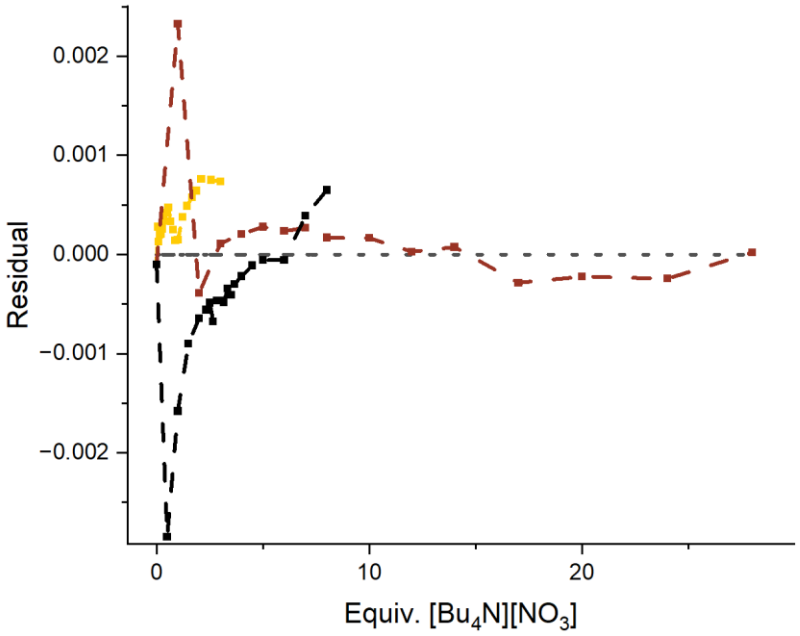

Supplementary Figure 21: Residuals of 2:1/1:1/1:2 fit for titration of **II-Zn** (colors denote different titrations).

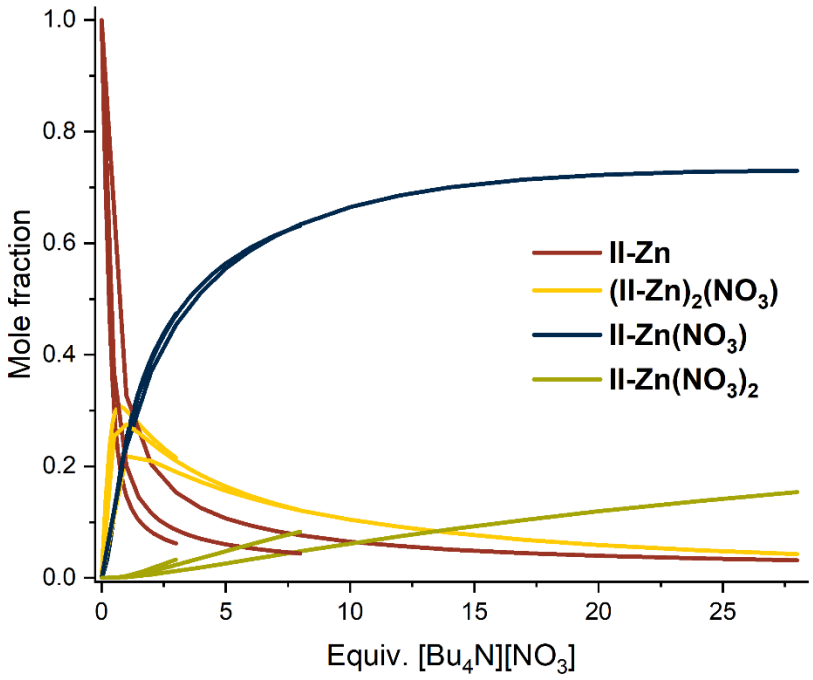

Supplementary Figure 22: Simulated mole fraction plots for **II-Zn** and its NO_3^- adducts.

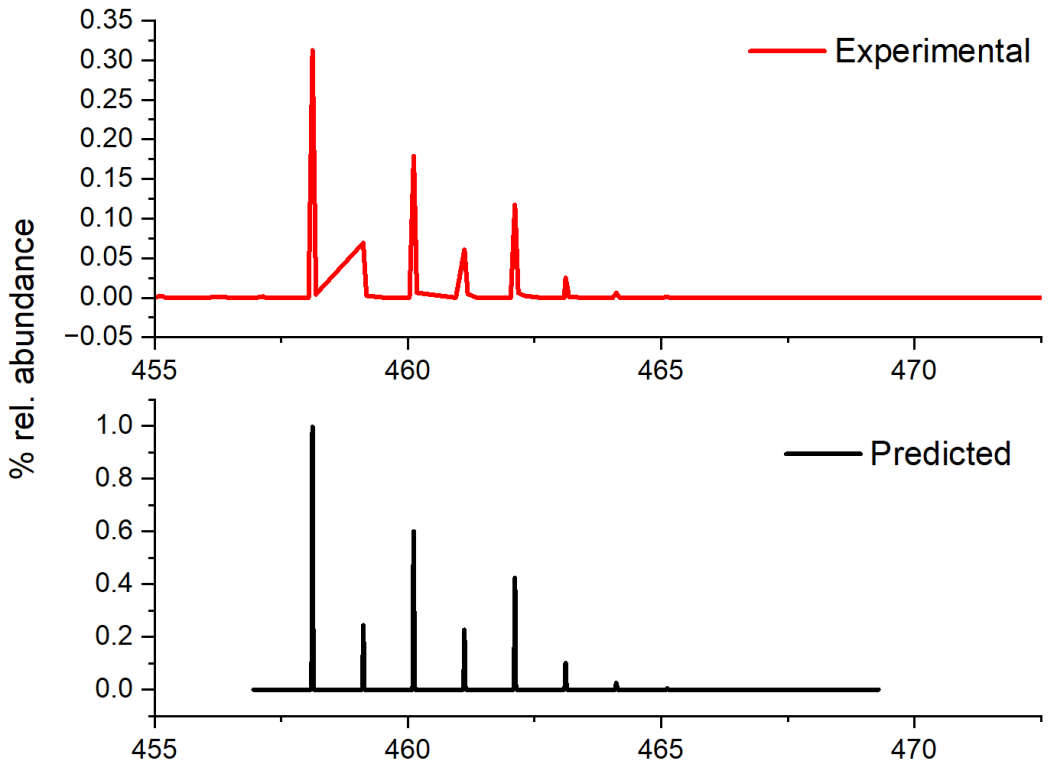

Supplementary Figure 23: ESI-MS of **II-Zn(NO_3)** stacked with its theoretical isotope envelope.

Stoichiometric Reactions between I-OTf and NO_3^-

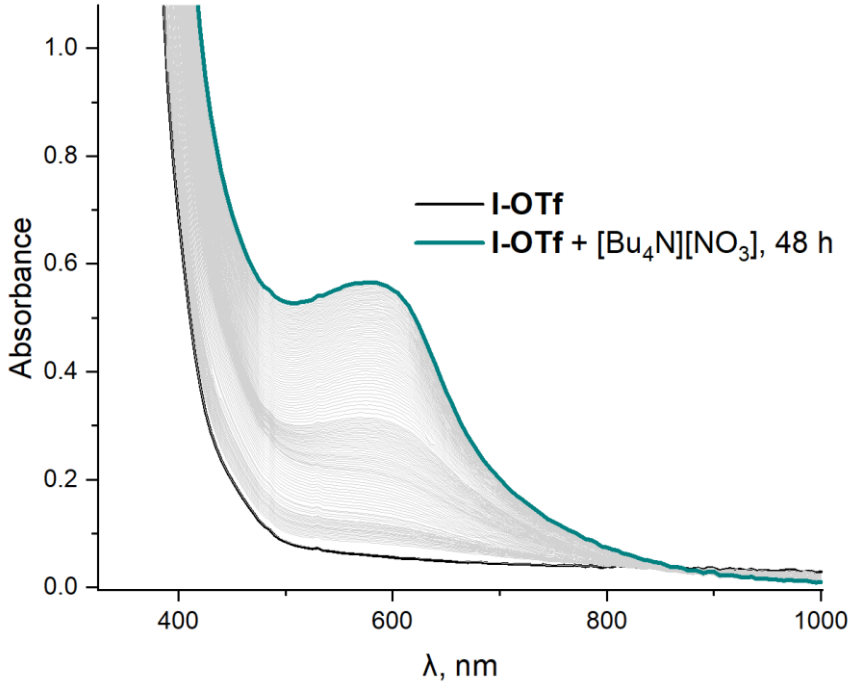

Supplementary Figure 24: UV-Vis time profile of reaction between **I-OTf** and 1 equiv. $[Bu_4N][NO_3]$ at 25 °C.

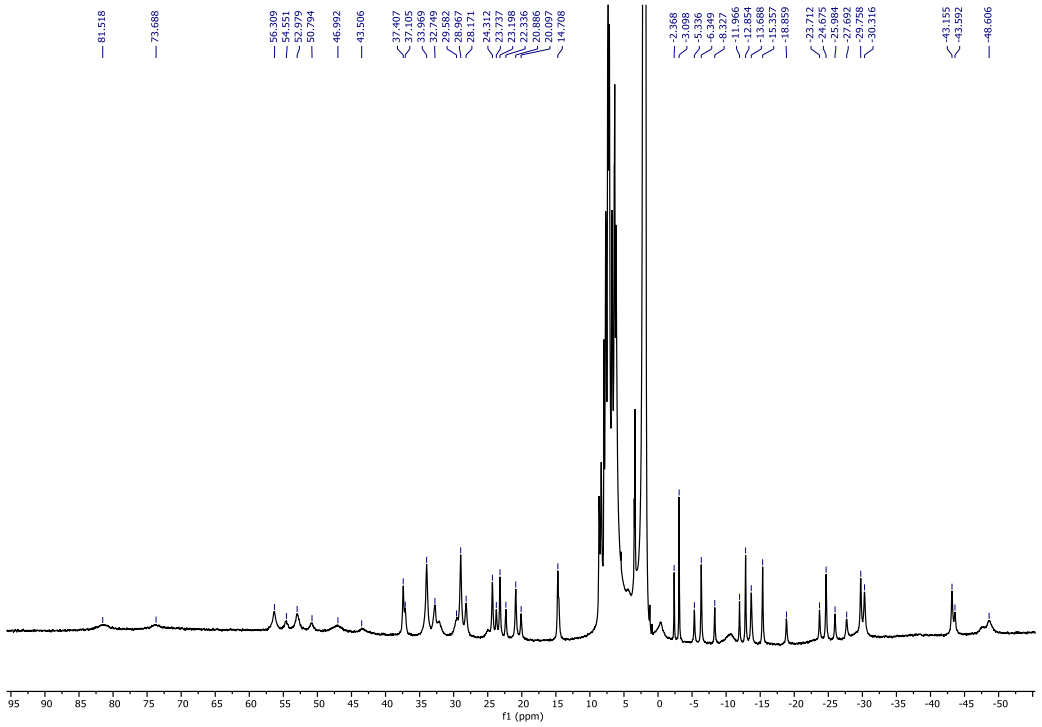

Supplementary Figure 25: H NMR spectrum (400 MHz, MeCN, 25 °C) of the terminal reaction product in Supplementary **Error! Reference source not found.**.

Note: We also observe the same species during NO_2^- reduction by **I-OTf**, which is the reaction that **V** was isolated from.

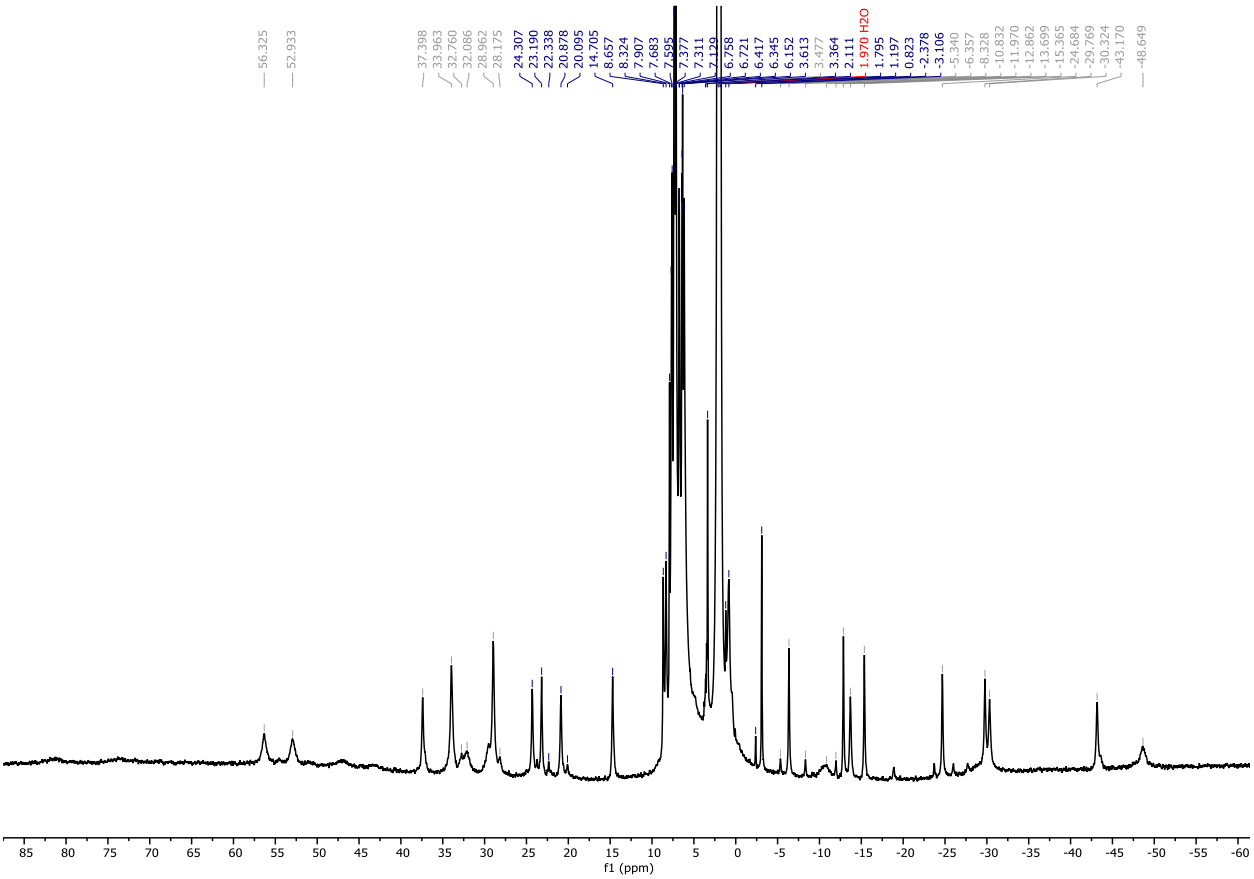

Supplementary Figure 26: ^{1}H-NMR spectrum (400 MHz, MeCN, 25 °C) of **V** isolated from NO_2^- reduction mediated by **I-OTf**.

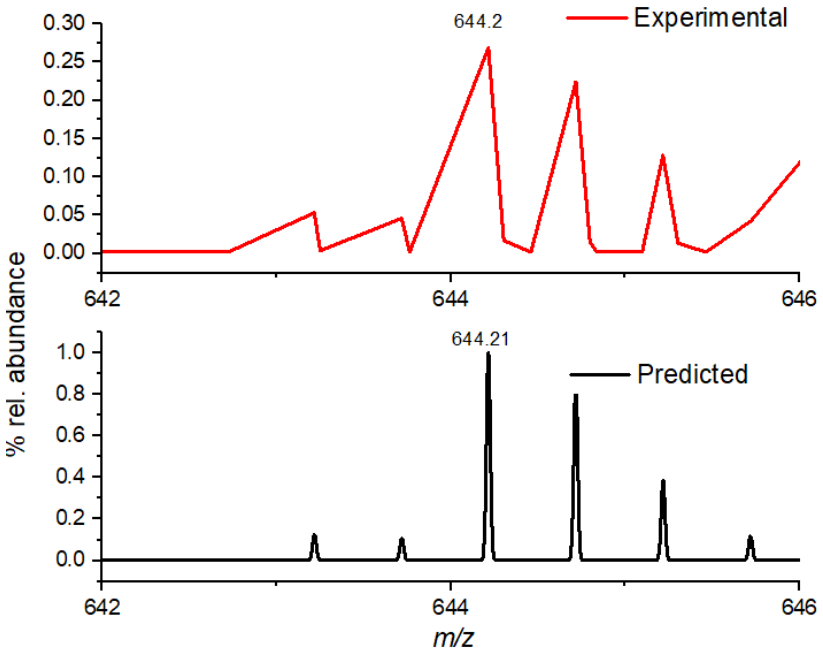

Supplementary Figure 27: ESI-MS of **V** stacked with its theoretical isotope envelope.

We show below that **V** decomposes to **IV** in presence of H^+ donors. The ESI-MS in our department elutes all samples through a short HPLC column with a 1% formic acid/formate buffer, a detail that may explain the low signal intensity.

Procedure for stoichiometric reaction at 80 °C: Inside a glove box, a J-young NMR tube was charged with $[Bu_4N][NO_3]$ (1.7 mg, 0.05 mmol, 1.0 equiv.) and complex **I-OTf** (4.6 mg, 0.05 mmol) in 1 mL MeCN. The tube was sealed with a Teflon cap and moved out of the glovebox, and it was kept in a pre-heated heating block set at 80 °C. After 16 h, ^{1}H NMR spectrum of the crude reaction mixture was recorded with an expanded spectral window.

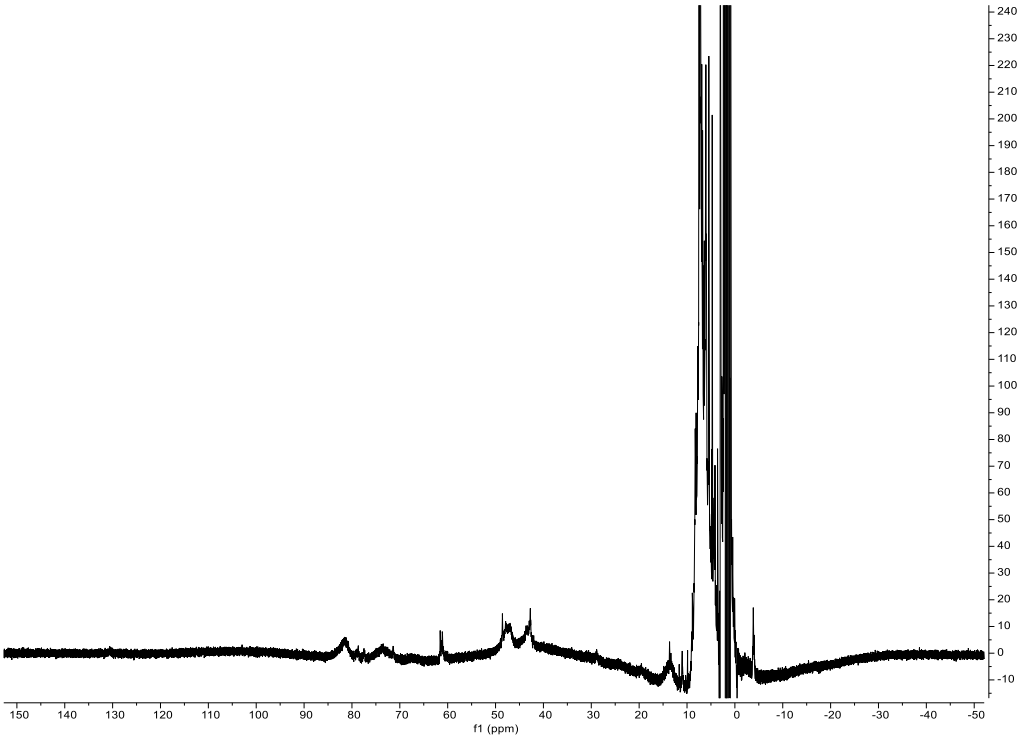

Supplementary Figure 28: ^{1}H NMR spectrum (600 MHz, MeCN, 25 °C) of the crude reaction mixture.

The major species in the crude reaction mixture is **IV**,[9] along with minor amounts of species **V** and other unidentified Fe-containing species.

Co(TPP) Trapping Experiment for Stoichiometric Reaction Between I-OTf and [Bu_4N][NO_3]: Inside a glove box, a Teflon-capped H-bridge setup was charged with [Bu_4N][NO_3] (1.2 mg, 0.004 mmol, 1.0 equiv.) and complex **I-OTf** (3.7 mg, 0.004 mmol) in 1 mL MeCN on one flask (side-1). The other flask was charged with Co(TPP) (2.7 mg, 0.004 mmol, 1.0 equiv) in 2 mL CH_2Cl_2 (side-2). The tube was sealed with three Teflon caps and moved out of the glovebox. The side-1 was heated and stirred in a pre-heated oil bath at 80 °C and the side-2 was kept stirring at room temperature (~25 °C). Teflon keys on both the sides were opened keeping the third (middle) Teflon key closed for flow of any evolved gas (from side-1 to side-2) during the reaction. After 16 h, the reaction was stopped and cooled to room temperature. An aliquot of the reaction mixture from side-2 was taken for ^{1}H NMR analysis that showed formation of Co(TPP)(NO) in 45% yield.

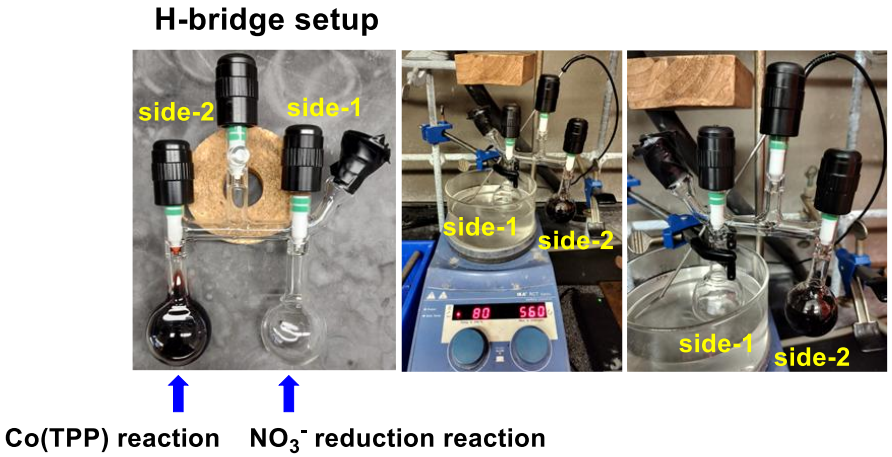

Supplementary Figure 29: Image of the reaction setup used for the flask -to-flask setup of tandem NO_3^- reduction to NO and Co(TPP) to Co(TPP)(NO) trapping**.**

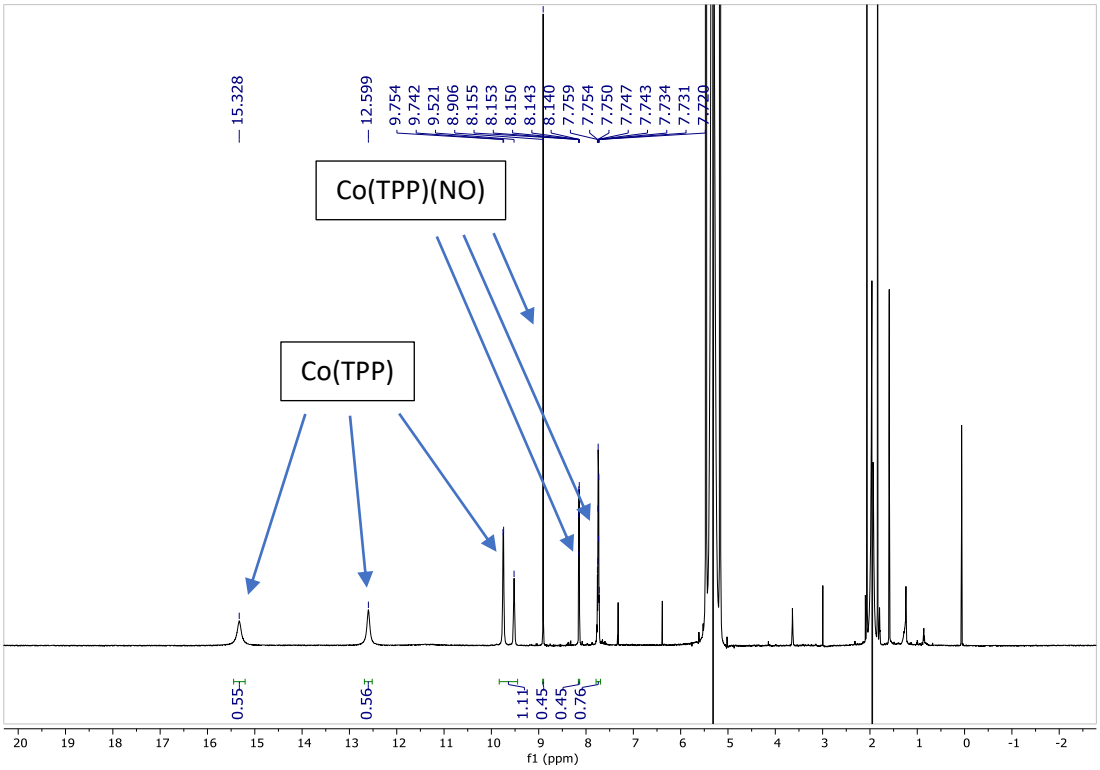

Supplementary Figure 30: ^{1}H NMR spectrum (400 MHz, CH_2Cl_2, 25 °C) of crude reaction mixture (side-2) of a stoichiometric reaction between **I-OTf** and $[Bu_4N][NO_3]$ giving 45% yield of Co(TPP)(NO).

Reactions between II-OTf and [Bu_4N][NO_3]

Procedure: Inside an N_2-filled glovebox, J-Young valved NMR tubes were charged with MeCN solutions containing **II-OTf**, and either 1, 10, or 100 equivalents of [Bu_4N][NO_3]. NMR spectra were recorded shortly after solution preparation and/or after 6 days.

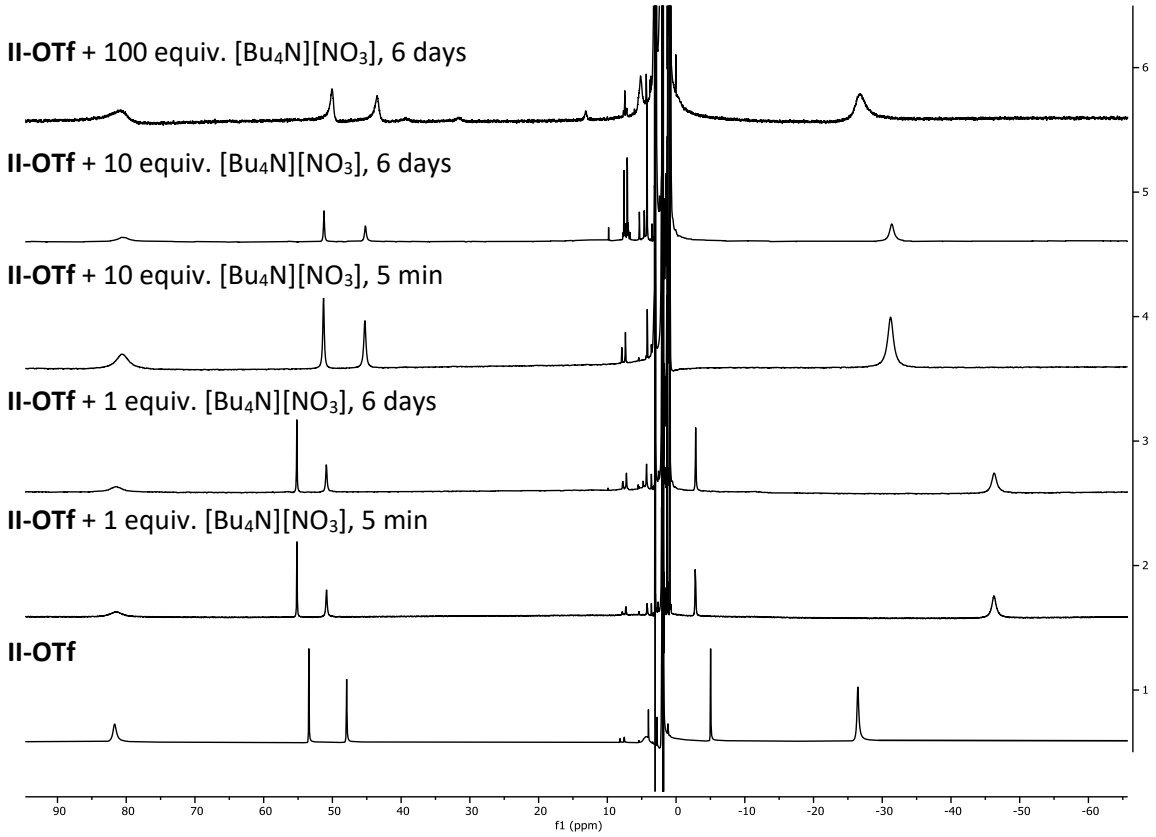

Supplementary Figure 31: Stacked ^{1}H-NMR spectra (400 MHz, CH_2Cl_2, 25 °C) of reactions between **II-OTf** and increasing amounts of [Bu_4N][NO_3].

After an initial binding event (resonances shifted with respect to **II-OTf**), the reactions undergo no further change, even after 6 days. The small additional peaks in the presence of 100 equiv. [Bu_4N][NO_3] could correspond to a 1:2 adduct, $TPA^{Me}Fe(II)(NO_3)_2$. Assuming identical binding affinities between Zn and Fe, such a state would be a small portion of the solution-state speciation, based on the simulated mole fraction plot for **II-Zn** (**Error! Reference source not found.**). Single crystals of **II-NO_3** were grown from the 1:1 stoichiometric reaction after 50 h via slow diffusion of Et_2O in CH_2Cl_2 (Supplementary Error! Reference source not found.).

Procedure: Inside an N_2-filled glovebox, a 20 mL scintillation vial was charged with **II-OTf** (0.003 mmol) and 1, 10, or 100 equivalents of [Bu_4N][NO_3]. The samples were dissolved in 3.0 mL of MeCN and transferred to a custom UV-Vis cuvette, stoppered, brought out of the glovebox, and inserted into spectrophotometer with its cryostat set to 25 °C. UV-Vis spectra were recorded after 5 min and 48 h.

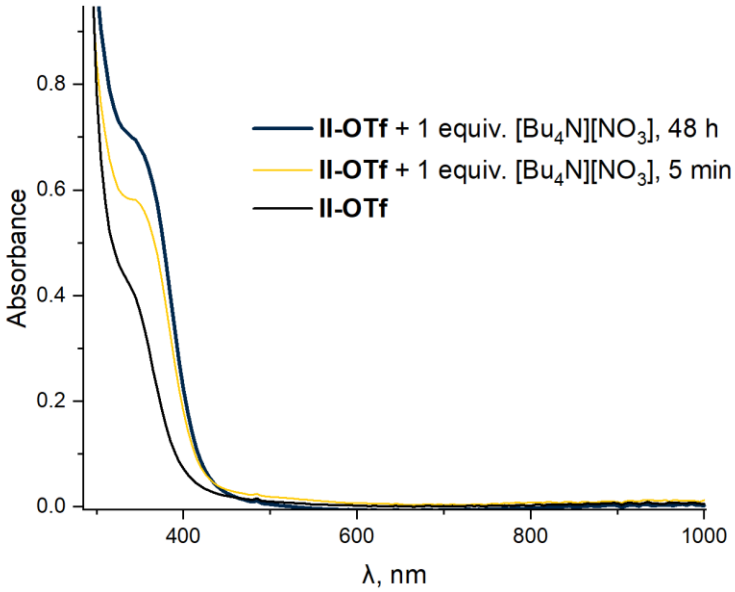

Supplementary Figure 32: Stacked UV-Vis traces of reactions between **II-OTf** and 1 equiv. of $[Bu_4N][NO_3]$ at t = 5 min and t = 48 h.

We note that minor slow changes in the absorbance feature at 375 nm occur over the reaction time frame. We attribute this to changes in solution state structures over the course of the reaction.

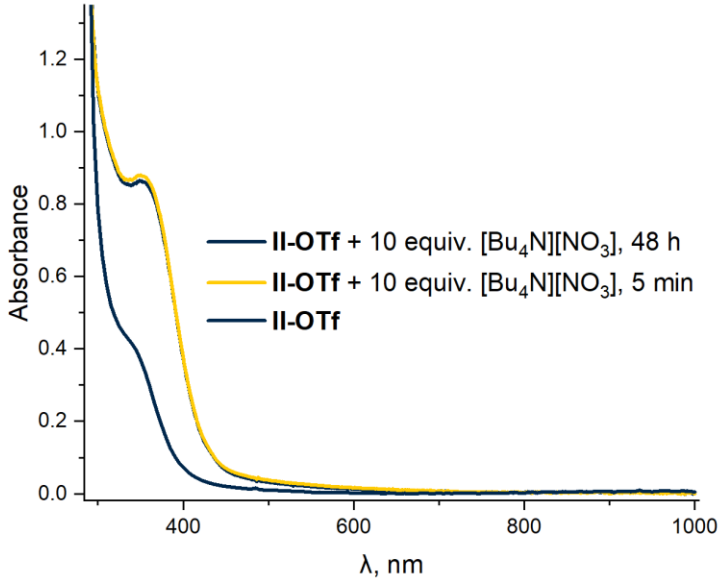

Supplementary Figure 33: Stacked UV-Vis traces of reactions between **II-OTf** and 10 equiv. of $[Bu_4N][NO_3]$ at t = 5 min and t = 48 h.

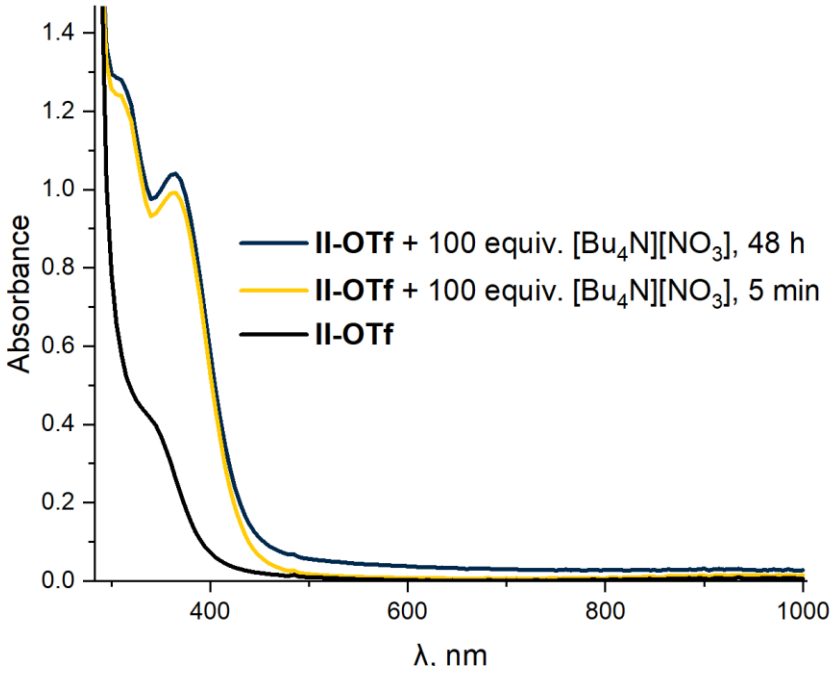

Supplementary Figure 34: Stacked UV-Vis traces of reactions between **II-OTf** and 100 equiv. of $[Bu_4N][NO_3]$ at t = 5 min and t = 48 h.

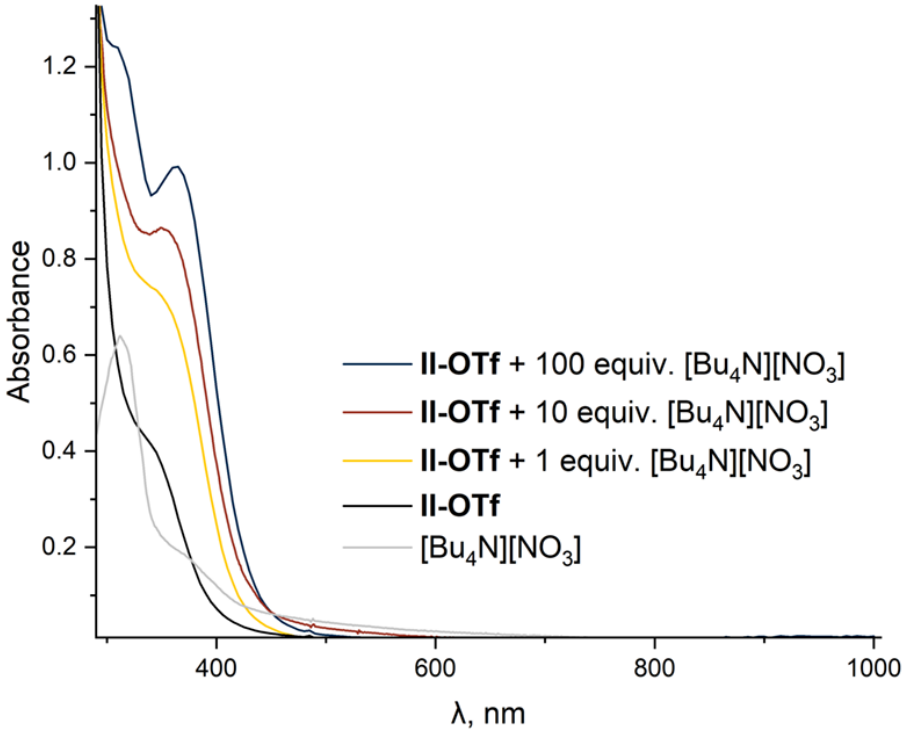

Supplementary Figure 35: Stacked UV-Vis traces of reactions between **II-OTf** and increasing amounts of $[Bu_4N][NO_3]$ after 48 h at 25 °C.

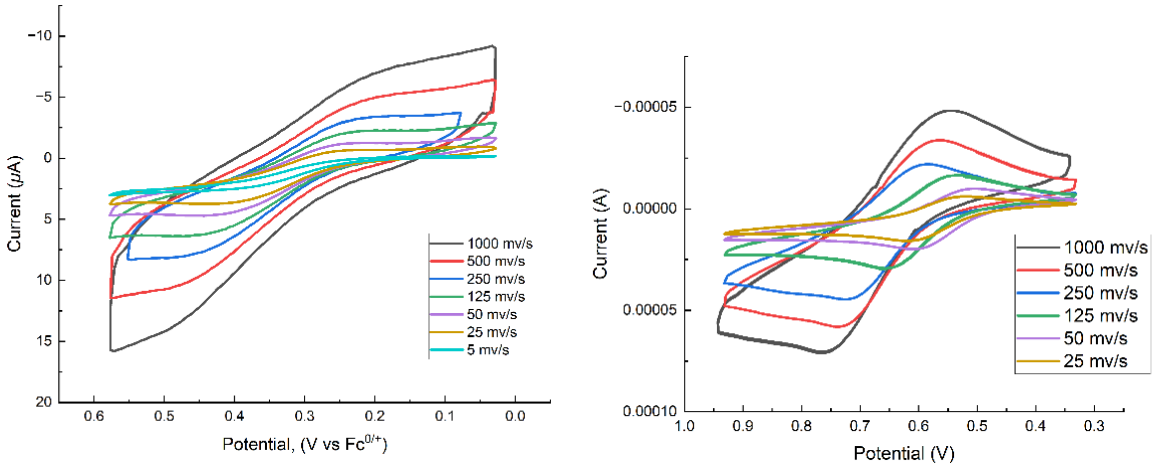

Supplementary Figure 36: Scan-rate dependent cyclic voltammograms of **I-OTf** (left) and **II-OTf** (right) (0.1 M $[Bu_4N][OTf]$ in MeCN)

These compounds feature *ca*. 0.3 V separation of their $E_{1/2}$ values (**I-OTf** ~ + 0.35 V; **II-OTf** ~ +0.65 V), which we attribute to differences in binding affinities for OTf^- ions, in analogy to our findings using NTf_2-based systems.[8]

Reactions of III with lutidine and IV with [DMFH][OTf]

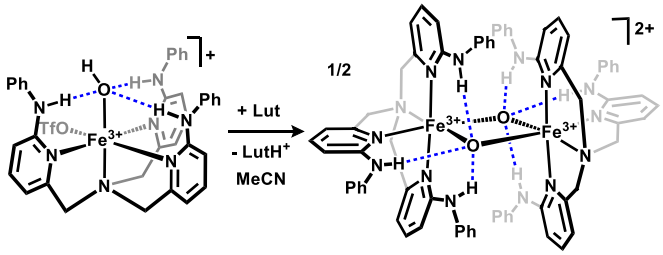

Procedure: Inside an N_2 filled glovebox, a 3 mL sample of a 0.75 mM solution of $TPA^{NHPh}Fe(III)OH(OTf)_2$ in MeCN in a modified UV-Vis quartz cuvette was titrated with successive aliquots (0.025 mL or 0.050 mL) of a 3 mM 2,6-lutidine solution in MeCN, while stirring, until full conversion was achieved (500 µL total volume added). Scans taken 10 s after addition of the aliquot.

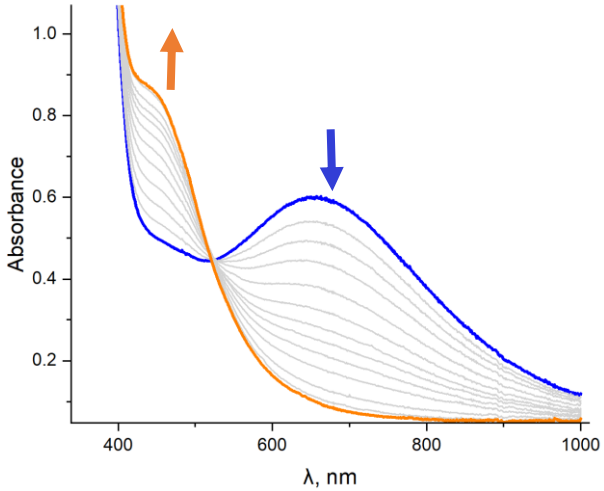

Supplementary Figure 37: Spectrophotometric titration of **III** with lutidine.

The final absorbance of **IV** at 433 nm corresponds to quantitative conversion of **III** to **IV**. (Abs_{433} = 0.856, ε = 2.63 $mM^{-1}cm^{-1}$ ∴ c = 0.27 mM).

Procedure: Analogous to the above titration, but with a single addition of 1 equiv. [DMFH][OTf].

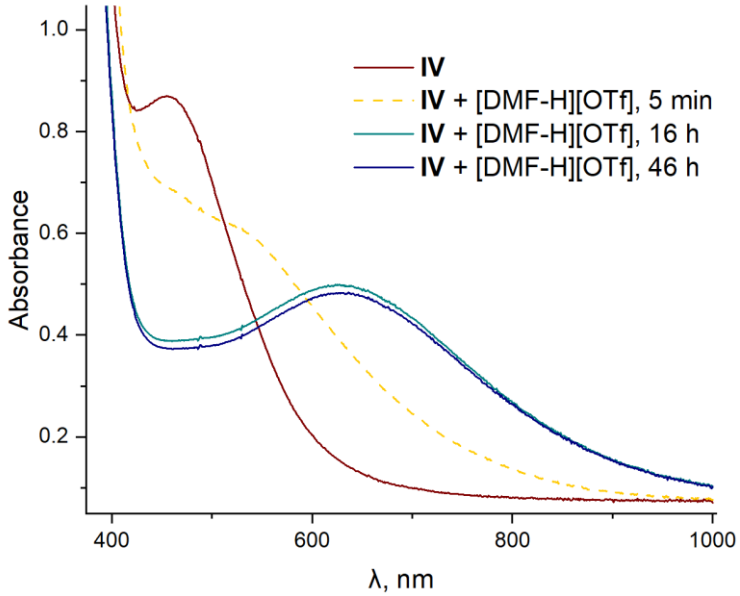

Supplementary Figure 38: Stacked UV-Vis spectra of a reaction between **IV** and [DMFH][OTf].

Reaction of $TPA^{NHPh}Fe(III)(OH)(OTf)(BArF_{20})$ with NO_2^-

Procedure: $TPA^{NHPh}Fe(III)(OH)(OTf)(BArF_{20})$ (5.0 mg, 0.003 mmol) was dissolved in 3.0 mL of MeCN and transferred to a modified quartz cuvette, sealed with a high vacuum 4 mm Teflon valve and a rubber septum, then inserted into the UV-Vis spectrophotometer set to 25 °C. Next, 0.1 mL of a 30 mM $[Bu_4N][NO_2]$ stock solution was injected into the cuvette immediately before spectral acquisition.

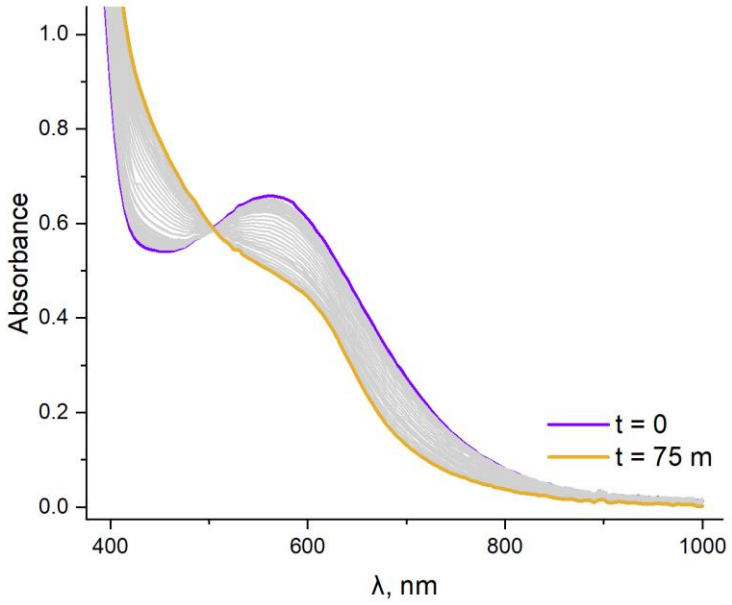

Supplementary Figure 39: UV-Vis time course of the reaction of **III** and 1 equiv. of $[Bu_4N][NO_2]$.

The previously reported UV-Vis feature of **III** at 645 shifted immediately to a peak at 590 nm which then decayed to a shoulder feature over 75 minutes. ε^{590} = 0.47 $mM^{-1}cm^{-1}$.

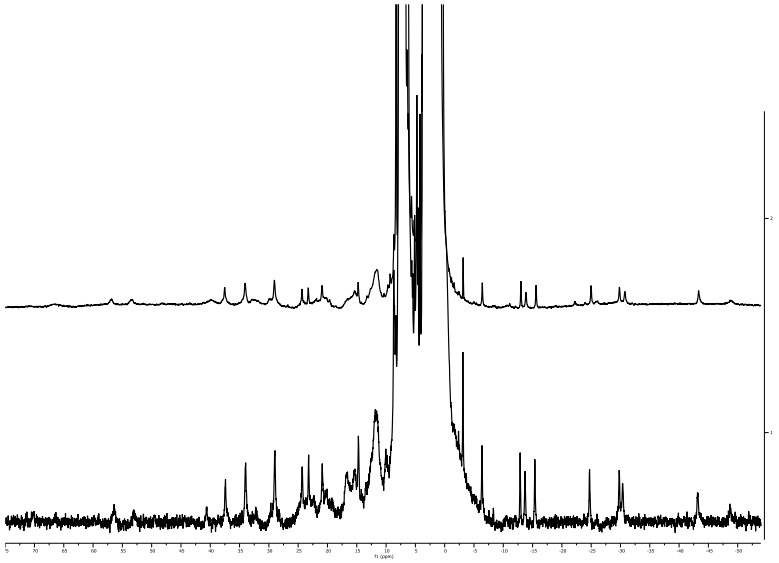

Supplementary Figure 40: Stacked ^1H NMR (400 MHz, MeCN, 25 °C) spectra of crude NO_3^- reduction product from **Error! Reference source not found.** (top, t = 23 h) and the product of the reaction between **III** with NO_2^- in MeCN (bottom)**.**

Procedure: Inside an N_2-filled glovebox, a 4 mL vial containing 0.005 mmol **III** and 0.005 mmol $[Bu_4N][NO_3]$ was placed into a 20 mL vial containing 10 mL CH_2Cl_2 and 0.005 mmol Co(TPP). Stirbars were added to each vial. MeCN was added to the inner vial, the outer vial was capped tightly, then the reaction was stirred for 2 h under ambient conditions. After 2 h, an FT-IR (ATR, dropcast) spectrum of the Co(TPP) trap

was recorded (Supplementary Figure 39). We observed a prominent peak at 1692 cm^{-1}, consistent with formation of Co(TPP)(NO).

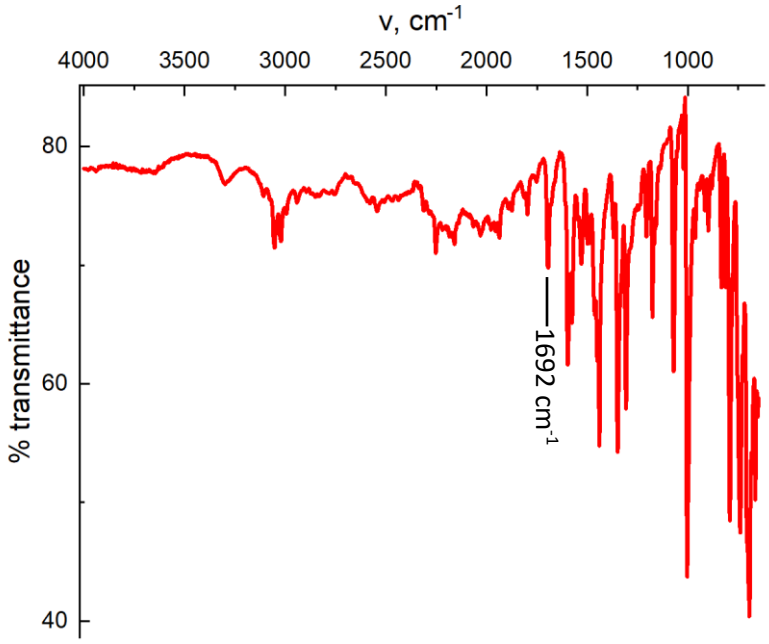

Supplementary Figure 41: FT-IR (ATR) spectrum of the Co(TPP) trapping experiment of the reaction between **III** and $[Bu_4N][NO_2]$.

As **V** retains two Fe(III)OH centers (i.e., no proton transfer or oxidation state changes), we propose that the formation of NO from NO_2^- and **III** follows an H^+-mediated disproportionation pathway, rather than formal $2H^+/1e^-$ reduction.

Procedure: Inside an N_2 filled glovebox, **III** (2.1 mg dissolved in 2.5 mL MeCN) was transferred to a UV-Vis cuvette, then treated with 0.5 mL of a MeCN solution containing 1 equiv. of $[Bu_4N][NO_3]$, then stirred for 20 h.

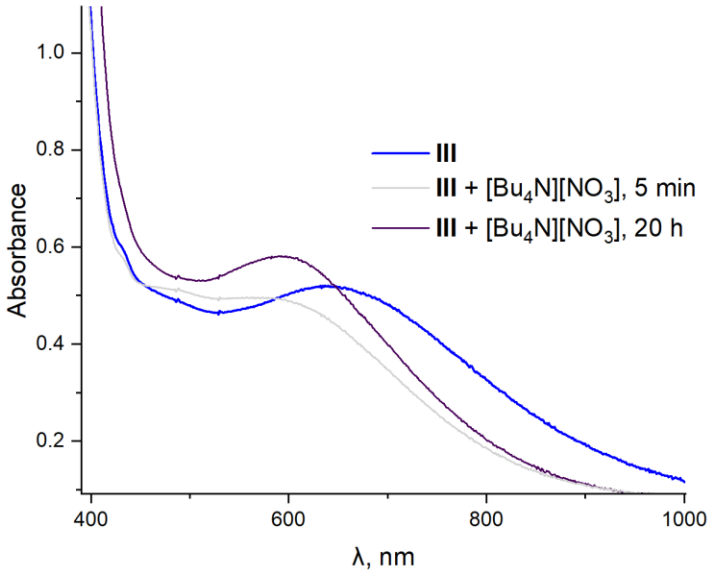

Supplementary Figure 42: Stacked UV-Vis spectra of the reaction between **III** and $[Bu_4N][NO_3]$.

λ_{max} shifts from 645 nm to 590 nm. The curvature of this product is different than the crude reaction product formed from **I-OTf** reacting with $[Bu_4N][NO_3]$ after 48 h, a difference that we attribute to the multiple products present in the terminal NO_3^- reduction mixture.

Reaction between III and 1,2-diphenylhydrazine

Procedure: Inside an N_2 filled glovebox, a 4 mL vial was charged with **III** (1.7 mg, 0.0018 mmol), 1.2 mg 1,2-diphenylhydrazine (1.4 mg, 0.0077 mmol, 4.2 equiv.), and 1,3,5-trimethoxybenzene (1.4 mg, 0.0083 mmol) as an internal standard. Then, 1.5 mL of MeCN was added, causing the blue color of **III** to bleach to yellow instantly upon mixing. The solution was then transferred to an NMR tube and analyzed by ^{1}H NMR spectroscopy to quantify azobenzene formation.

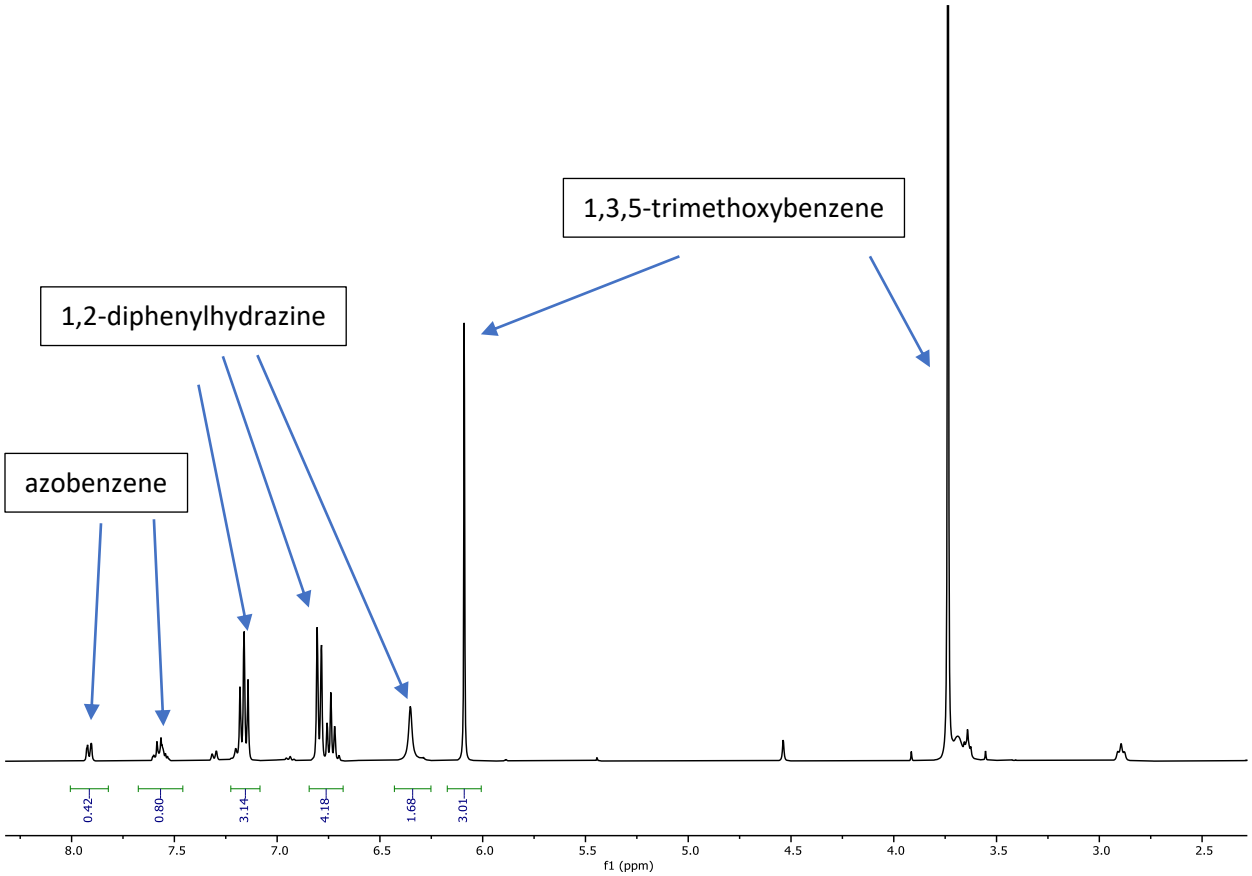

Supplementary Figure 43: ^{1}H q-NMR spectrum (400 MHz, MeCN, 25 °C) of reaction between **III** and $Ph_2N_2H_2$.

The respective integrals of azobenzene and trimethoxybenzene correspond to quantitative consumption of **III** and concomitant formation of 1/2 equivalent of azobenzene.

$$\text{mmol azobenzene} = \left(\frac{3\text{H}}{4\text{H}}\right)\left(\frac{0.43}{3}\right) * (0.0083\ \text{mmol}) = 0.009; 100\%\ \text{yield}$$

This reaction afforded a mixture of **I-OTf** and **VI** as the terminal products:

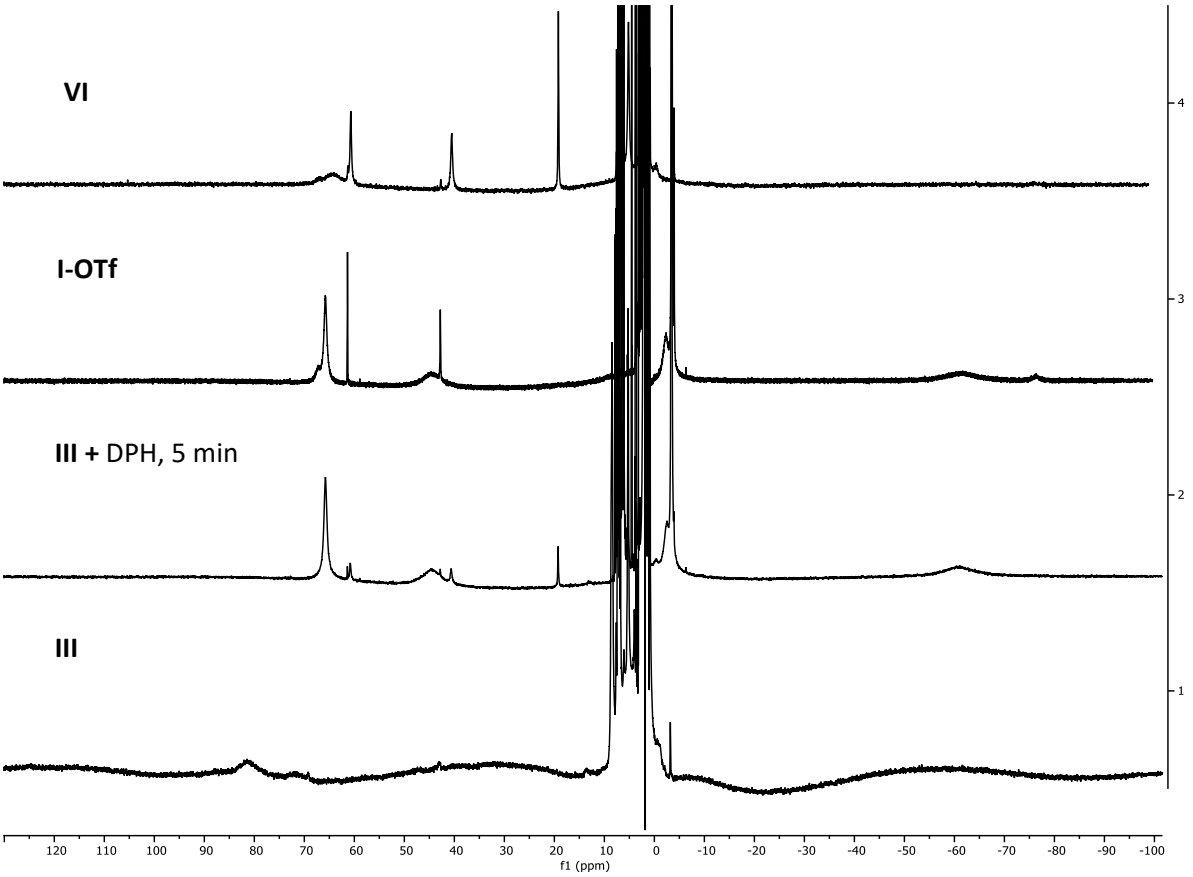

Supplementary Figure 44: Stacked ^{1}H-NMR spectra (400 MHz, MeCN, 25 °C) with expanded spectral window of **III**, its product after reduction with DPH, an authentic sample of **I-OTf**, and an authentic sample of **VI**.

Reaction Between IV and $[Bu_4N][NO_3]$ at 25 °C

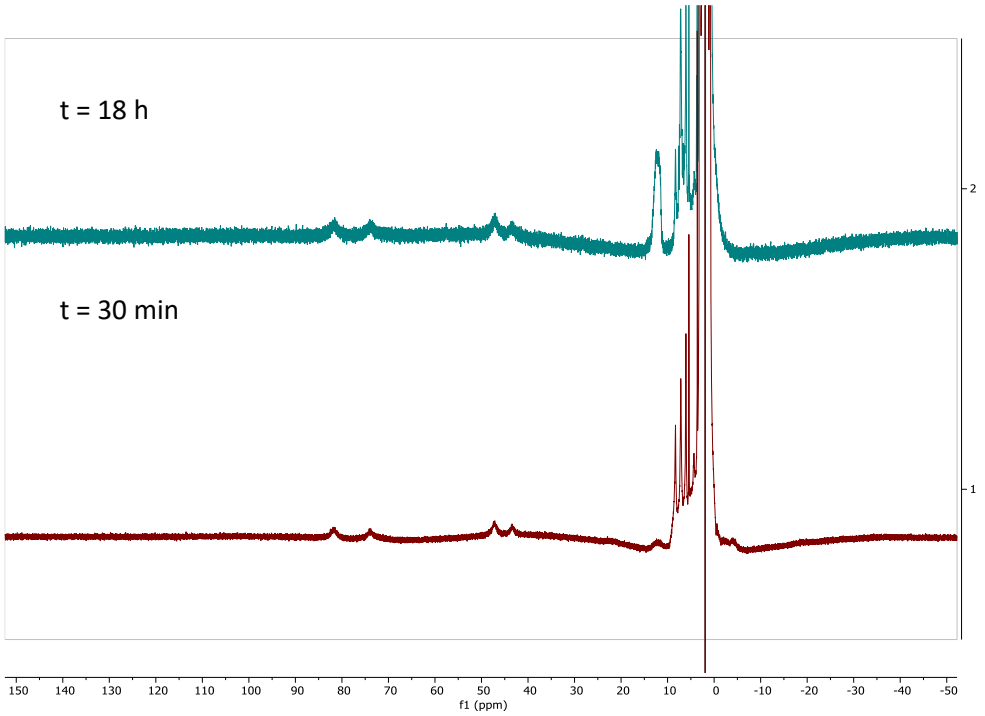

Supplementary Figure 45: Stacked ^{1}H NMR spectra (600 MHz, MeCN, 25 °C) of the crude reaction mixture of complex **IV** (1.0 equiv.) reacting with $[Bu_4N][NO_3]$ (10.0 equiv.).

No reaction was observed.

Reaction Between Complex V and $[Bu_4N][NO_3]$ at 25 °C

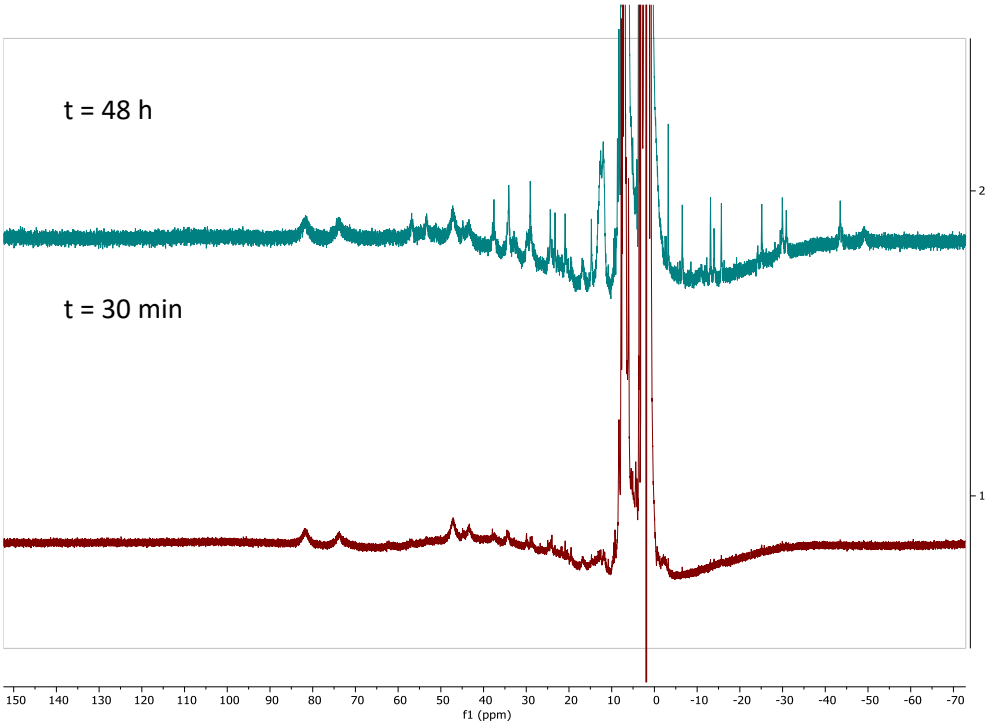

Supplementary Figure 46: Stacked ^1H NMR spectrum (600 MHz, CH_3CN, 25 °C) of the crude reaction mixture of **V** reacting with $[Bu_4N][NO_3]$ (10.0 equiv.).

No reaction was observed.

Reaction Between VI and $[Bu_4N][NO_2]$ at 25 °C: NMR

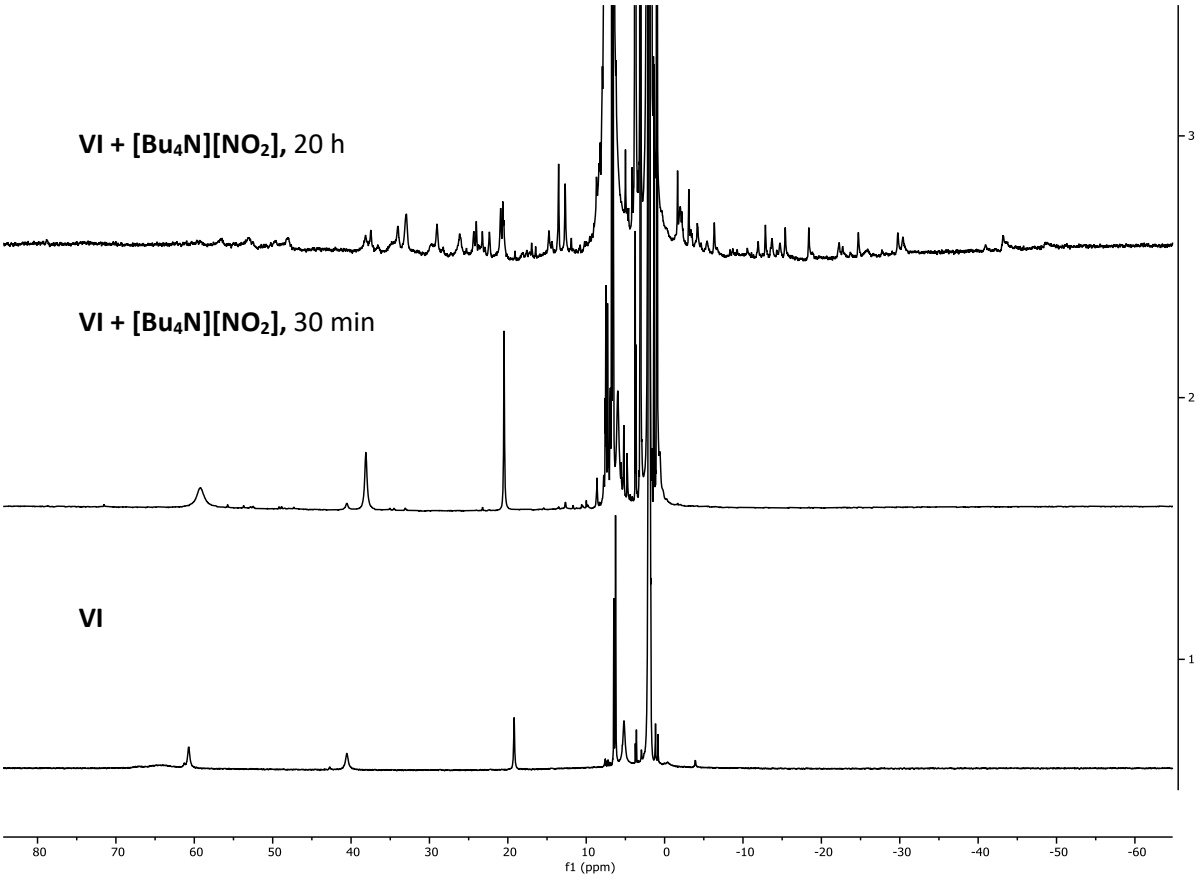

Supplementary Figure 47: Stacked ^{1}H NMR spectrum (400 MHz, MeCN, 25 °C) of crude reaction mixture of a reaction between complex **VI** and $[Bu_4N][NO_2]$ (1.0 equiv.).

One set of resonances in the reaction mixture matches the paramagnetically shifted ^{1}H NMR resonances of **V** while the remainder correspond to an unidentified paramagnetic product.

Reaction of VI with $[Bu_4N][NO_2]$ at 25 °C: UV-Vis

Procedure: In an N_2-filled glovebox, a modified quartz cuvette was charged with 3 mL of a 2.0 mM stock solution of **VI**. The cuvette was sealed, then transferred to the spectrometer and held at 25 °C. A 0.5 mL aliquot of a 30 mM $[Bu_4N][NO_2]$ solution in MeCN was then added immediately before data acquisition.

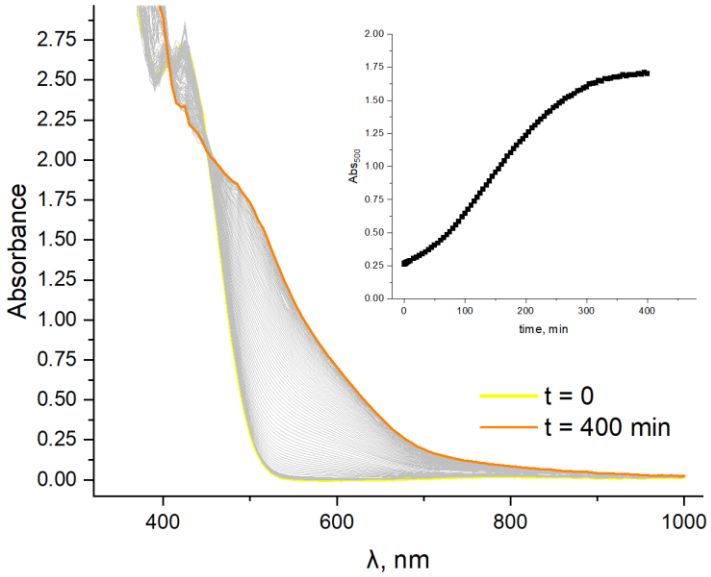

Supplementary Figure 48: UV-Vis time course of **VI** reacting with 4.6 equiv. $[Bu_4N][NO_2]$ (1.8 mM VI, 8.3 mM $[Bu_4N][NO_2]$, MeCN, 25 °C). Inset: kinetic trace of absorbance growth at 500 nm.

The sigmoidal shape of the kinetic trace suggests a slow equilibrium (NO_2^- binding) before the rate determining step, or a radical chain autocatalysis/auto-oxidation pathway.

Reaction Between VI and $[Bu_4N][NO_3]$ at 25 °C

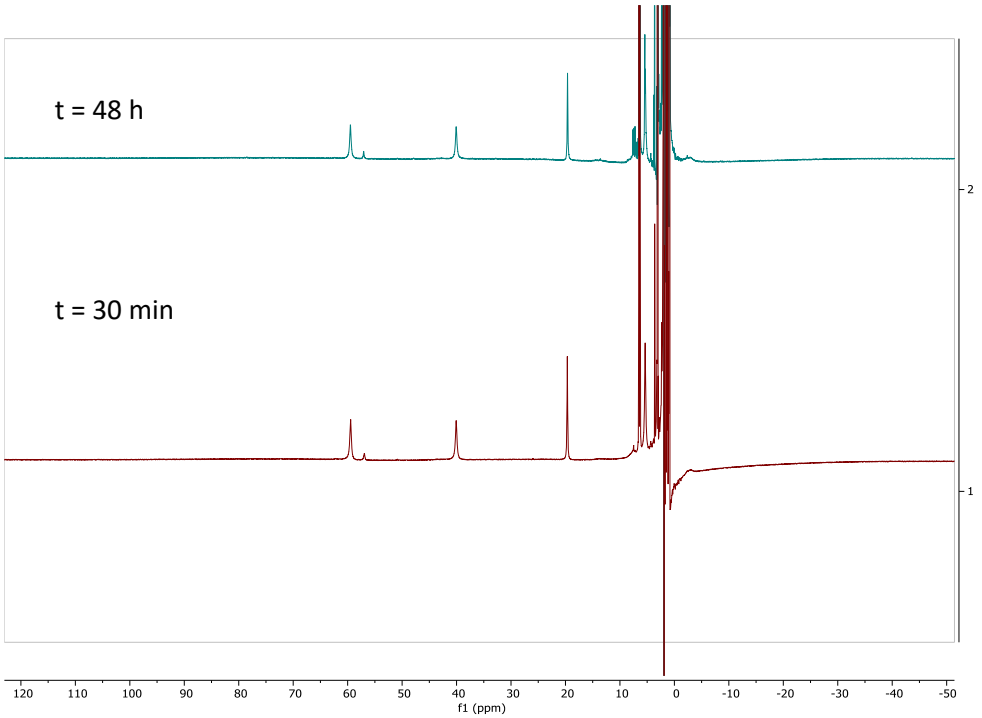

Supplementary Figure 49: Stacked ^{1}H NMR spectrum (600 MHz, CH_3CN, 25 °C) of crude reaction mixture of a reaction between complex **VI** (1.0 equiv.) and $[Bu_4N][NO_3]$ (10.0 equiv.).

No reaction was observed.

Reaction between V and [PhNH$_3$][OTf]

Procedure: Inside an N_2 filled glovebox, a 20 mL vial was charged with equimolar amounts of **V** and [PhNH$_3$][OTf] and 1 mL of MeCN, then transferred to an NMR tube for analysis.

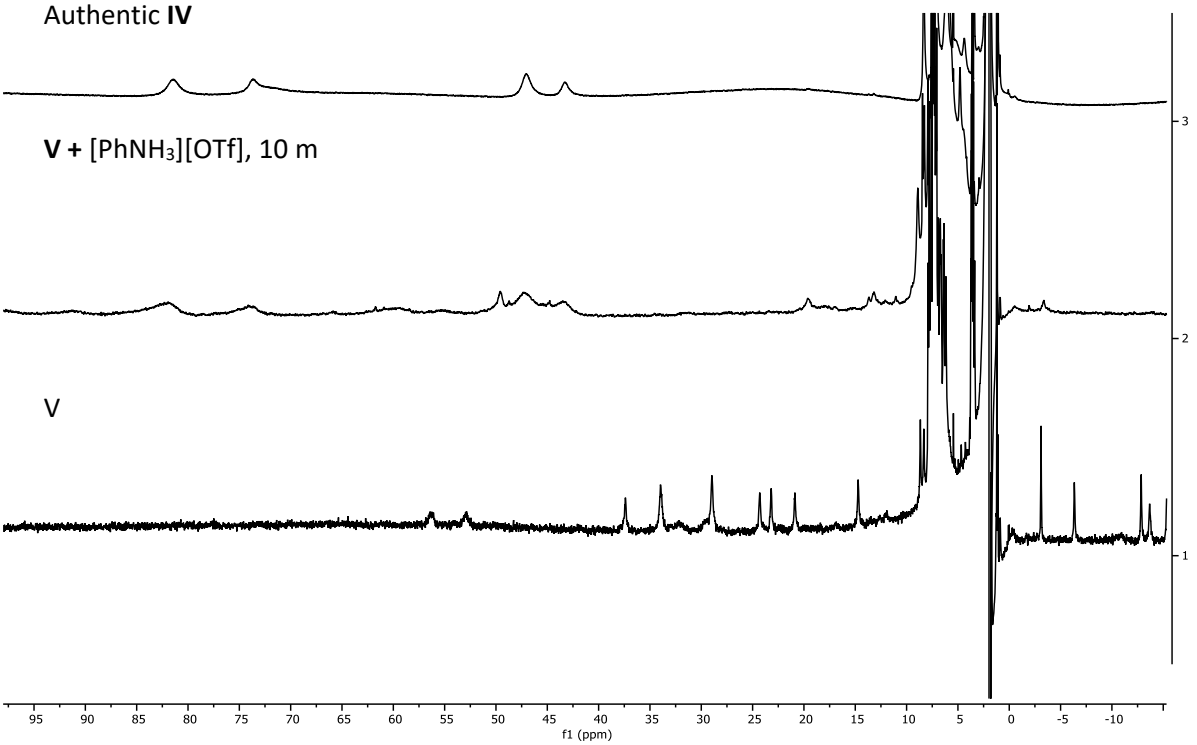

Supplementary Figure 50: Stacked ^{1}H NMR spectrum (400 MHz, MeCN, 25 °C) of crude reaction mixture of a reaction between complex **V** (1.0 equiv.) and [PhN][OTf] (10.0 equiv.).

Reaction of VI with $[Ph_2NH_2][OTf]$

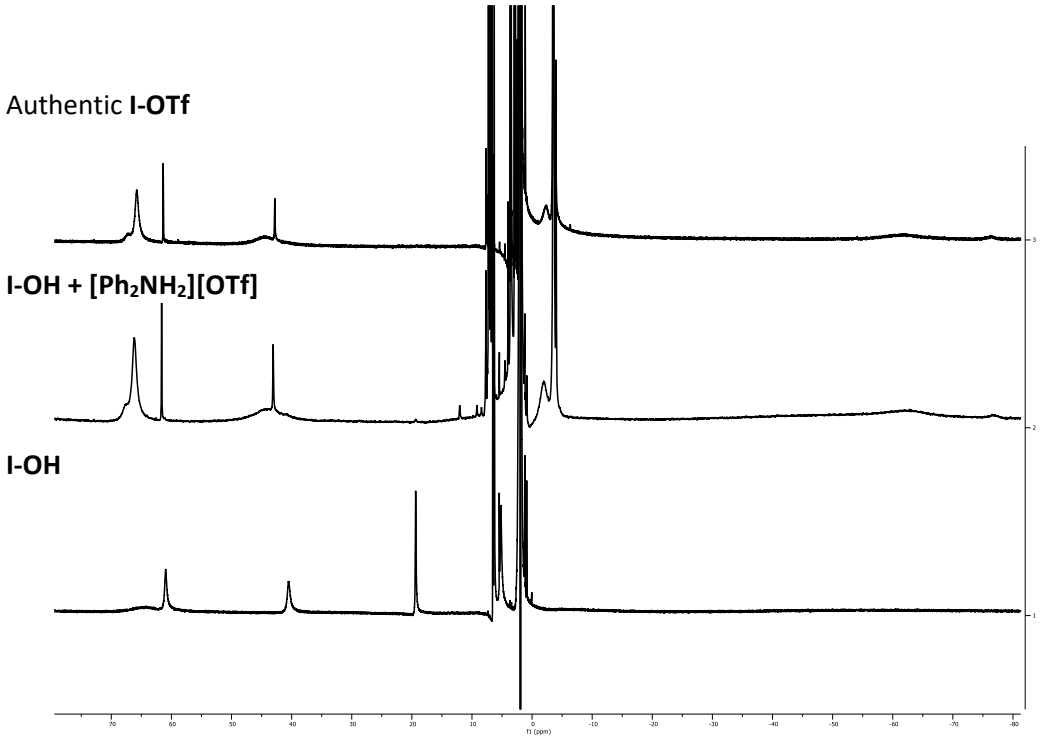

Supplementary Figure 51: Stacked ^{1}H NMR (400 MHz, MeCN, 25 °C) spectra of **I-OH**, its reaction with $[Ph_2NH_2][OTf]$, and an authentic sample of **I-OTf**.

Weaker acids such as $PhNH_3^+$, 2,4,6-Me_3PyH^+, or NEt_3H^+ afforded no conversion of **VI** to **I-OTf**.

Optimization Studies for Catalytic NO_3^- Reduction Using 1,2-diphenylhydrazine as a H^+/e^- Source

Representative Procedure for Optimization Using 1,2-diphenylhydrazine ($Ph_2N_2H_2$): Inside a glove box, a 10 mL Teflon-capped Schlenk tube was charged with $[Bu_4N][NO_3]$ (12.2 mg, 0.04 mmol, 1.0 equiv.), $Ph_2N_2H_2$ (7.4 mg, 0.04 mmol, 1.0 equiv.), and catalyst **I-OTf** (7.3 mg, 0.008 mmol) in 1 mL MeCN. The tube was sealed with a Teflon cap and moved out of the glovebox, and it was heated in a pre-heated oil bath at 80 °C. After 18 h, the reaction was stopped and cooled to room temperature. The reaction mixture was transferred to a pipette filter packed with silica gel (ca. 3 cm height) and the residual reaction mixture was washed/transferred using CH_2Cl_2 (3 x 2 mL), passed through the silica plug into a scintillation vial containing 1,3,5-trimethoxybenzene (6.7 mg, 0.04 mmol, 1.0 equiv) internal standard, and then the solvent was evaporated in vacuo. The yield of the oxidized product, azobenzene (Ph_2N_2) was determined using ^{1}H q-NMR (quantitative NMR) of the resulting crude reaction mixture (no. of scans = 8, relaxation delay = 25 sec, pulse width = 90, ^{13}C decoupling ON) which showed the formation of Ph_2N_2 in 38% yield (Figure 4c, entry 2 in the manuscript).

Supplementary Table 3: Additional optimization of oxidation of 1,2-diphenylhydrazine ($Ph_2N_2H_2$):[a]

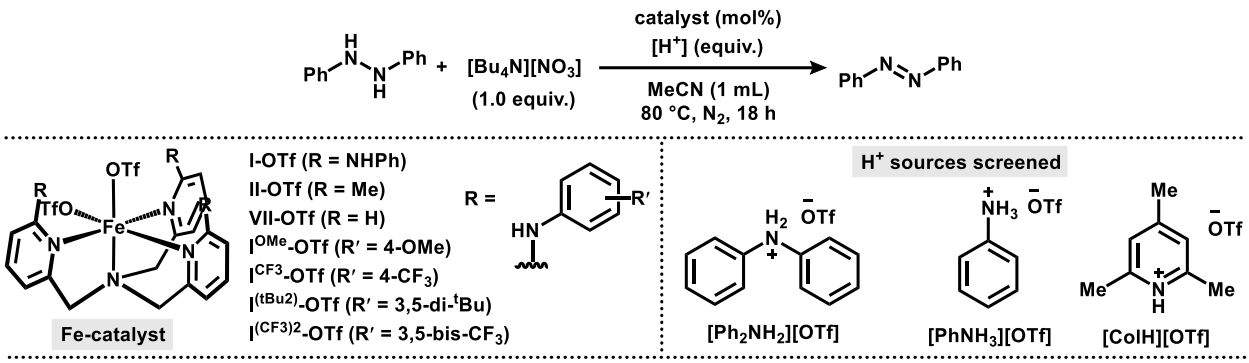

entry	catalyst (mol%)	$Ph_2N_2H_2$ (equiv.)	[H⁺] (equiv.)	yield of Ph_2N_2 (%)[b]
1	**I-OTf** (10)	1.0	$[Ph_2NH_2][OTf]$ (1.0)	63
2	**I-OTf** (10)	1.0	$[PhNH_3][OTf]$ (1.0)	91
3	-	1.0	$[Ph_2NH_2][OTf]$ (1.0)	23
4	-	1.0	$[PhNH_3][OTf]$ (1.0)	46
5	-	1.0	[ColH][OTf] (1.0)	2
6	**I-OTf** (1)	1.5	[ColH][OTf] (2.0)	73
7[c]	**I-OTf** (1)	1.5	[ColH][OTf] (3.0)	2
8[d]	**I-OTf** (1)	1.5	[ColH][OTf] (3.0)	2
9	**I-OTf** (0.015)	1.5	[ColH][OTf] (3.0)	2
10[e]	**$Fe(OTf)_2$** (1)	1.5	[ColH][OTf] (3.0)	85
11	**$Fe(OTf)_2$** (1)	1.5	[ColH][OTf] (3.0)	8
12[f]	**I^{CF3}-OTf** (0.15)	1.5	[ColH][OTf] (3.0)	12 ± 1

[a]Reaction conditions: $[Bu_4N][NO_3]$ (0.04 mmol, 1.0 equiv.), $Ph_2N_2H_2$ (equiv.), catalyst (mol%), [H⁺] (equiv), solvent (mL), 80 °C, N_2, 18 h. [b]^{1}H NMR yield using 1,3,5-trimethoxybenzene (same equiv. as $Ph_2N_2H_2$) as internal standard. [c]$[Bu_4N][NO_3]$ was not used. [d]reaction was run at 25 °C. [e]L^H (1 mol%) was used. Purity of catalyst **I-OTf** lies in the range of 92% to >99% (mixture of $[Fe(OTf)_2L^H]$ + $[Fe(OTf)(MeCN)(TPA^{NHPh})][OTf]$). [f]average yields with standard deviations after triplicate results.

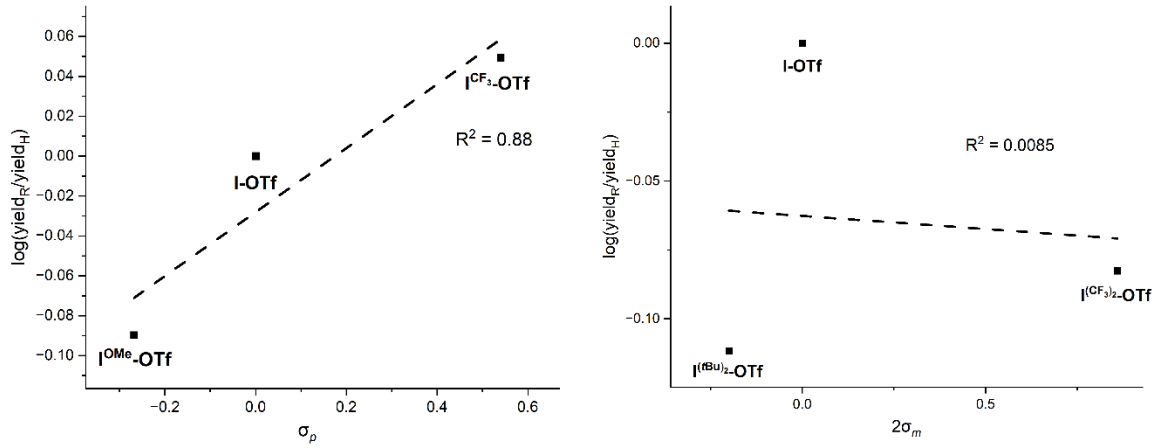

Supplementary Figure 52: Left: Hammett correlation for azobenzene yields across *para*-substituted catalyst variants. Right: Hammett correlation for azobenzene yields across 3,5-di-*meta*-substituted catalyst variants.

The modest correlation between Ph_2N_2 yields and σ_p parameters for *para*-substituted catalyst variants suggest that stronger hydrogen bond donors and more electrophilic Fe centers aid the reaction by 1) further polarizing the N–O bonds, and 2) anodically shifting the reduction potential of Fe(III) species. The absence of correlation between 3,5-di *meta*-substituted catalysts suggest that the larger steric profiles of **$I^{(CF3)2}$-OTf** an **I^{tBu2}-OTf** inhibit the reaction.

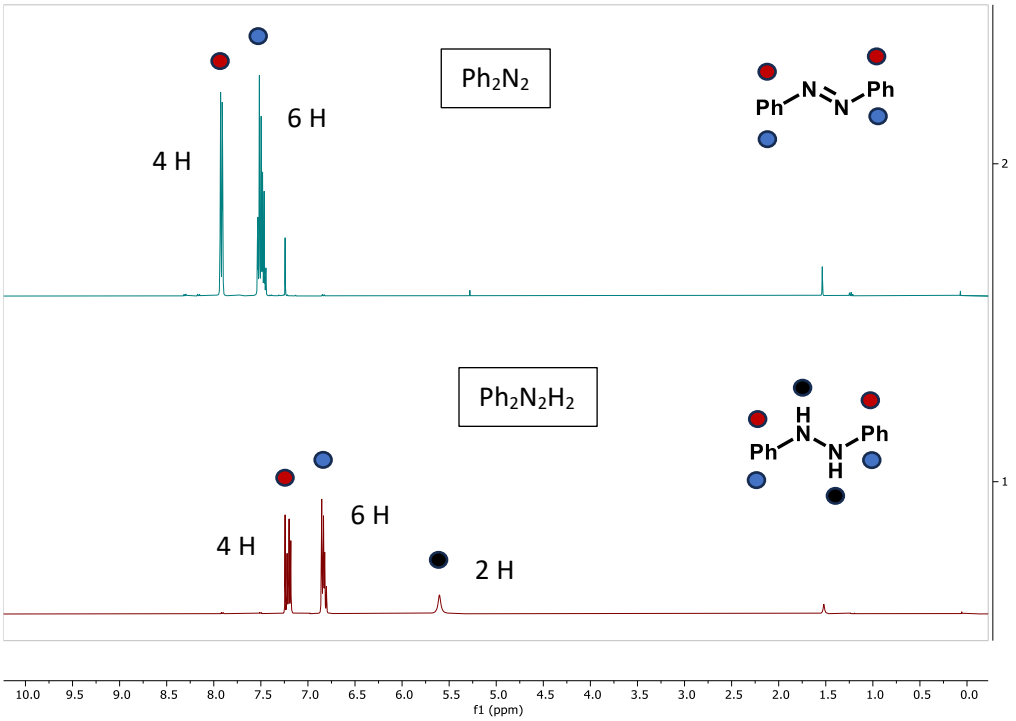

Supplementary Figure 53: Stacked ^{1}H NMR spectra (400 MHz, $CDCl_3$, 25 °C) of $Ph_2N_2H_2$ and Ph_2N_2.

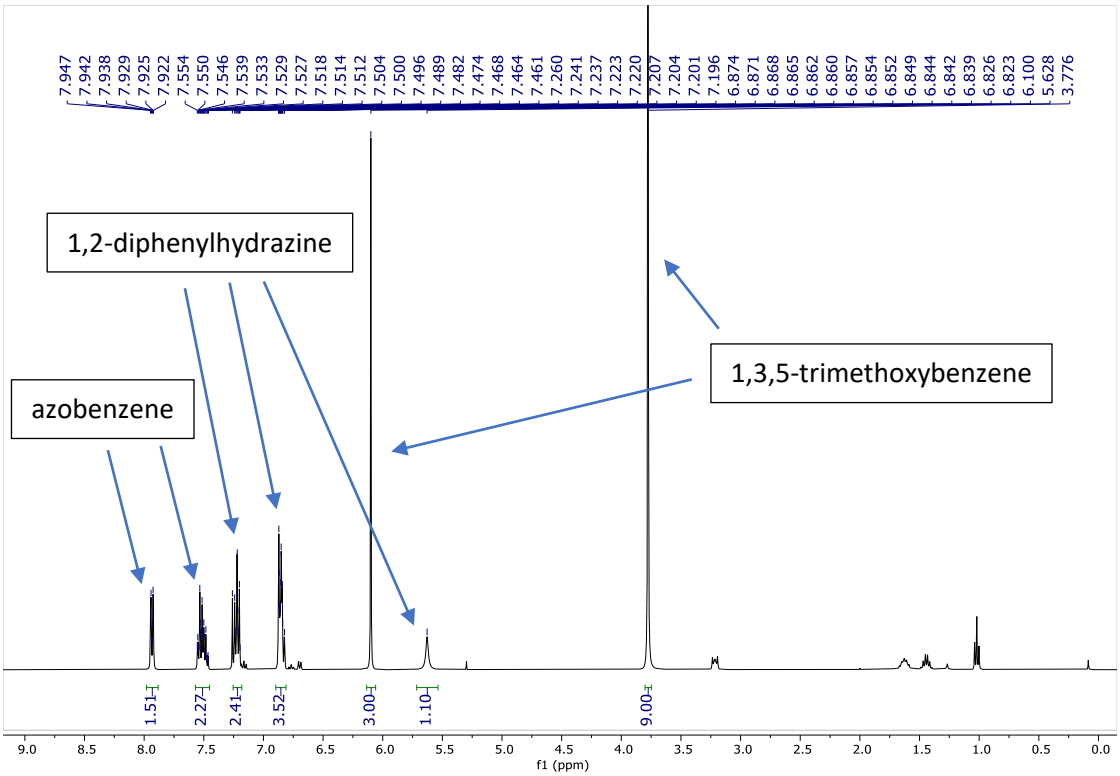

Supplementary Figure 54: ^{1}H q-NMR spectrum (400 MHz, $CDCl_3$, 25 °C) of crude reaction mixture corresponding to the experiment depicted in Figure 4c, entry 2 (main text).

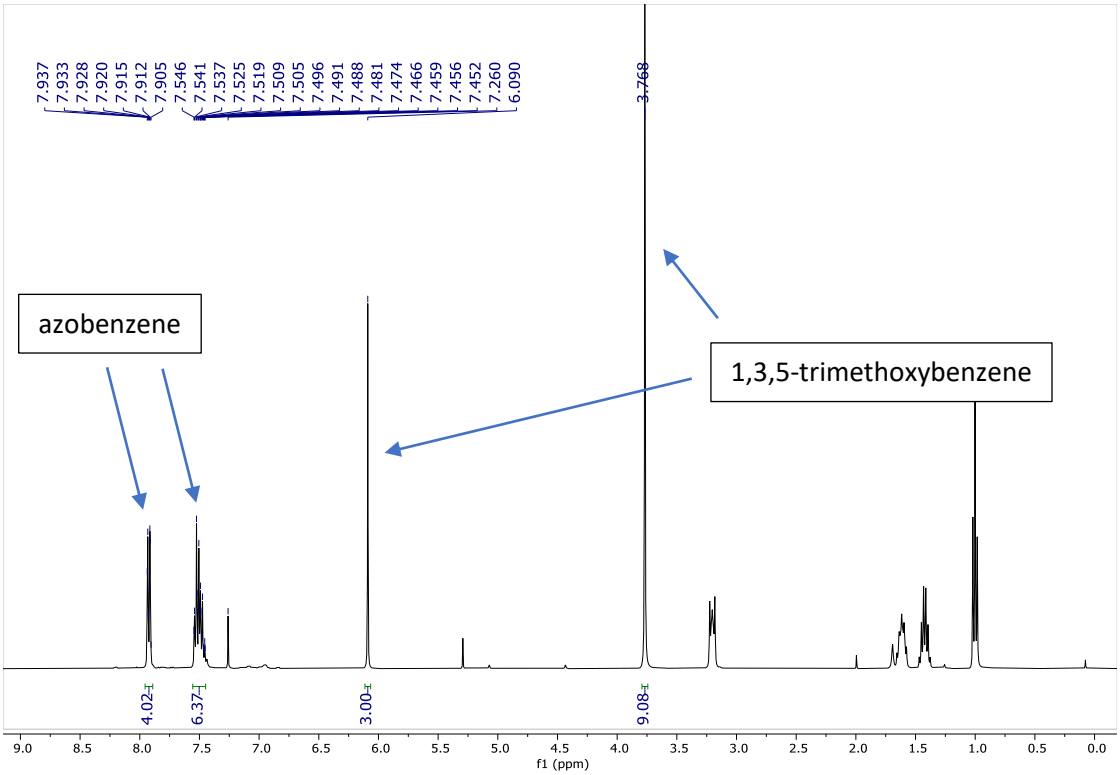

Supplementary Figure 55: ^{1}H q-NMR spectrum (400 MHz, $CDCl_3$, 25 °C) of crude reaction mixture corresponding to the experiment depicted in Figure 4c, entry 3 (main text).

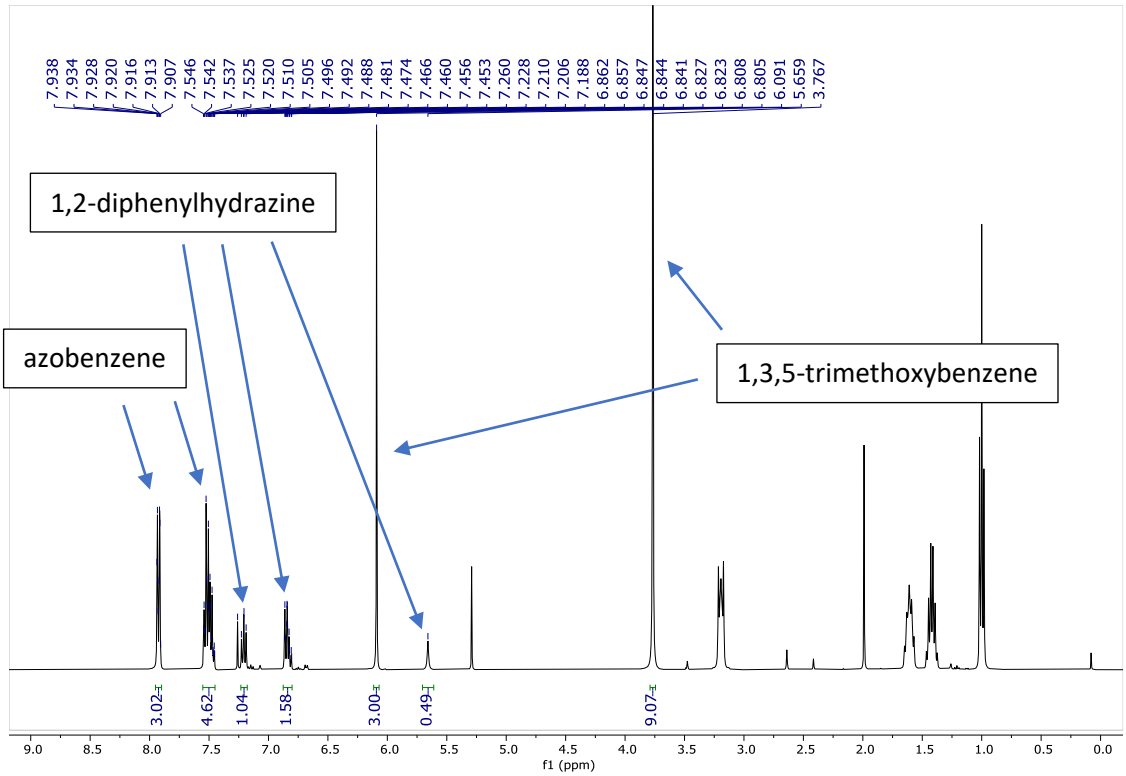

Supplementary Figure 56: ^{1}H q-NMR spectrum (400 MHz, $CDCl_3$, 25 °C) of crude reaction mixture corresponding to the experiment depicted in Table 1, entry 2 (main text).

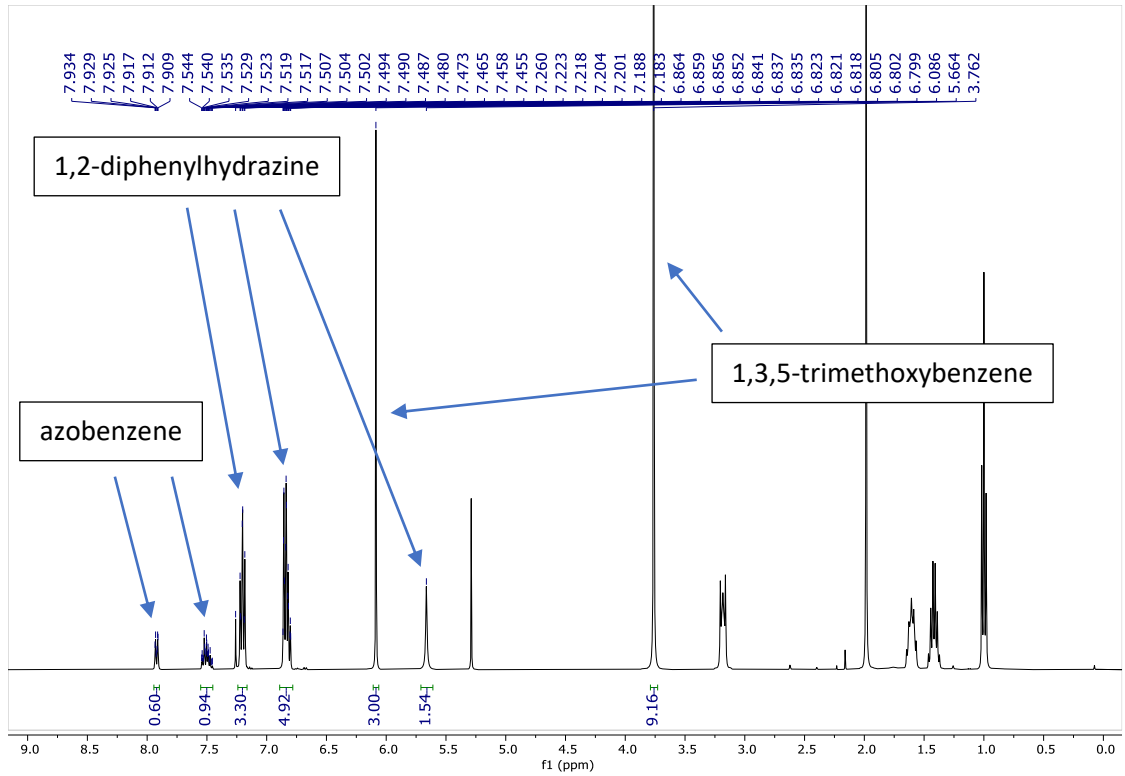

Supplementary Figure 57: ^{1}H q-NMR spectrum (400 MHz, $CDCl_3$, 25 °C) of crude reaction mixture corresponding to the experiment depicted in Table 1, entry 4 (main text).

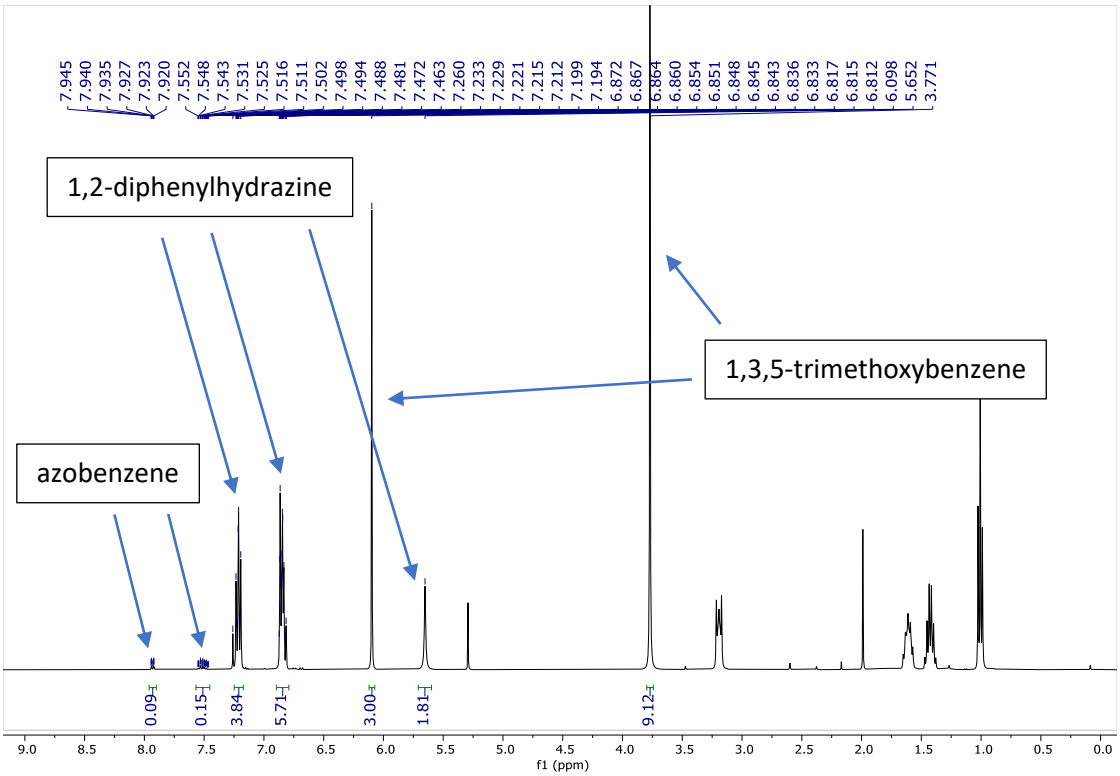

Supplementary Figure 58: ^{1}H q-NMR spectrum (400 MHz, $CDCl_3$, 25 °C) of crude reaction mixture corresponding to the experiment depicted in Table 1, entry 5 (main text).

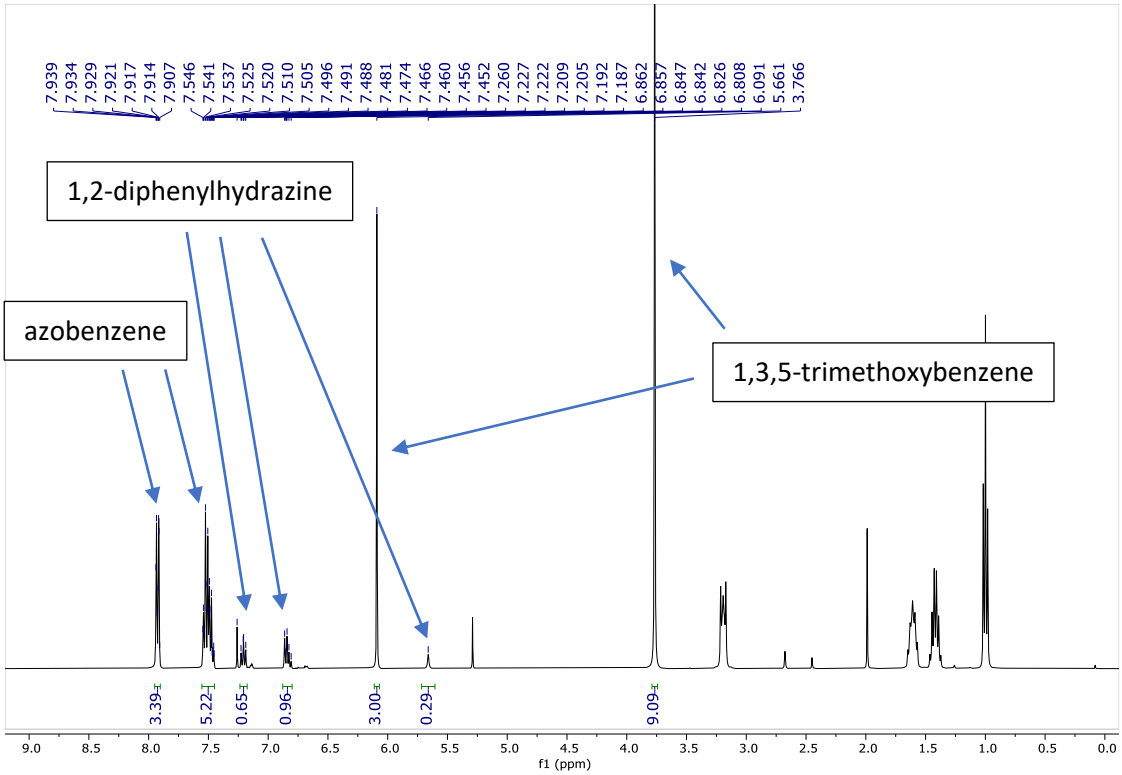

Supplementary Figure 59: ^{1}H q-NMR spectrum (400 MHz, $CDCl_3$, 25 °C) of crude reaction mixture corresponding to the experiment depicted in Table 1, entry 10 (main text).

Representative Procedure for Gas-phase IR Studies of Thermal Catalytic Reaction with $Ph_2N_2H_2$: Inside a glove box, a J-young NMR tube was charged with $[Bu_4N][^{14}NO_3]$ (12.2 mg, 0.04 mmol, 1.0 equiv.), $Ph_2N_2H_2$ (7.4 mg, 0.04 mmol, 1.0 equiv.), [ColH][OTf] (10.9 mg, 0.04 mmol) and catalyst **I-OTf** (3.7 mg, 0.004 mmol) in 1 mL MeCN (experiment in Figure 4c, entry 3 in the main text). The tube was sealed with a Teflon cap and moved out of the glovebox, and it was kept in a pre-heated heating block set at 80 °C. After 18 h, the reaction was stopped and cooled to room temperature. Then the NMR tube was frozen, and the volatiles of the reaction mixture were vacuum transferred to a gas-phase IR cell. After collecting a background infrared spectrum of the IR cell under vacuo, the infrared spectrum of the IR cell containing the reaction volatiles was collected with 32 scans which showed the characteristic P, Q, and R bands corresponding to ^{14}NO (g) at 1845, 1875, and 1902 cm^{-1}.

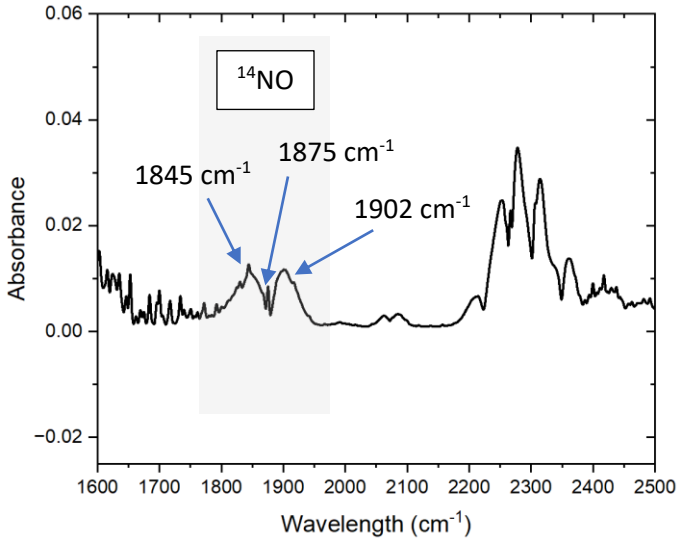

Supplementary Figure 60: FT-IR (gas-phase) of reaction corresponding to the experiment depicted in Figure 4c, entry 3 (main text) using $[Bu_4N][^{14}NO_3]$.

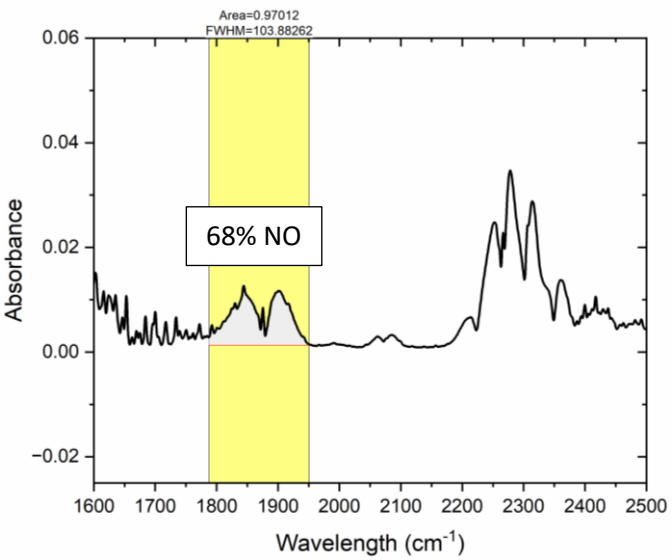

Supplementary Figure 61: Integrated gas-phase IR spectrum of the headspace from the reaction corresponding to Figure 4c, entry 3 of the main text.

The concentration of NO(g) was determined to be 0.025 mM in the 95 mL IR-cell ($\varepsilon \bullet l$ = 137 $cm^{-2}atm^{-1}$)[25], corresponding to 0.028 mmol of NO(g) (68% yield).[26]

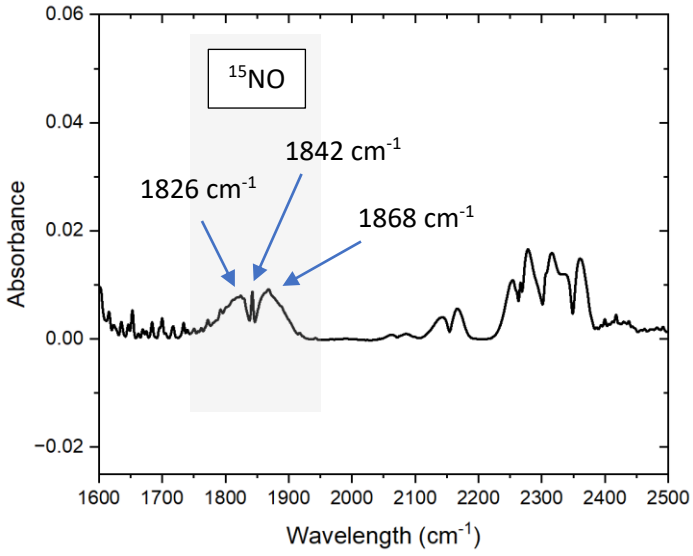

Supplementary Figure 62: FT-IR (gas-phase) of the headspace reaction corresponding to the experiment depicted in Figure 4c, entry 3 (main text) using $[Bu_4N][^{15}NO_3]$.

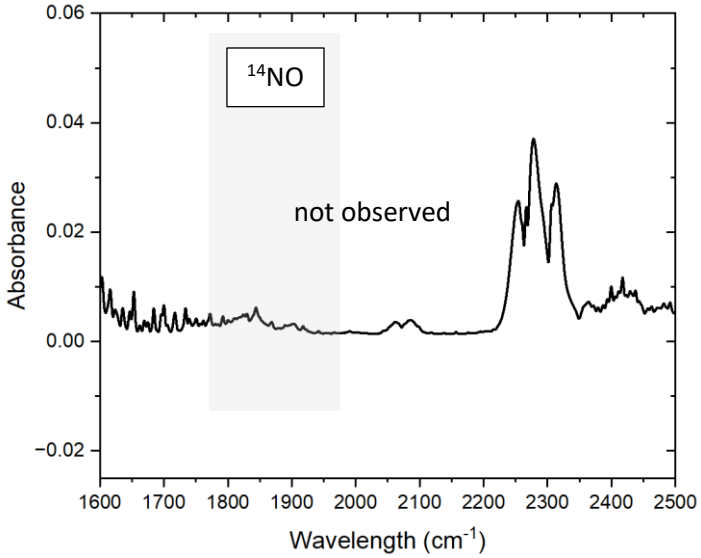

Supplementary Figure 63: FT-IR (gas-phase) of the headspace of the reaction corresponding to the experiment depicted in Supplementary **Error! Reference source not found.**, entry 5 using $[Bu_4N][^{14}NO_3]$.

Co(TPP) to Co(TPP)(NO) Trapping Experiments and Validation with $Ph_2N_2H_2$ to Ph_2N_2 Conversion

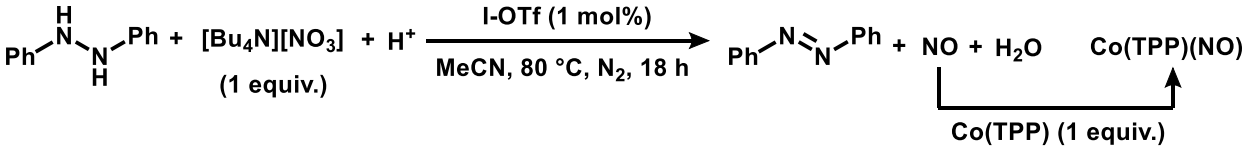

Representative Procedure for NO quantification using Co(TPP) Trapping: Inside a glove box, a Teflon-capped H-bridge setup was charged with $[Bu_4N][NO_3]$ (12.2 mg, 0.04 mmol, 1.0 equiv.), $Ph_2N_2H_2$ (7.4 mg, 0.04 mmol, 1.0 equiv.), [ColH][OTf] (10.9 mg, 0.12 mmol), and catalyst **I-OTf** (7.3 mg, 0.008 mmol) in 1 mL CH_3CN on one flask (side-1). The other flask was charged with Co(TPP) (26.9 mg, 0.04 mmol, 1.0 equiv) in 20 mL CH_2Cl_2 (side-2). The Teflon keys were sealed and moved out of the glovebox. The side-1 was heated and stirred in a pre-heated oil bath at 80 °C and the side-2 was kept stirring at room temperature (~25 °C). Teflon keys on both the sides were opened keeping the third (middle) Teflon key closed for flow of any evolved gas (from side-1 to side-2) during the reaction. After 18 h, the reaction was stopped and cooled to room temperature. An aliquot of the reaction mixture from side-2 was taken for ^{1}H NMR analysis that showed 68% yield of Co(TPP)(NO) product, corresponding to 68% NO(g) generation. This result was in good agreement with the maximum amount of NO generation that was possible from the corresponding observed yield of azobenzene (>99%) for this experimental condition (Figure 4c, entry 3 in the main text).

Photos of the glassware setup used in this operation are presented above in Supplementary **Error! Reference source not found.**29.

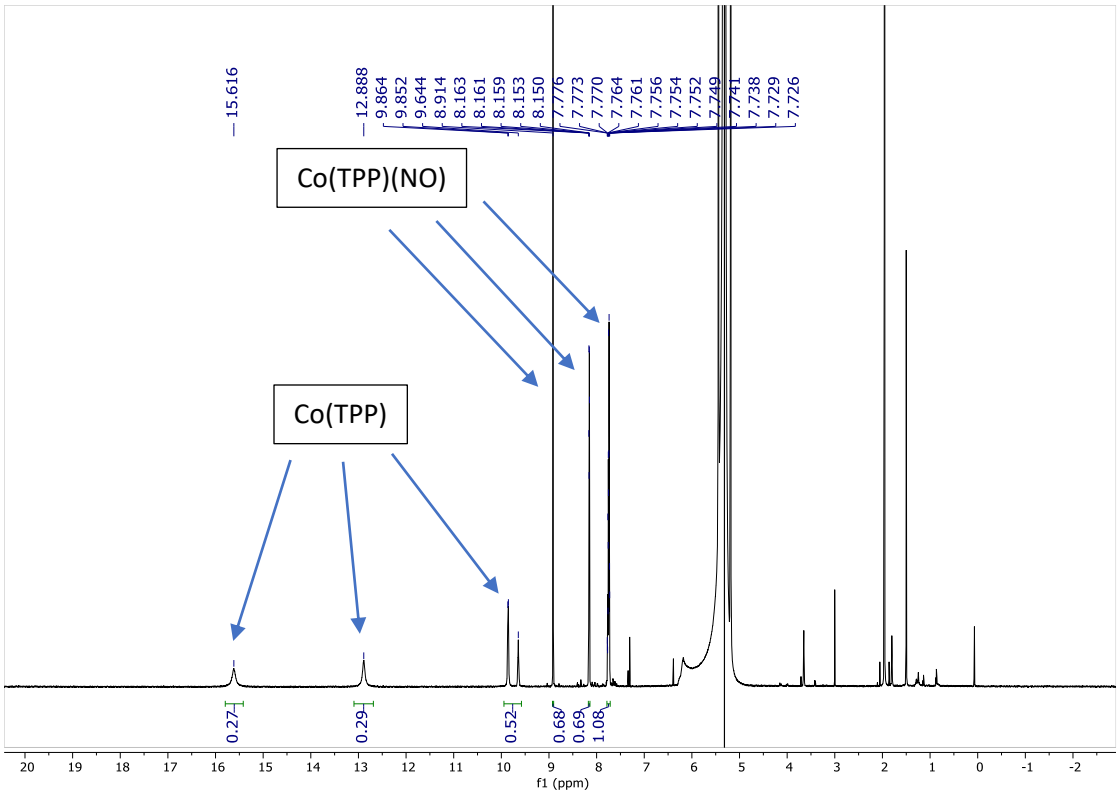

Supplementary Figure 64: ^{1}H NMR spectrum (400 MHz, CH_2Cl_2, 25 °C) of crude reaction mixture (side-2) corresponding to the experiment depicted in Figure 4c, entry 3 (main text).

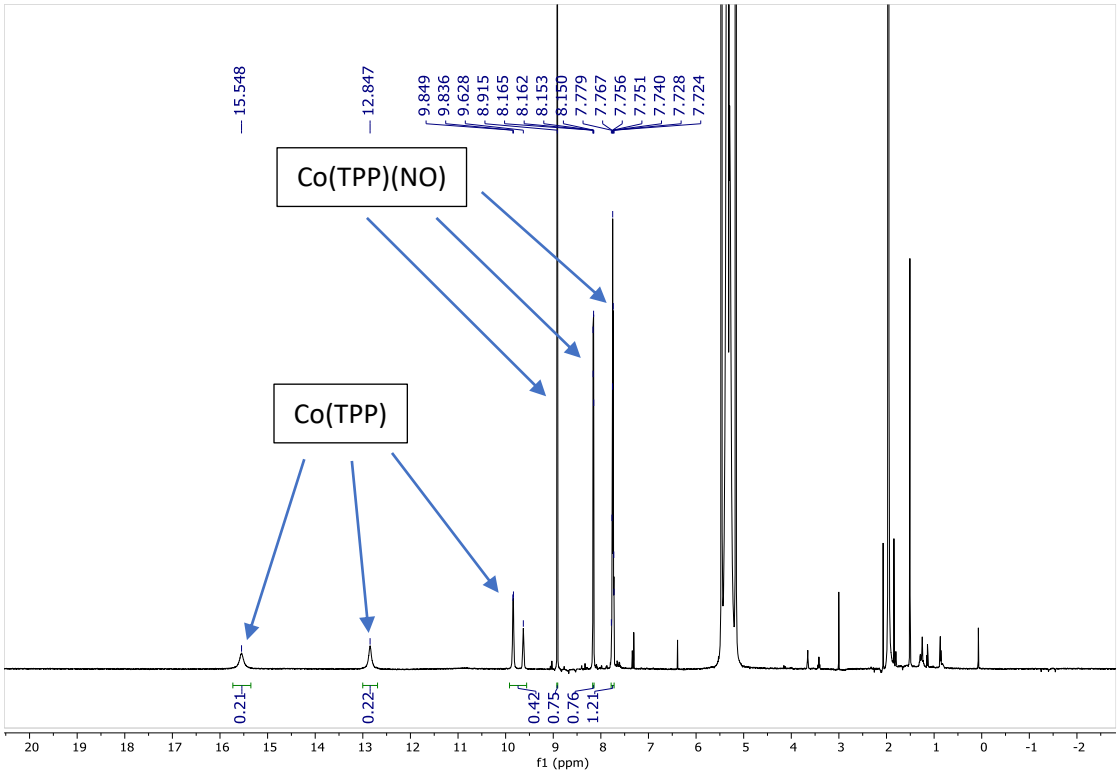

Supplementary Figure 65: ^{1}H NMR spectrum (400 MHz, CH_2Cl_2, 25 °C) of crude reaction mixture (side-2) corresponding to the experiment depicted in Table 1, entry 2 (main text).

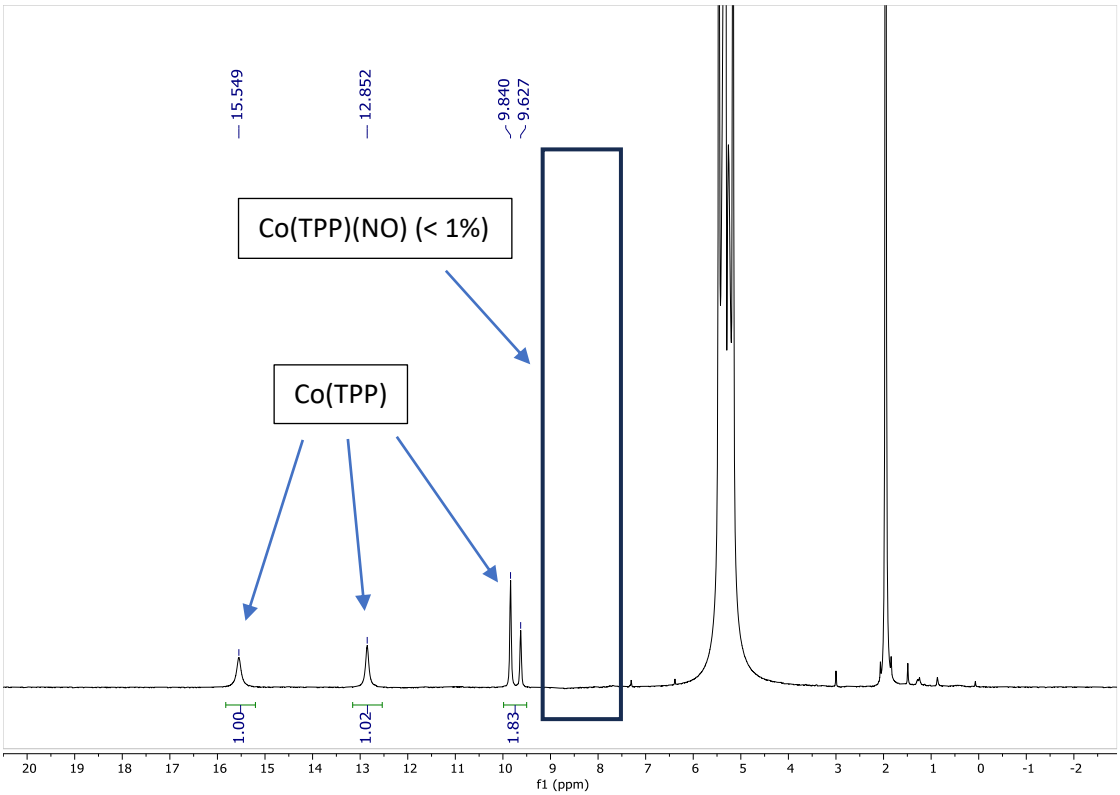

Supplementary Figure 66: ^{1}H NMR spectrum (400 MHz, CH_2Cl_2, 25 °C) of crude reaction mixture (side-2) corresponding to the experiment depicted in Table 1, entry 5 (main text).

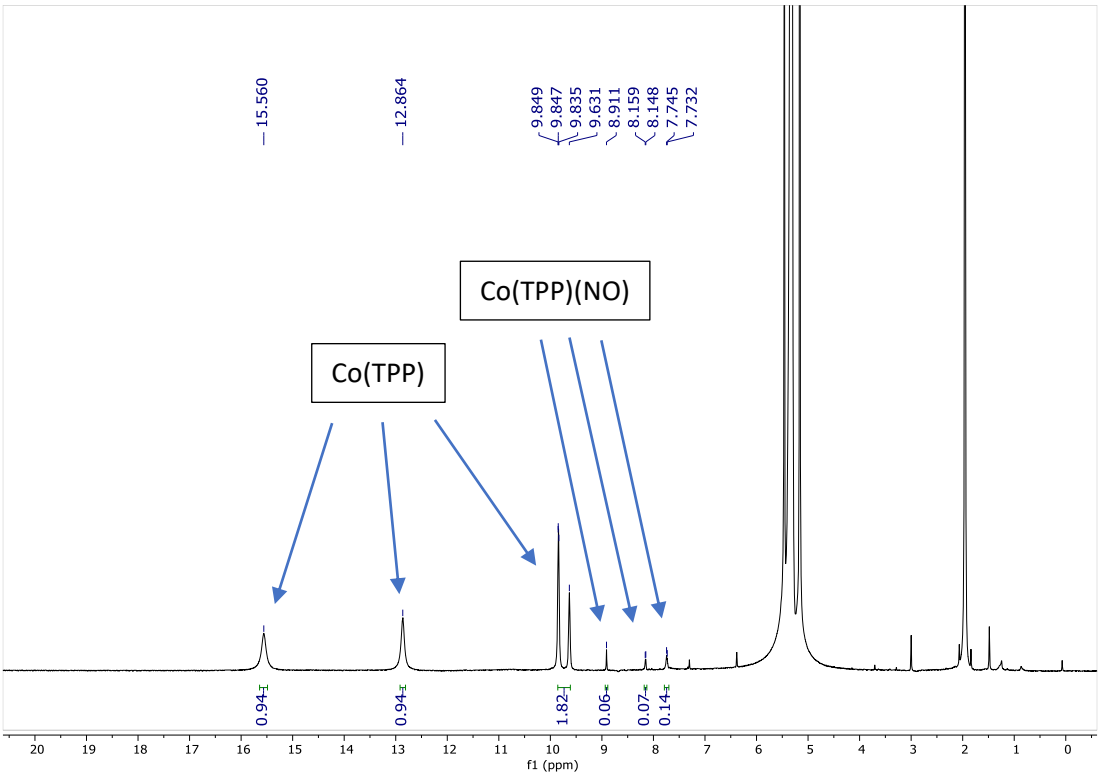

Supplementary Figure 67: ^{1}H NMR spectrum (400 MHz, CH_2Cl_2, 25 °C) of crude reaction mixture (side-2) corresponding to the experiment depicted in Table 1, entry 4 (main text).

As an alternative, we performed additional validation using the Co(TPP) trapping technique for Table 1, entry 4 using an H-bridge setup. We observed a lower value of 6% Co(TPP)(NO) in comparison to 13-17% Ph_2N_2 formation for the same reaction. At this lower scale, the Co(TPP)(NO) trapping is not quantitative, a result we attribute to mass transport issues of low NO quantities (~ 0.15 mL).

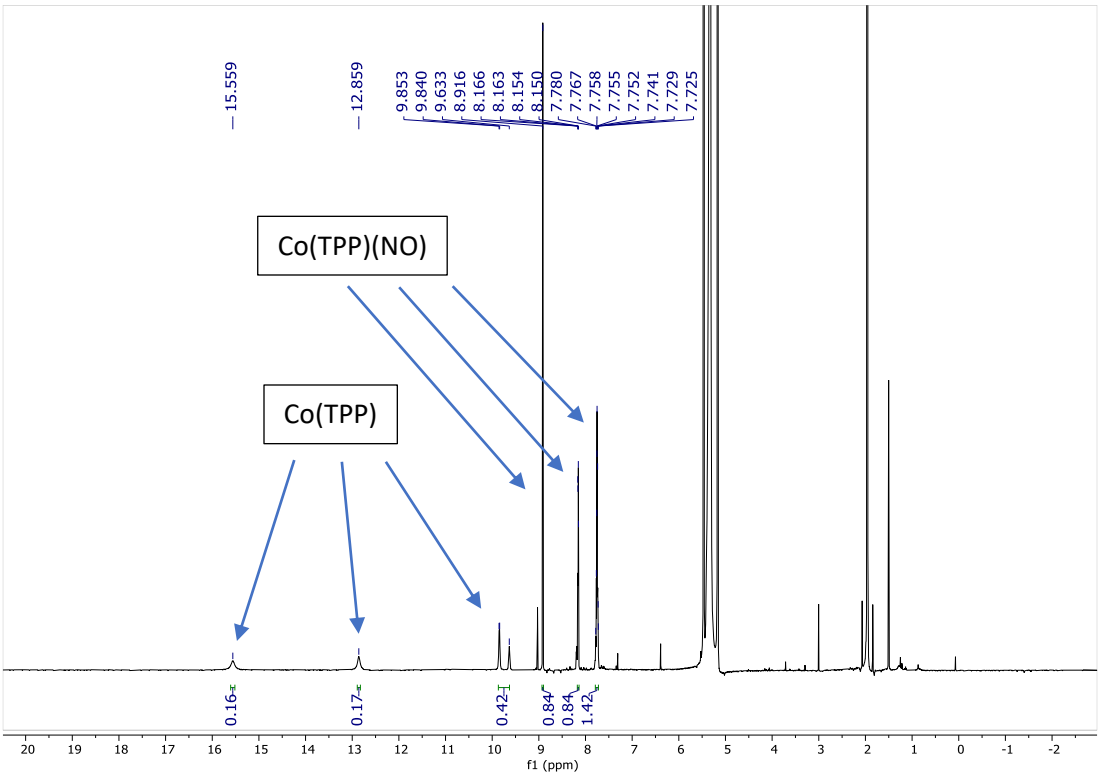

Supplementary Figure 68: ^{1}H NMR spectrum (400 MHz, CH_2Cl_2, 25 °C) of crude reaction mixture (side-2) corresponding to the experiment depicted in Table 1, entry 11 (main text)**.**

Validation of Co(TPP)(NO) Yields with Ph_2N_2 Yields for $TON_{NO3-/NO}$ Calculation

balanced chemical reaction

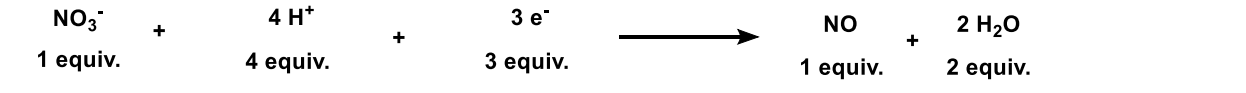

conditions used in figure 4c, entry 3 of main text

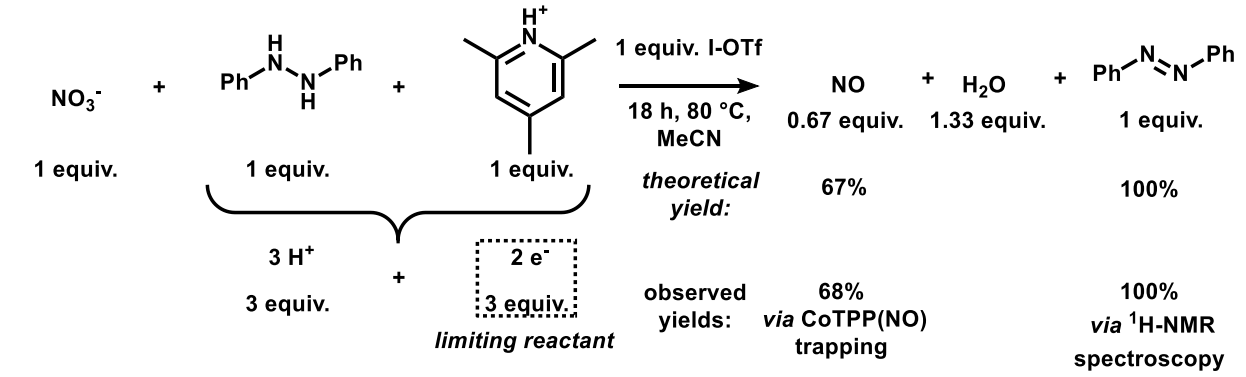

conditions used in table 1, entry 2 of main text

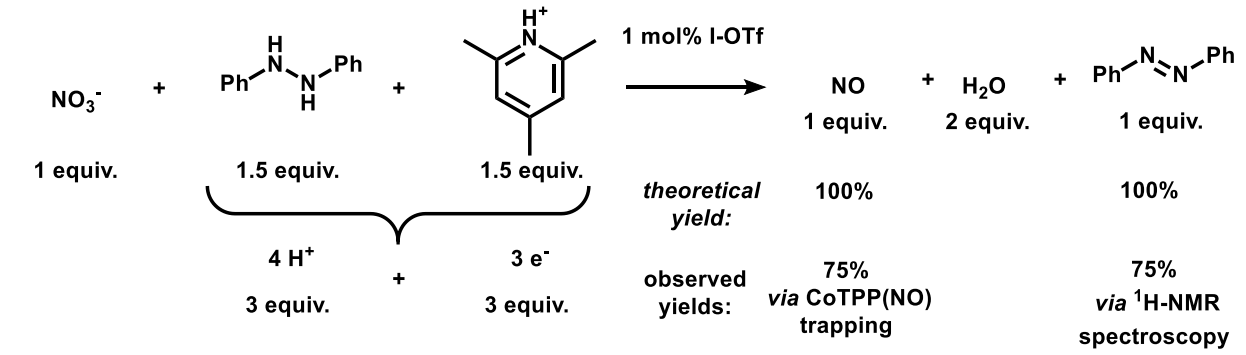

conditions used in table 1, entry 5 of main text

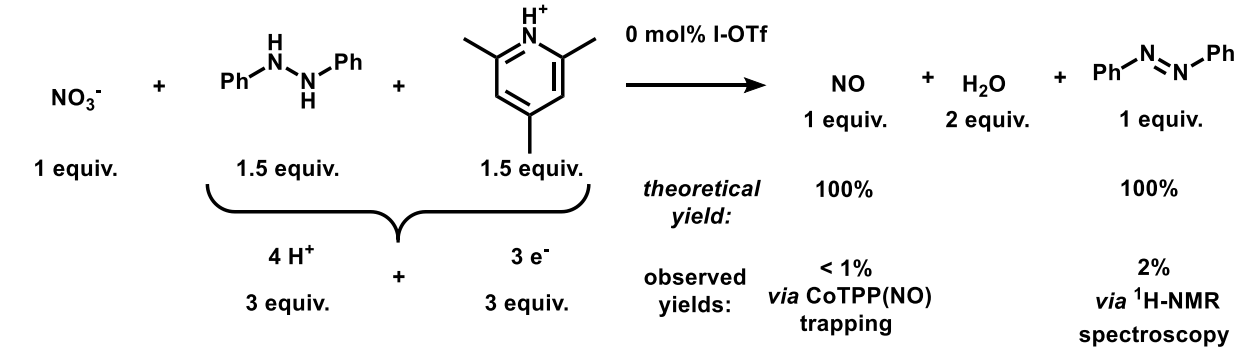

We observed >99% yield of azobenzene and observed 68% yield of Co(TPP)(NO) in a separate CoTPP trapping experiment using the conditions in entry 3 of Figure 4c (main text), consistent with the theoretical yields. Similarly, in entry 2 of Table 1 (main text), we observed 75% yield of Ph_2N_2 and 75% yield of Co(TPP)(NO) – equimolar amounts, consistent with the theoretical yields. In the absence of **I-OTf**, we observe minimal background reactivity, affording 2% Ph_2N_2 and <1% Co(TPP)(NO).

Based on these results we calculated $TON_{NO3-/NO}$ for NO_3^- to NO was based off yields of Ph_2N_2 observed in the catalytic optimization experiments as a surrogate for determining NO yields from all entries.

Optimization Studies for Catalytic NO_3^- Reduction Using Hantzsch Ester as a H^+/e^- Source

Representative Procedure for Optimization Using Hantzsch ester (HEH_2): Inside a glove box, a 10 mL Teflon-capped Schlenk tube was charged with $[Bu_4N][NO_3]$ (12.2 mg, 0.04 mmol, 1.0 equiv.), HEH_2 (10.1 mg, 0.04 mmol, 1.0 equiv.), and catalyst **I-OTf** (7.3 mg, 0.008 mmol) in 1 mL MeCN. The tube was sealed with a Teflon cap and moved out of the glovebox, and it was stirred in a pre-set oil bath at 25 °C. The reaction was stirred and irradiated with a 390 nm Kessil LED lamp at ~4-5 cm distance from the tube. After 18 h, the reaction was stopped and cooled to room temperature. The reaction mixture was transferred to a pipette filter packed with silica gel (ca. 3 cm height) and the residual reaction mixture was washed/transferred using CH_2Cl_2 (3 x 2 mL), passed through the silica plug into a scintillation vial containing 1,3,5-trimethoxybenzene (6.7 mg, 0.04 mmol, 1.0 equiv) internal standard, and then the solvent was evaporated in vacuo. The yield of the oxidized product, diethyl 2,6-dimethylpyridine-3,5-dicarboxylate (HE) was determined using ^1H q-NMR (quantitative NMR) of the resulting crude reaction mixture (no. of scans = 8, relaxation delay = 25 sec, pulse width = 90, ^{13}C decoupling ON), which showed the formation of HE in 47% yield (Supplementary Table 4, entry 1).

Supplementary Table 4: Additional optimization of oxidation of Hantzsch ester (HEH_2):[a]

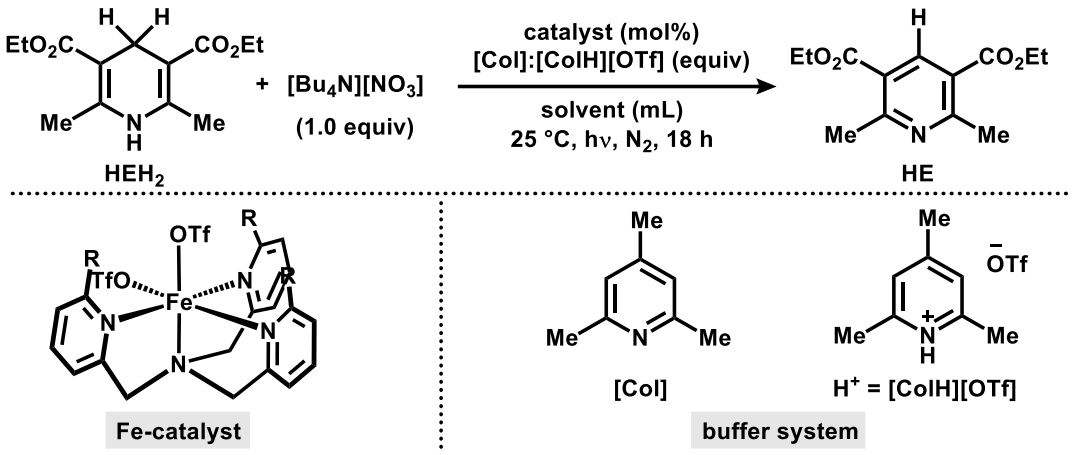

entry	catalyst (mol%)	HEH_2 (equiv.)	[Col]:[ColH][OTf] (equiv.)	solvent (mL)	light wavelength (nm)	yield of HE (%)[b]
1	**I-OTf** (20)	1.0	-	MeCN (1)	390	47
2	**I-OTf** (20)	1.0	-	EtCN (1)	390	74
3	**I-OTf** (20)	1.0	-	THF (1)	390	80
4	**I-OTf** (20)	1.0	-	PhF (1)	390	nd
5	**I-OTf** (20)	1.0	-	CH_2Cl_2 (1)	390	nd
6	**I-OTf** (20)	1.0	-	THF (0.4)	390	98
7	**I-OTf** (10)	1.0	-	THF (0.4)	390	58

8	**I-OTf** (2.5)	1.0	-	THF (0.4)	390	42
9	**I-OTf** (2.5)	1.0	-	THF (0.4)	427	83
10	**I-OTf** (2.5)	1.0	-	THF (0.4)	440	64
11[c]	**I-OTf** (2.5)	2.0	-	THF (0.8)	427	62 ± 2
12	**I^{OMe}-OTf** (2.5)	2.0	-	THF (0.8)	427	12
13	**I^{CF3}-OTf** (2.5)	2.0	-	THF (0.8)	427	83
14	**I^{tBu2}-OTf** (2.5)	2.0	-	THF (0.8)	427	66
15	**$I^{(CF3)2}$-OTf** (2.5)	2.0	-	THF (0.8)	427	31
16	**II-OTf** (2.5)	2.0	-	THF (0.8)	427	49
17	**VII-OTf** (2.5)	2.0	-	THF (0.8)	427	56
18[d]	**I-OTf** (2.5)	4.0	1:1 (3.0 equiv)	THF (1.2)	427	25
19	**I-OTf** (2.5)	4.0	-	THF (1.2)	427	49
20	**I-OTf** (2.5)	4.0	1:1 (3.0 equiv)	THF (1.2)	-	3
21	**$Fe(OTf)_2$** (2.5)	4.0	1:1 (3.0 equiv)	THF (1.2)	427	56
22[e]	**$Fe(OTf)_2$** (2.5)	4.0	1:1 (3.0 equiv)	THF (1.2)	427	81
23[f]	**II-OTf** (2.5)	4.0	1:1 (3.0 equiv)	THF (1.2)	427	89
24[f]	**VII-OTf** (2.5)	4.0	1:1 (3.0 equiv)	THF (1.2)	427	88
25[f]	**I-OTf** (0.1)	4.0	1:1 (3.0 equiv)	THF (1.2)	427	39 ± 3
26[f]	**I-OTf** (0.01)	4.0	1:1 (3.0 equiv)	THF (1.2)	427	38 ± 2
27[f]	**I^{CF3}-OTf** (2.5)	4.0	1:1 (3.0 equiv)	THF (1.2)	427	90
28[f]	**I^{CF3}-OTf** (1.0)	4.0	1:1 (3.0 equiv)	THF (1.2)	427	77
29[f]	**I^{CF3}-OTf** (0.1)	4.0	1:1 (3.0 equiv)	THF (1.2)	427	41
30[f]	**I^{CF3}-OTf** (0.01)	4.0	1:1 (3.0 equiv)	THF (1.2)	427	39

[a]Reaction conditions: $[Bu_4N][NO_3]$ (0.04 mmol, 1.0 equiv.), HEH_2 (equiv.), catalyst (mol%), [Col]:[ColH][OTf] (equiv), solvent (mL), 25 °C, N_2, Kessil lamp, 18 h. [b]^{1}H NMR yield using 1,3,5-trimethoxybenzene (same equiv. as HEH_2) as internal standard. [c]average yields with standard deviation after triplicate results. [d]$[Bu_4N][NO_3]$ was not used. [e]L^H (2.5 mol%) was used. [f]stock solution of the catalyst (5 mg in 2 mL THF) was prepared and diluted accordingly before usage using a 500 µL or 50 µL Hamilton syringe for catalytic experiments. Purity of catalyst **I-OTf** lies in the range of 92% to >99% (mixture of $[Fe(OTf)_2L^H]$ + $[Fe(OTf)(MeCN)(TPA^{NHPh})][OTf]$). Temperature of the oil bath reaches ~40 °C over the duration of the reactions under light irradiation. nd = not detected.

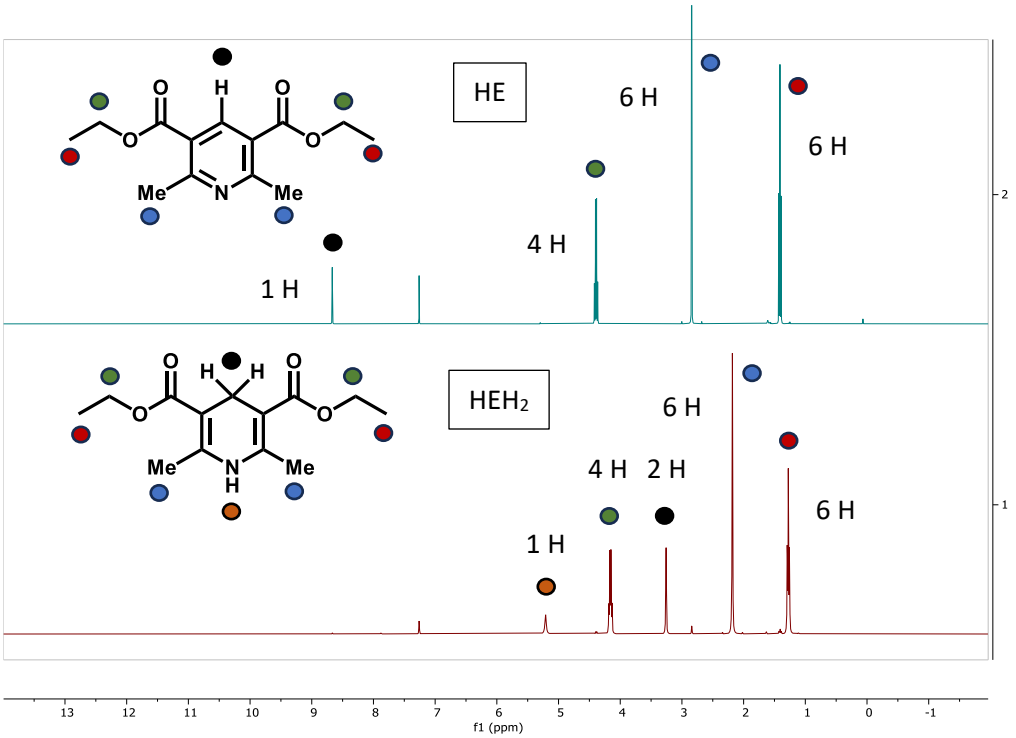

Supplementary Figure 69: Stacked ^{1}H NMR spectra (400 MHz, $CDCl_3$, 25 °C) of HEH_2 and HE.

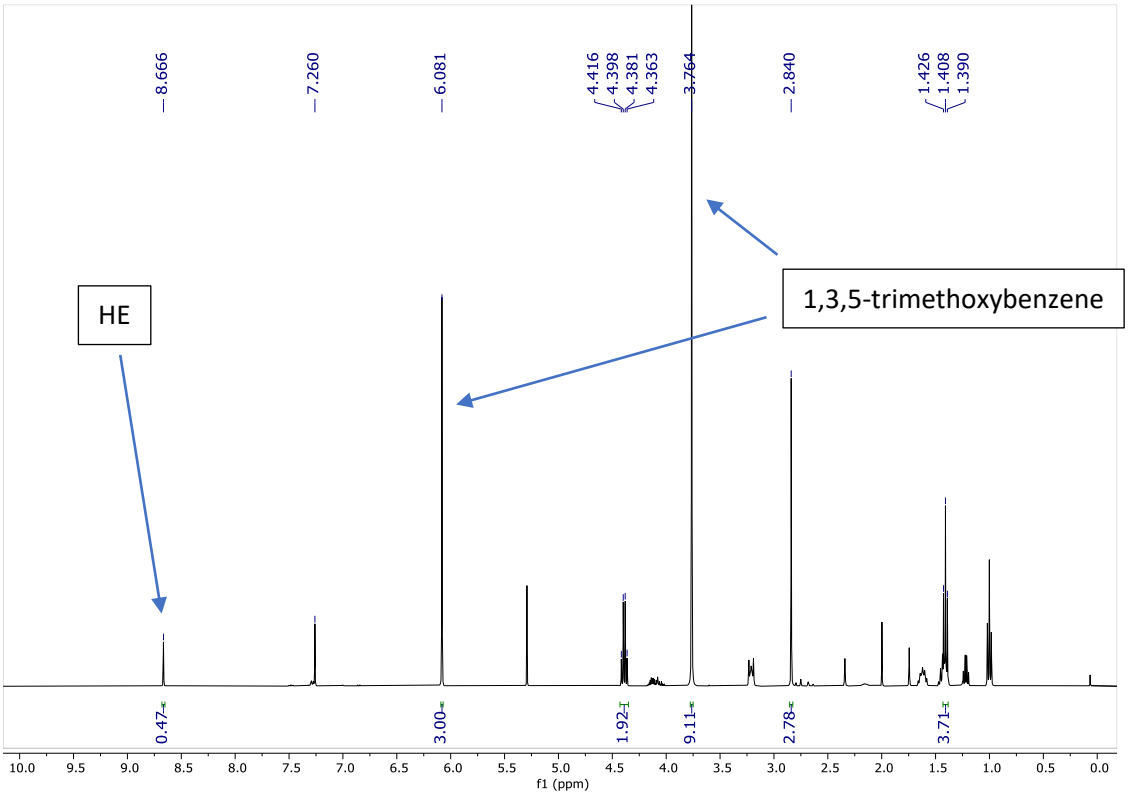

Supplementary Figure 70: ^{1}H q-NMR spectrum (400 MHz, $CDCl_3$, 25 °C) of crude reaction mixture corresponding to the experiment depicted in Supplementary Table 4, entry 1.

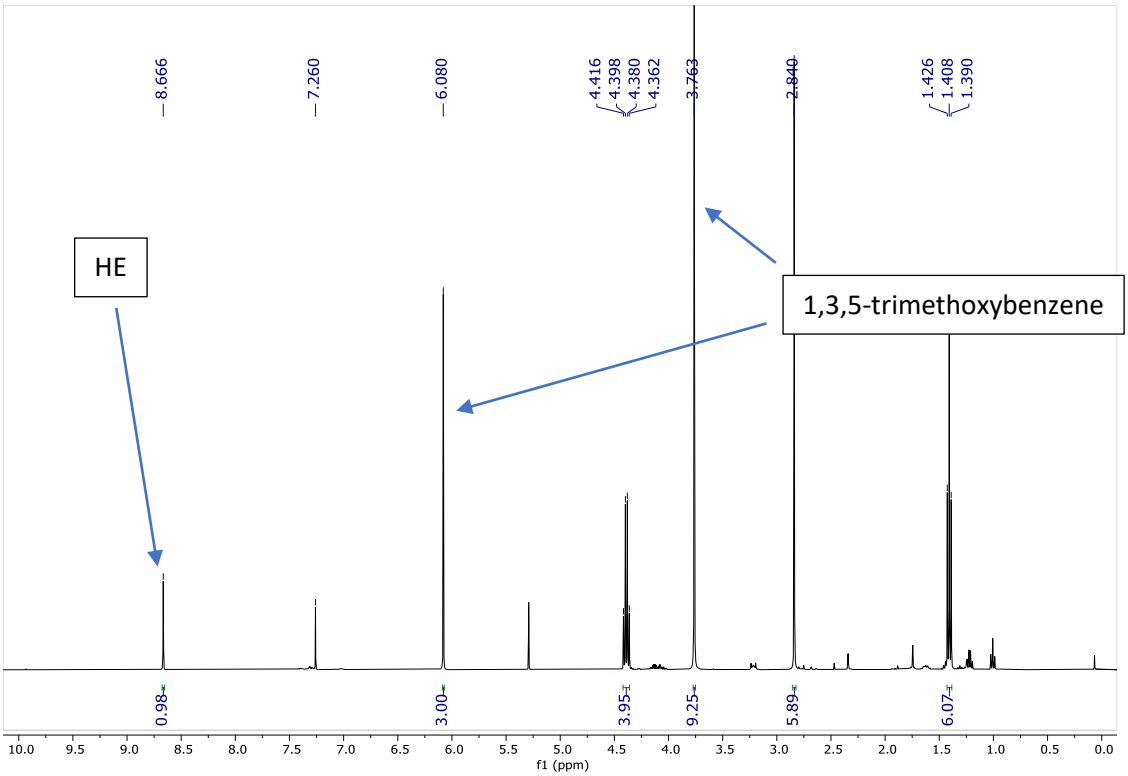

Supplementary Figure 71: ^{1}H q-NMR spectrum (400 MHz, $CDCl_3$, 25 °C) of crude reaction mixture corresponding to the experiment depicted in Supplementary Table 4 entry 6.

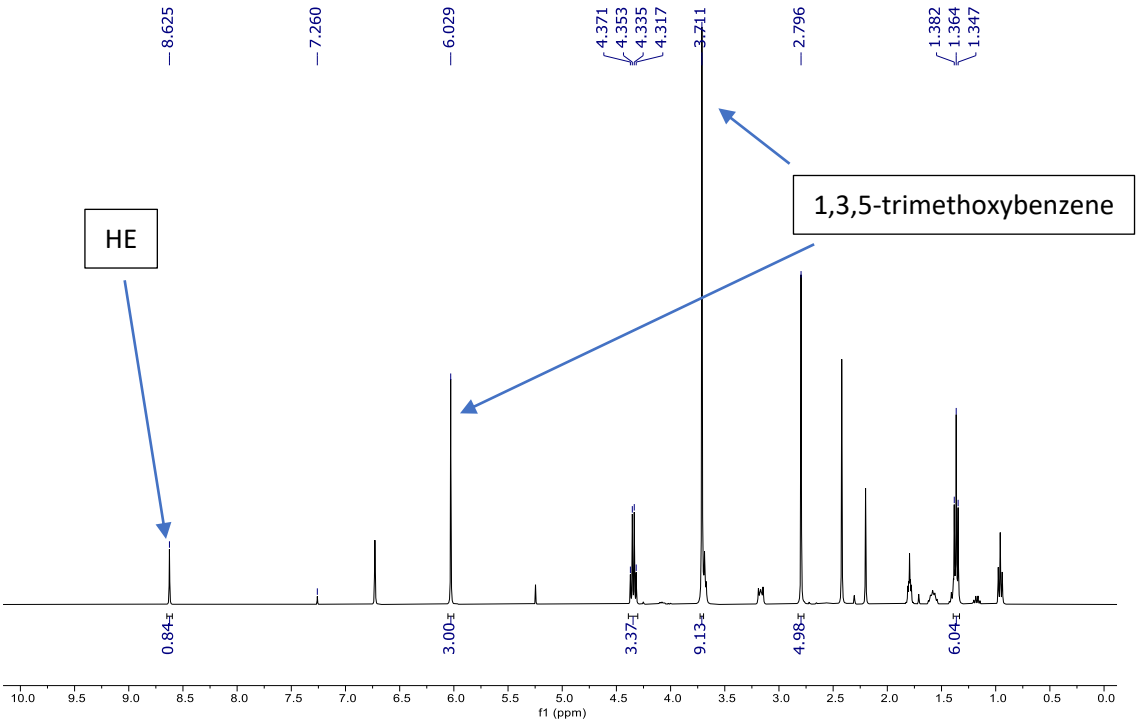

Supplementary Figure 72: ^{1}H q-NMR spectrum (400 MHz, $CDCl_3$, 25 °C) of crude reaction mixture corresponding to the experiment depicted in Table 2, entry 3 (main text).

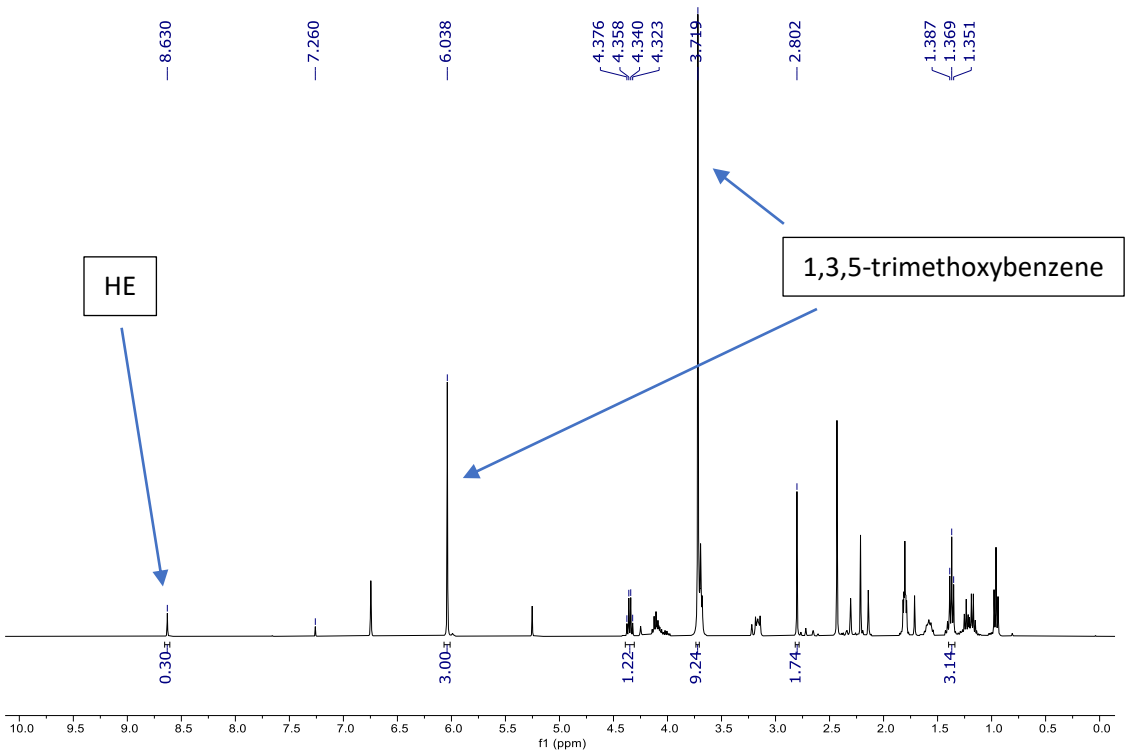

Supplementary Figure 73: ^{1}H q-NMR spectrum (400 MHz, $CDCl_3$, 25 °C) of crude reaction mixture corresponding to the experiment depicted in Table 2, entry 4 (main text).

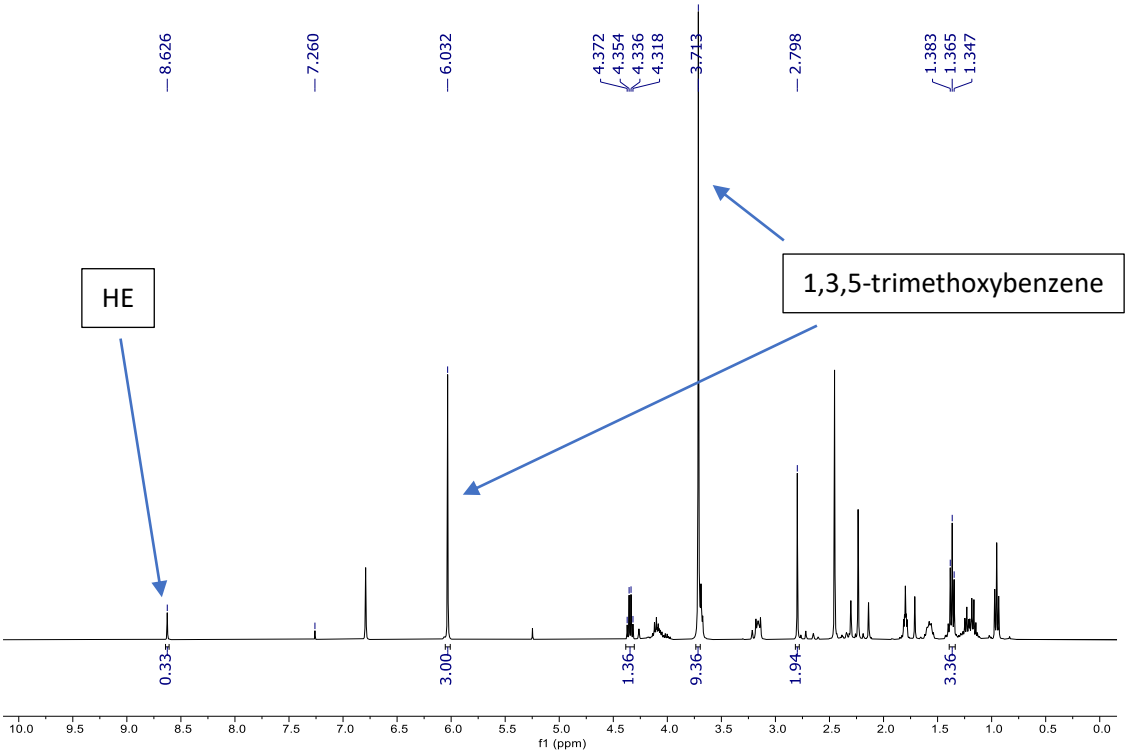

Supplementary Figure 74: ^{1}H q-NMR spectrum (400 MHz, $CDCl_3$, 25 °C) of crude reaction mixture corresponding to the experiment depicted in Table 2, entry 7 (main text).

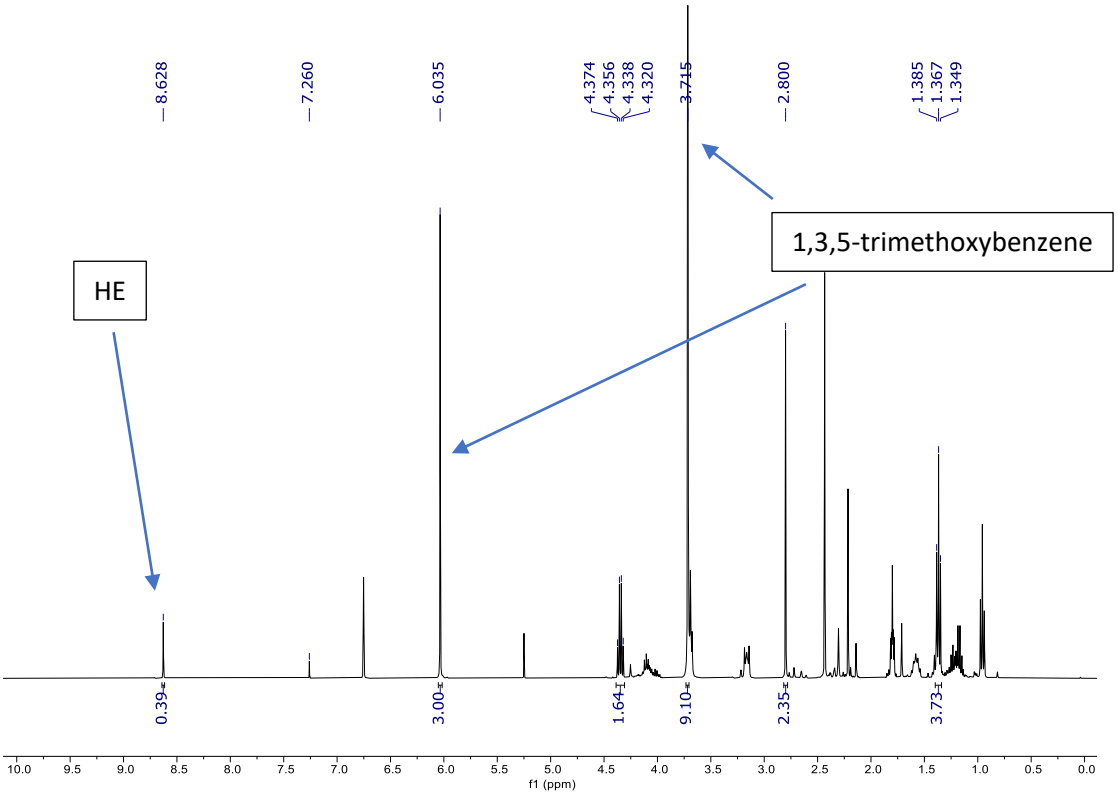

Supplementary Figure 75: ^{1}H q-NMR spectrum (400 MHz, $CDCl_3$, 25 °C) of crude reaction mixture corresponding to the experiment depicted in Table 2, entry 8 (main text).

^{1}H NMR and Gas-phase IR Studies for Reaction Between HEH_2 and NO or NH_2OH:

^{1}H NMR studies-

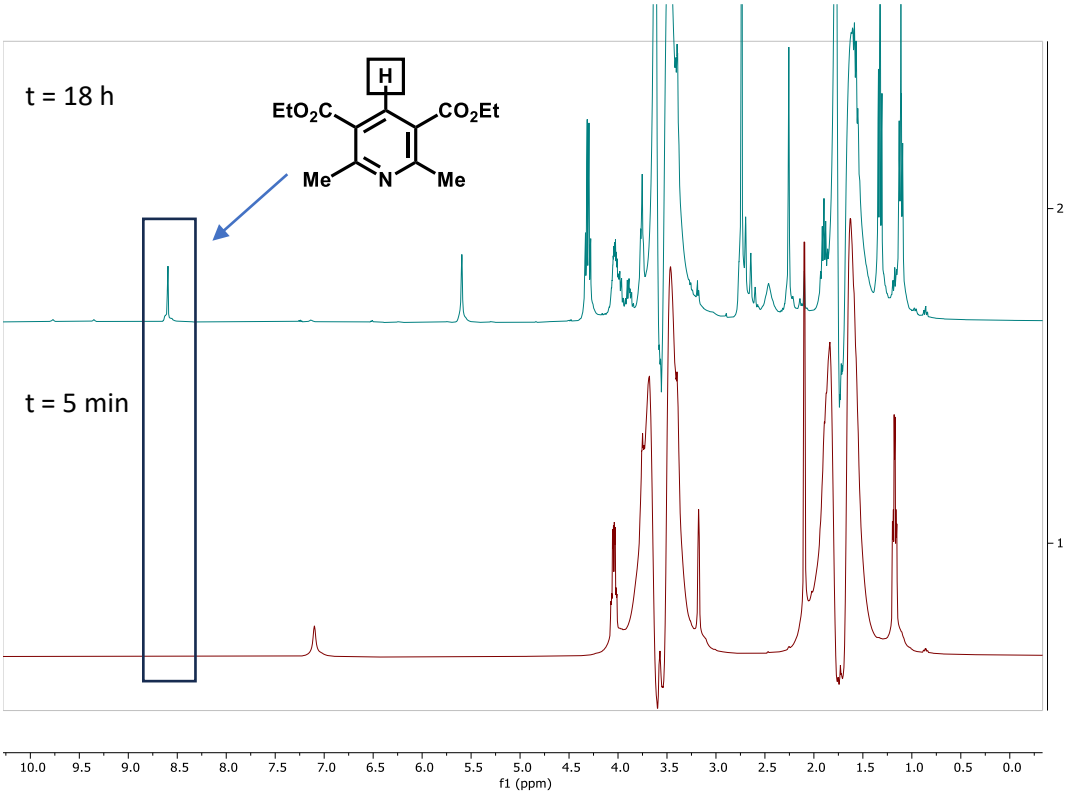

Supplementary Figure 76: Stacked ^{1}H NMR spectra (400 MHz, THF, 25 °C) of reaction between HEH_2 and NO (g) at 25 °C under 427 nm Kessil lamp irradiation. Bottom: spectra at t = 5 min, top: t = 18 h.

Gas-phase IR studies-

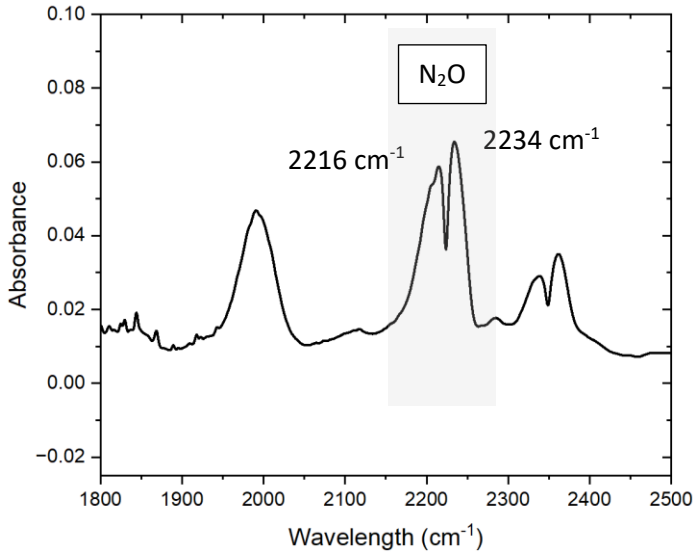

Supplementary Figure 77: FT-IR spectrum (gas phase) of reaction between HEH_2 and NO(g) ran at 25 °C under 427 nm Kessil lamp irradiation at t = 18 h timepoint.

Under the optimized photochemical reaction conditions (Table 2, entry 3 in the main text)-

reaction with NO(g):

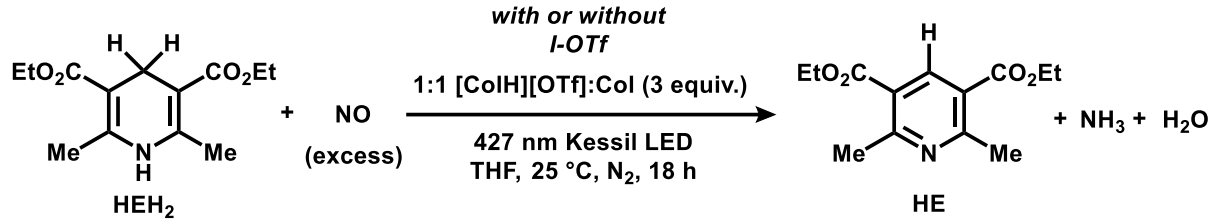

reaction with $NH_2OH.HCl$:

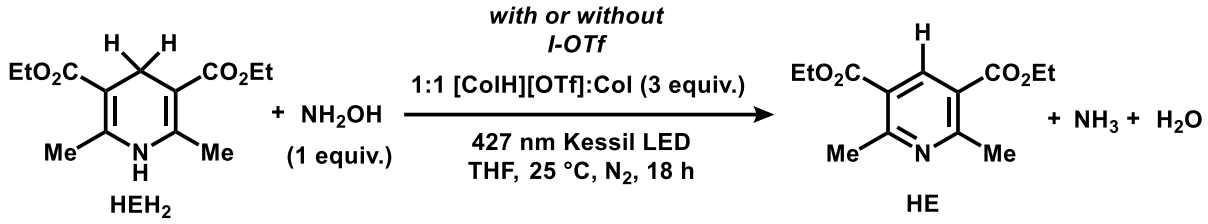

Procedure: Inside a glove box, a J-young NMR tube was charged with NO(g) (~1 mL, excess) or $NH_2OH.HCl$ (0.05 mmol, 1.0 equiv.), HEH_2 (4.0 equiv.), 1:1 [Col]/[ColH][OTf] (3 equiv.), and with or without catalyst **I-OTf** (2.5 mol%) in THF. The tube was sealed with a Teflon cap and moved out of the glovebox, and it was stirred in a pre-set oil bath at 25 °C. The reaction was stirred and irradiated with a 427 nm Kessil LED lamp at ~4-5 cm distance from the tube. After 18 h, the reaction was stopped and cooled to room temperature. The reaction mixture was acidified with ~1 mL of 2 M HCl in Et_2O. ^1H NMR of the sample was then recorded in DMSO-d_6 which showed the formation of NH_4^+ in all the cases.

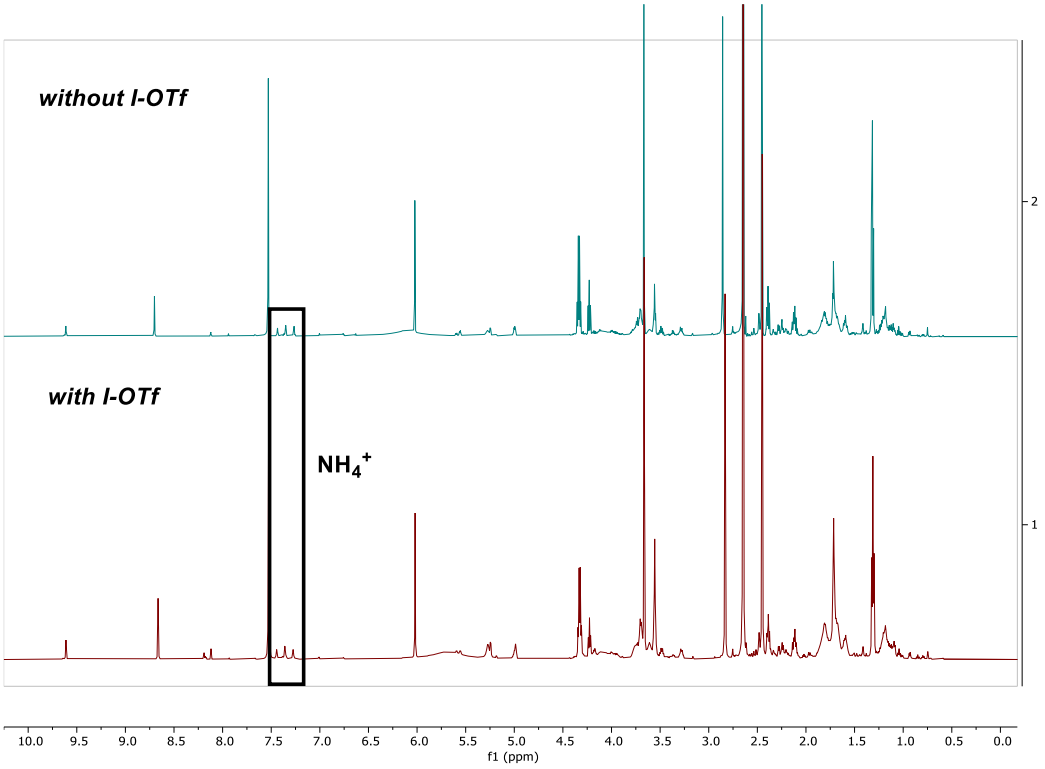

Supplementary Figure 78: Stacked ^{1}H NMR spectra (600 MHz, DMSO-d_6, 25 °C) of the reaction with NH_2OH•HCl under the optimized conditions (Table 2, entry 3 in the min text) with and without catalyst **I-OTf**.

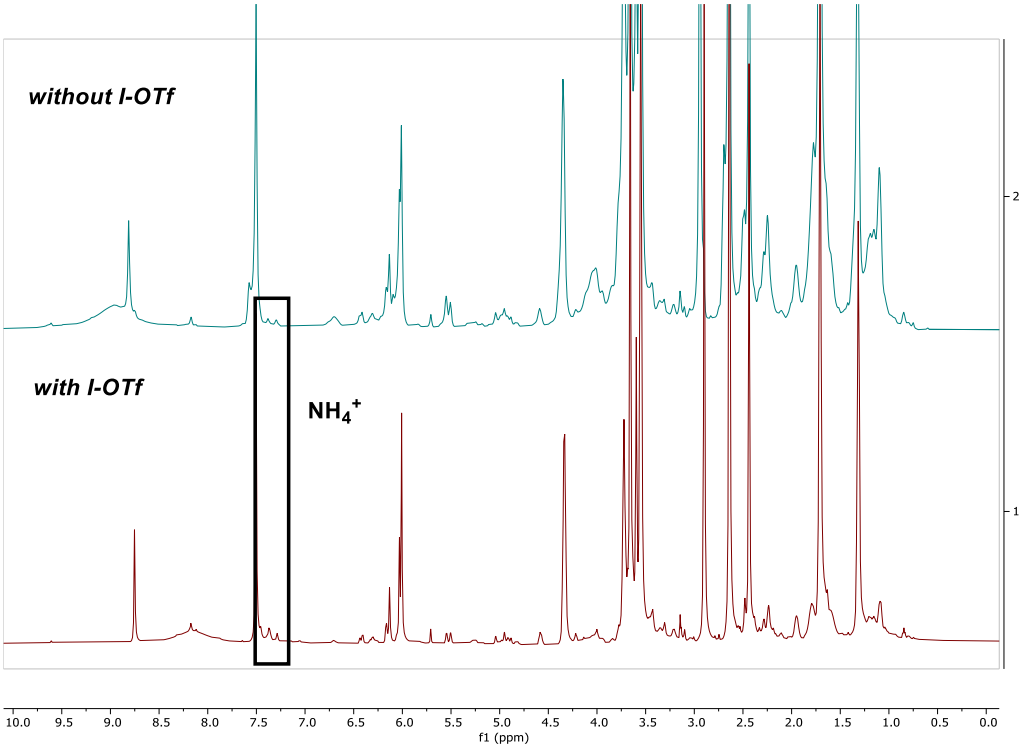

Supplementary Figure 79: Stacked ^{1}H NMR spectra (600 MHz, DMSO-d_6, 25 °C) of the reaction with NO(g) under the optimized conditions (Table 2, entry 3 in the min text) with and without catalyst **I-OTf**.

Gas-phase IR Studies of Photochemical Catalytic Reaction with HEH_2:

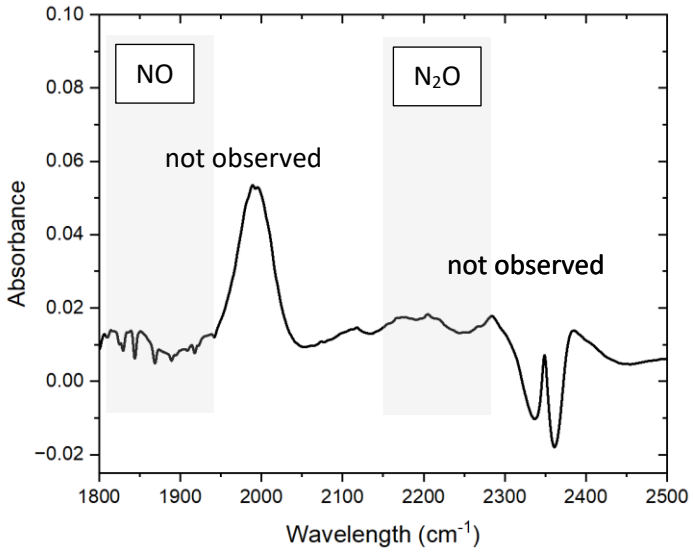

Supplementary Figure 80: FT-IR spectrum (gas-phase) of reaction corresponding to the experiment depicted in Supplementary Table 4, entry 11.

^{15}N NMR Studies for NH_3 detection: Inside a glove box, a J-young NMR tube was charged with $[Bu_4N][^{15}NO_3]$ (12.2 mg, 0.04 mmol, 1.0 equiv.), HEH_2 (20.3 mg, 0.08 mmol), and catalyst **I-OTf** (0.9 mg, 0.001 mmol) in 0.8 mL THF (experiment corresponding to Supplementary Table 4, entry 1). The tube was

sealed with a Teflon cap and moved out of the glovebox. ^{15}N NMR of the crude reaction mixture was taken after 5 min. The peak for $^{15}NO_3^-$ was observed as a broad singlet signal at -3.90 ppm. The tube was then kept standing in a pre-set oil bath stirring at 25 °C and the NMR tube was irradiated with a 427 nm Kessil LED lamp at ~4-5 cm distance from the tube. After 18 h, the reaction was stopped and cooled to room temperature. ^{15}N NMR of the crude reaction mixture was taken at the 18 h timepoint. The peak for $^{15}NO_3^-$ was now observed as a sharp singlet signal at -1.67 ppm and a new peak for $^{15}NH_3$ was observed at -387.29 ppm. The peak for $^{15}NO_3^-$ of $[Bu_4N][^{15}NO_3]$ in THF was at -1.72 ppm.

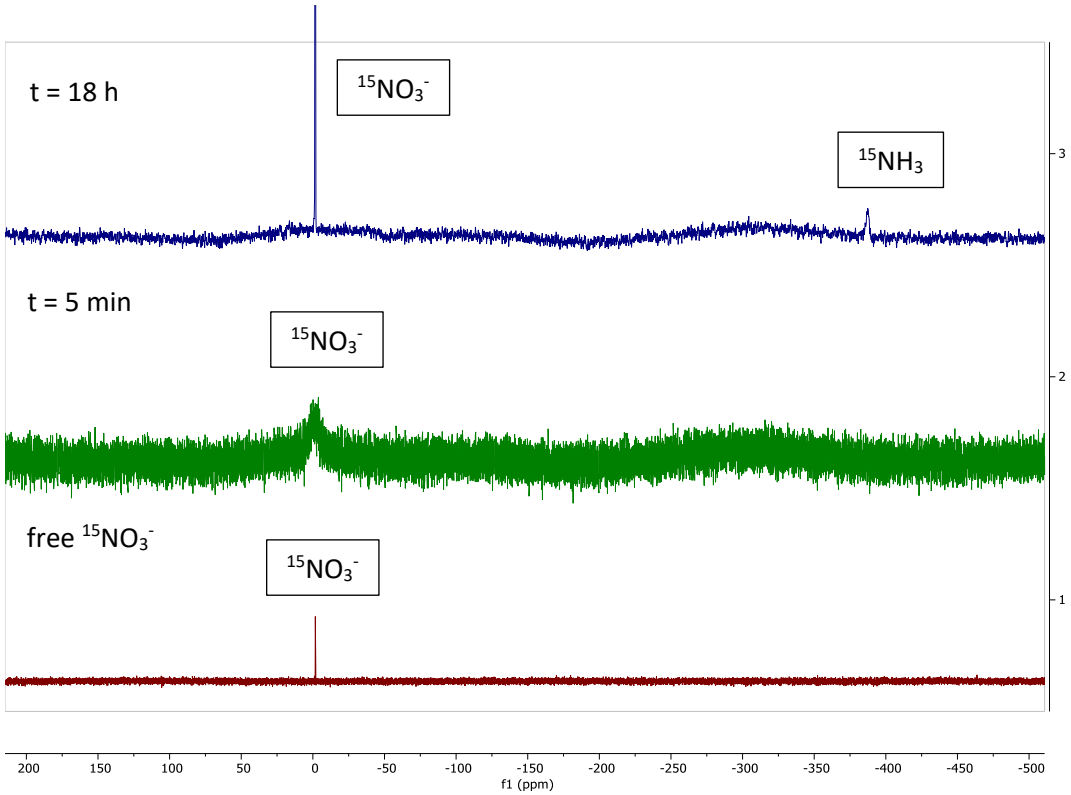

Supplementary Figure 81: Stacked ^{15}N NMR spectra (700 MHz, THF, 25 °C) of $[Bu_4N][^{15}NO_3]$ and crude reaction mixture at t = 5 min and t = 18 h, corresponding to the experiment depicted in Supplementary Table 4, entry 11.

NH_3 Quantification Experiments and Validation with HEH_2 to HE Conversion

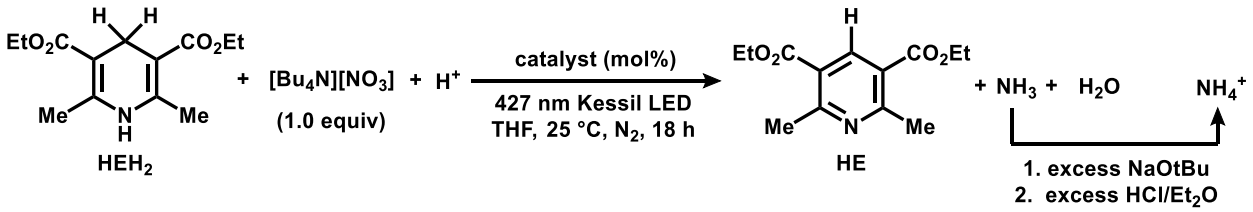

Representative Procedure for NH_3 quantification: Inside a glove box, a 10 mL Teflon-capped Schlenk tube was charged with $[Bu_4N][^{15}NO_3]$ (12.2 mg, 0.04 mmol, 1.0 equiv.), HEH_2 (20.3 mg, 0.08 mmol), and catalyst **I-OTf** (0.9 mg, 0.001 mmol) in 0.8 mL THF. The tube was sealed with a Teflon cap and moved out of the glovebox, and it was stirred in a pre-set oil bath at 25 °C. The reaction was stirred and irradiated with a 427 nm Kessil LED lamp at ~4-5 cm distance from the tube. After 18 h, the reaction was stopped and

cooled to room temperature. 4.0 mL of a 0.125 M NaO^{t}Bu solution in MeOH was added to the crude reaction mixture under liquid nitrogen temperature and then stirred while thawing at room temperature. Another 10 mL Teflon-capped Schlenk tube was equipped with 2 mL of 2 M HCl in Et_2O and stirred at room temperature. Both the solutions were connected through an H-bridge setup and they were separately freeze-pump-thawed three times using liquid nitrogen. Then, the volatiles of the reaction mixture flask were vacuum transferred to the flask containing HCl/Et_2O and was then stirred for 10 min after completion of the process. The resulting mixture was then transferred into a scintillation vial containing 1,3,5-trimethoxybenzene (6.7 mg, 0.04 mmol, 1.0 equiv) internal standard using THF and then the solvent was evaporated in vacuo. ^{1}H q-NMR (quantitative NMR) of the sample was then recorded in DMSO-d_6 which showed the formation of NH_4^+ in 31% yield (experiment in Supplementary Table 4, entry 11).

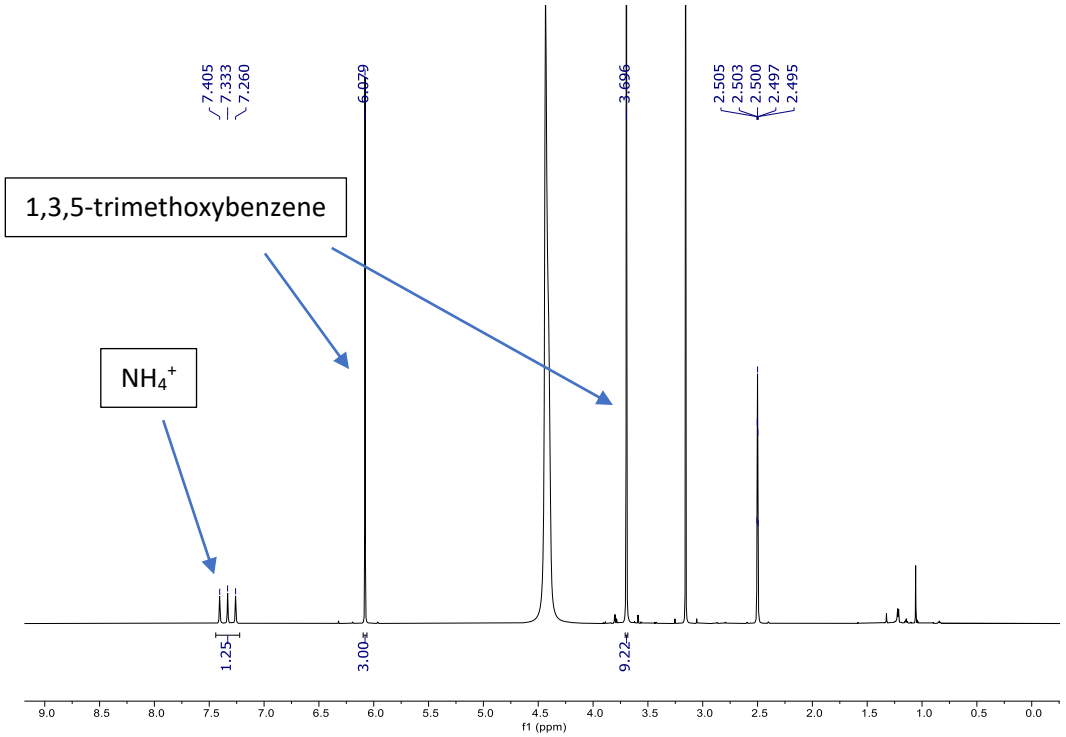

Supplementary Figure 82: ^{1}H q-NMR spectrum (700 MHz, DMSO-d_6, 25 °C) of the acidified mixture containing volatiles of the crude reaction corresponding to the experiment depicted in Supplementary Table 4, entry 11.

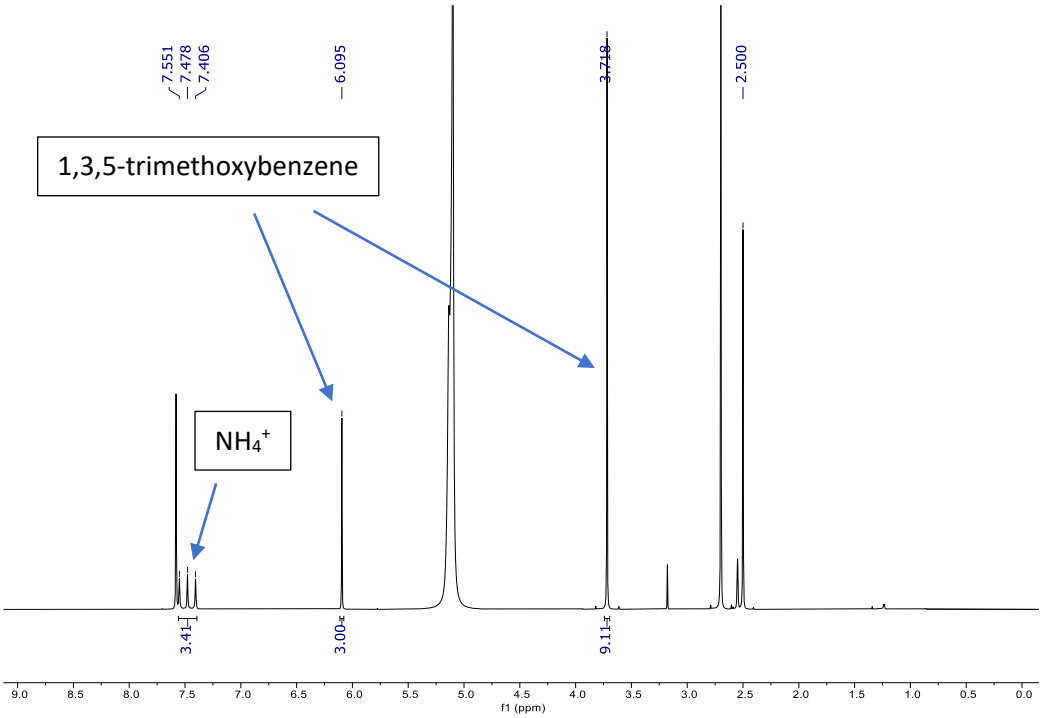

Supplementary Figure 83: ^{1}H q-NMR spectrum (700 MHz, DMSO-d_6, 25 °C) of the acidified mixture containing volatiles of the crude reaction corresponding to the experiment depicted in Table 2, entry 3 in the main text.

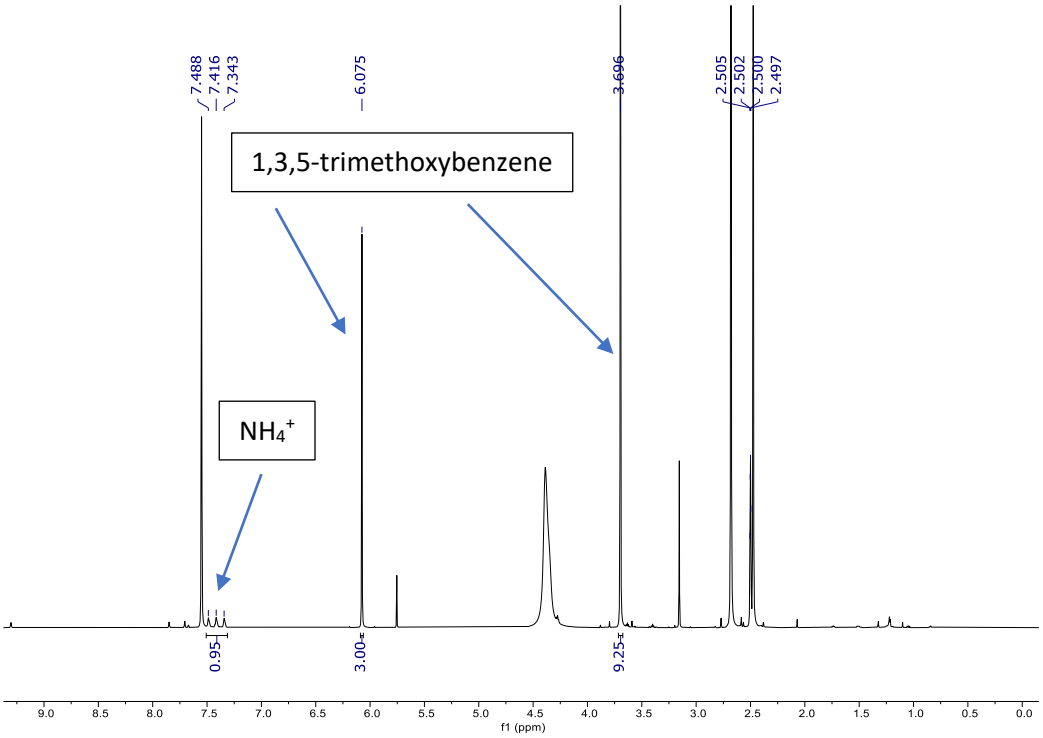

Supplementary Figure 84: ^{1}H q-NMR spectrum (700 MHz, DMSO-d_6, 25 °C) of the acidified mixture containing volatiles of the crude reaction corresponding to the experiment depicted in Table 2, entry 4 in the main text.

Procedure for NH_3 Quantification at Ten-fold Scale of Optimization: Inside a glove box, one 25 mL bulb of an H-bridge cell was equipped with a stir bar and charged with $[Bu_4N][NO_3]$ (121.8 mg, 0.4 mmol, 1.0 equiv.), HEH_2 (405.2 mg, 1.6 mmol, 4.0 equiv.), [Col] (145.4 mg, 1.2 mmol, 3.0 equiv.), [ColH][OTf] (325.5 mg, 1.2 mmol, 3.0 equiv.) and with or without catalyst **I^{CF3}-OTf** (150µL, 0.001 mol%) in 12 mL THF. The bulb was sealed with a Teflon cap and moved out of the glovebox, and it was stirred in a pre-set oil bath at 25 °C. The reaction was stirred and irradiated with a 427 nm Kessil LED lamp at ~4-5 cm distance from the tube. After 18 h, the reaction was stopped and cooled to room temperature. The contents of the bulb were then cooled to -78°C over liquid nitrogen. Then, the bulb was lifted out of the liquid nitrogen, and NaO^tBu (600 mg in 4.5 mL MeOH, 6.25 mmol) was added slowly over the course of a few minutes. The bulb was then re-stoppered, the contents were frozen, and the headspace was evacuated twice. The mixture was then warmed to room temperature and allowed to stir for at least 20 minutes. Meanwhile, the other bulb was equipped with a stir bar and charged with 2 M HCl in Et_2O (3 mL, 6 mmol). The contents of this bulb were subjected to two de-gas cycles. Once the reaction bulb had stirred for at least 20 minutes, a third de-gas cycle was performed on it, without thawing to room temperature. Then, a final de-gas cycle was performed on the receiving bulb. Once the headspace of the vessel was fully evacuated, the vessel was closed to active vacuum, the Teflon keys for the reaction flask and receiving flask were opened, and the volatiles of the reaction flask were slowly vacuum transferred to the receiving flask. Once the reaction flask was devoid of all volatiles, the receiving flask's key was closed, the vessel was removed from liquid nitrogen, the contents were thawed to room temperature, and the thawed mixture was allowed to stir for 20 minutes. At this point, the contents of the receiving flask were transferred with a pipette to a scintillation vial containing 1,3,5-trimethoxybenzene (6.7 mg, 0.04 mmol, 0.1 equiv) internal standard, and then the solvent was evaporated in vacuo. The receiving bulb was then rinsed thrice with MeOH (3 x ~1 mL), which was then removed in vacuo. The yield of NH_4^+ was determined using ^1H NMR (quantitative NMR) in DMSO of the resulting residue.

Stock solution of **I^{CF3}-OTf** used: 6 mg in 2 mL THF, from which 100 µL was used for making a 100 µL in 10 mL stock, from which 150 µL was used for the 0.001 mol% catalytic loading reaction.

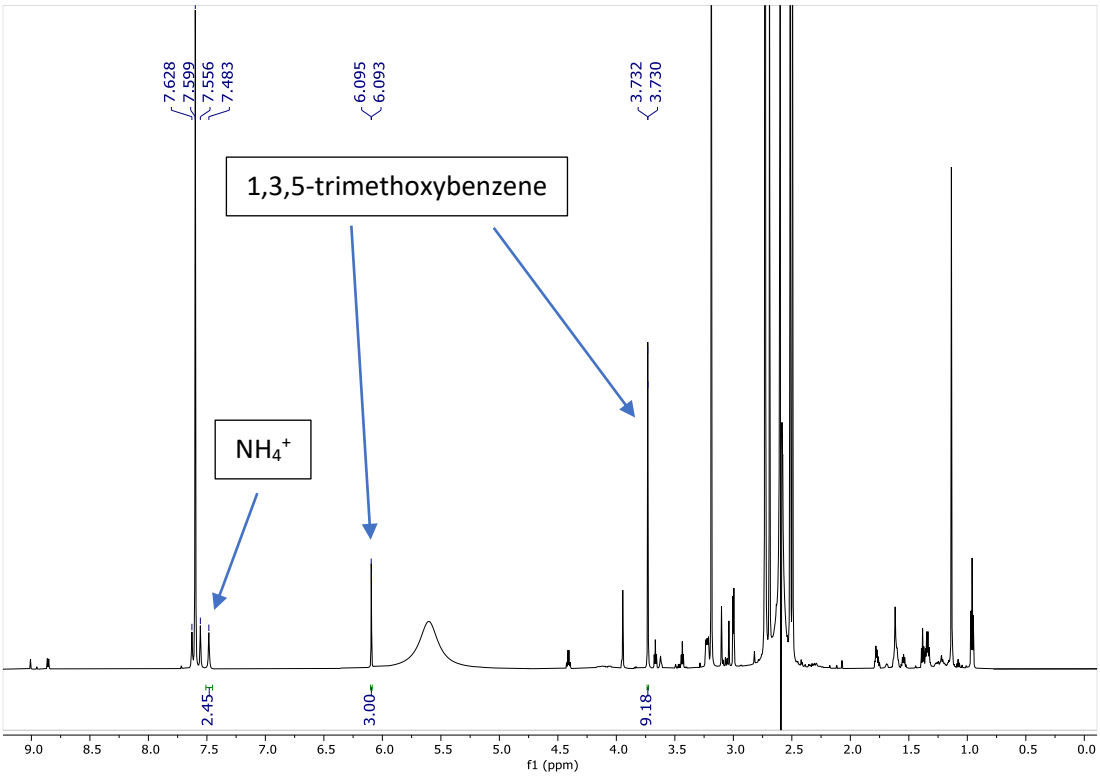

Supplementary Figure 85: ^{1}H q-NMR spectrum (700 MHz, DMSO, 25 °C) of the acidified mixture containing volatiles of the crude reaction corresponding to the experiment depicted in Table 2, entry 8 in the main text**.**

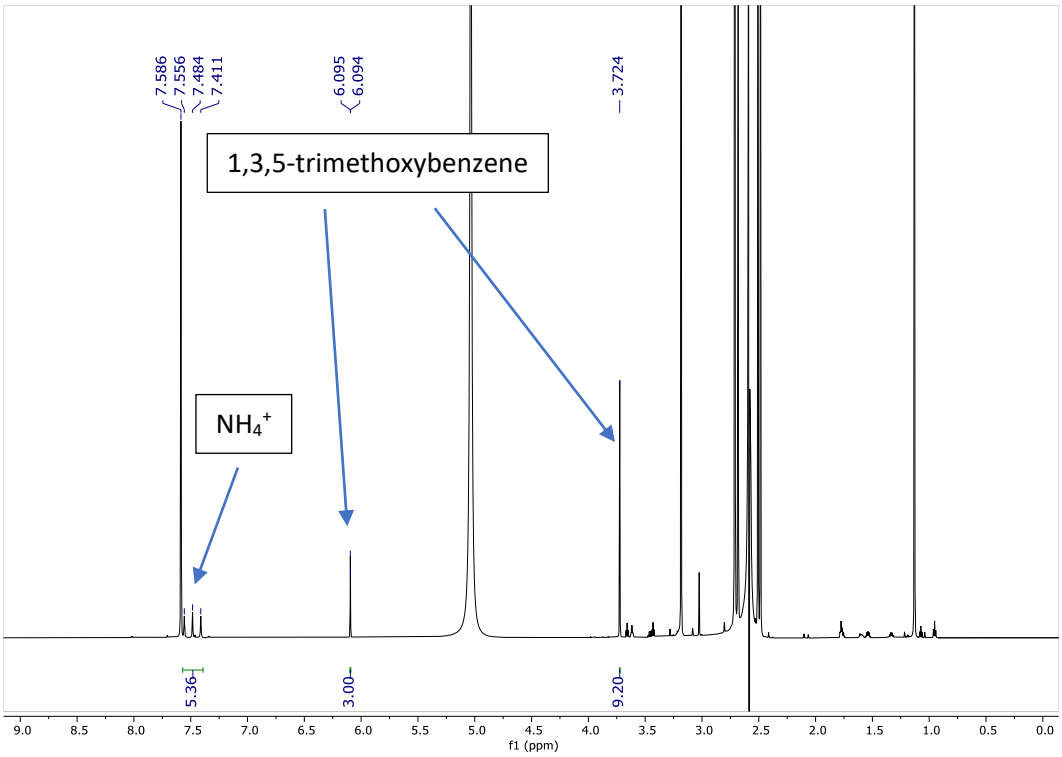

Supplementary Figure 86: ^{1}H q-NMR spectrum (700 MHz, DMSO, 25 °C) of the acidified mixture containing volatiles of the crude reaction corresponding to the experiment depicted in Table 2, entry 9 in the main text.

Supplementary Table 5: Tabulated triplicate results at 10-fold of the optimization scale (0.4 mmol $[Bu_4N][NO_3]$, 0.001 mol% catalyst)-

Experiment No.	**NH_4^+ yield (%) with I^{CF3}-OTf**	**NH_4^+ yield (%) without I^{CF3}-OTf**
1	18	13%
2	20	15%
3	17	12%
Average yield with standard deviation	18 ± 1	13 ± 1
Δ (average yield)	5%	-
$TON_{NO3-/NH3}$	**5000**	**-**

Validation of NH_3 Yields with HEH_2 Yields for $TON_{NO3-/NH3}$ Calculation

a) *balanced chemical reaction*

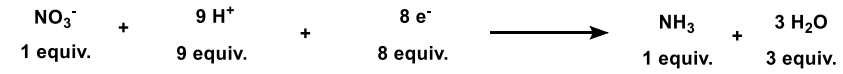

b) *conditions used in Table S4, entry 11*

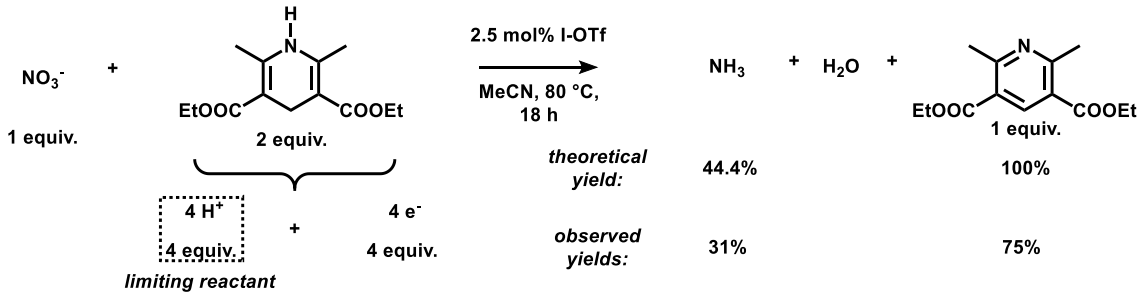

c) *conditions used in Table 2, entry 3 (main text)*

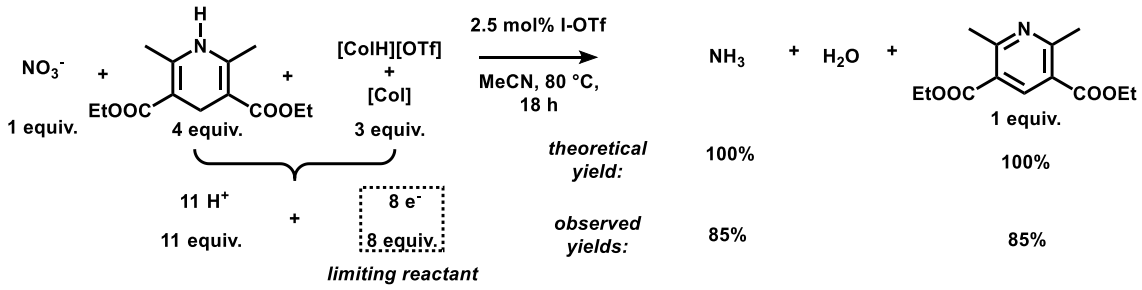

d) *conditions used in Table 2, entry 4 (main text)*

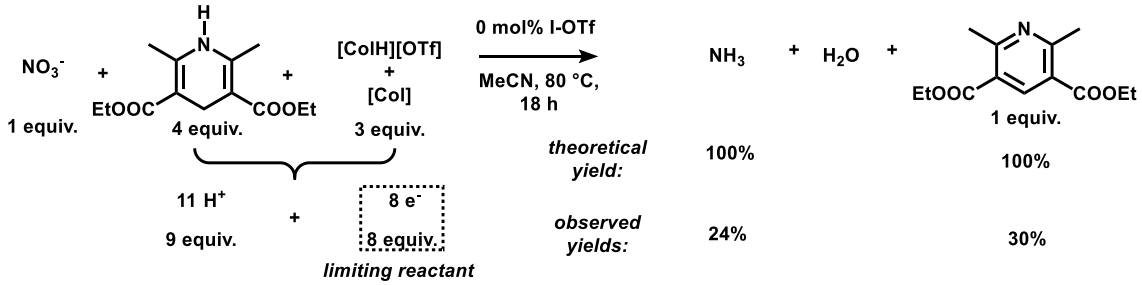

The % yield of non-metal mediated HEH_2 reduction (HE_{nocat}), and thus NH_3 formation, was subtracted from the yields of HE from entry *i* (HE_i) to calculate $TON_{NO3-/NH3}$, as shown below. Calculating TON in this manner denotes NH_3 formation as a direct consequence of catalyst presence.

$$TON_{\frac{NO_3^-}{NH_3}} = \frac{(HE_i - HE_{nocat})}{mol\,\%\,of\ catalyst}$$

From Table 2, entry 3, we therefore obtain:

$$TON_{\frac{NO_3^-}{NH_3}} = \frac{(85 - 30)}{2.5\,mol\%\,I-OTf} = 22$$

Supplementary Table 6: Tabulated triplicate results at the optimization scale (0.04 mmol $[Bu_4N][NO_3]$, 0.001 mol% catalyst)-

Experiment No.	HE yield (%) with I^{CF3}-OTf	HE yield (%) without I^{CF3}-OTf
1	38	31%
2	39	29%
3	42	30%
Average yield with std dev.	40 ± 2	30 ± 1
Δ (average yield)	10%	-
$TON_{NO3-/NH3}$	**10000**	**-**

H_2O Quantification Studies by Me_3SiCl Quenching Experiments

Procedure for H_2O Quantification for Thermal Catalytic Reaction using $Ph_2N_2H_2$: Inside a glove box, two 10 mL Teflon-capped Schlenk tubes were charged with $[Bu_4N][NO_3]$ (12.2 mg, 0.04 mmol, 1.0 equiv.), $Ph_2N_2H_2$ (11.1 mg, 0.06 mmol, 1.5 equiv.), [ColH][OTf] (32.6 mg, 0.12 mmol, 3.0 equiv), and catalyst **I-OTf** (0.4 mg, 0.0004 mmol) in 1 mL MeCN (experiment corresponding to Table 1, entry 2 in the main text). To one of them, Me_3SiCl (25.4 µL, 0.2 mmol, 5.0 equiv.) was added and ^1H q-NMR of the crude reaction mixture was taken using 1,3,5-trimethoxybenzene (10.1 mg, 0.06 mmol) as internal standard (no. of scans = 8, relaxation delay = 30 sec, pulse width = 90, ^{13}C decoupling ON). The other tube was heated in a pre-heated oil bath at 80 °C outside the glove box. After 18 h, the reaction was stopped and cooled to room temperature. Me_3SiCl (25.4 µL, 0.2 mmol, 5.0 equiv.) was added to this reaction mixture. ^1H q-NMR of the crude reaction mixture was taken using 1,3,5-trimethoxybenzene (10.1 mg, 0.06 mmol) as internal standard (no. of scans = 8, relaxation delay = 30 sec, pulse width = 90, ^{13}C decoupling ON). The difference in the amount of $(Me_3Si)_2O$ observed between the two timepoints showed an increase in the formation of $(Me_3Si)_2O$ after reaction which is known to form from a reaction between Me_3SiCl and H_2O. Therefore, we concluded the generation of H_2O in the catalytic reaction medium.

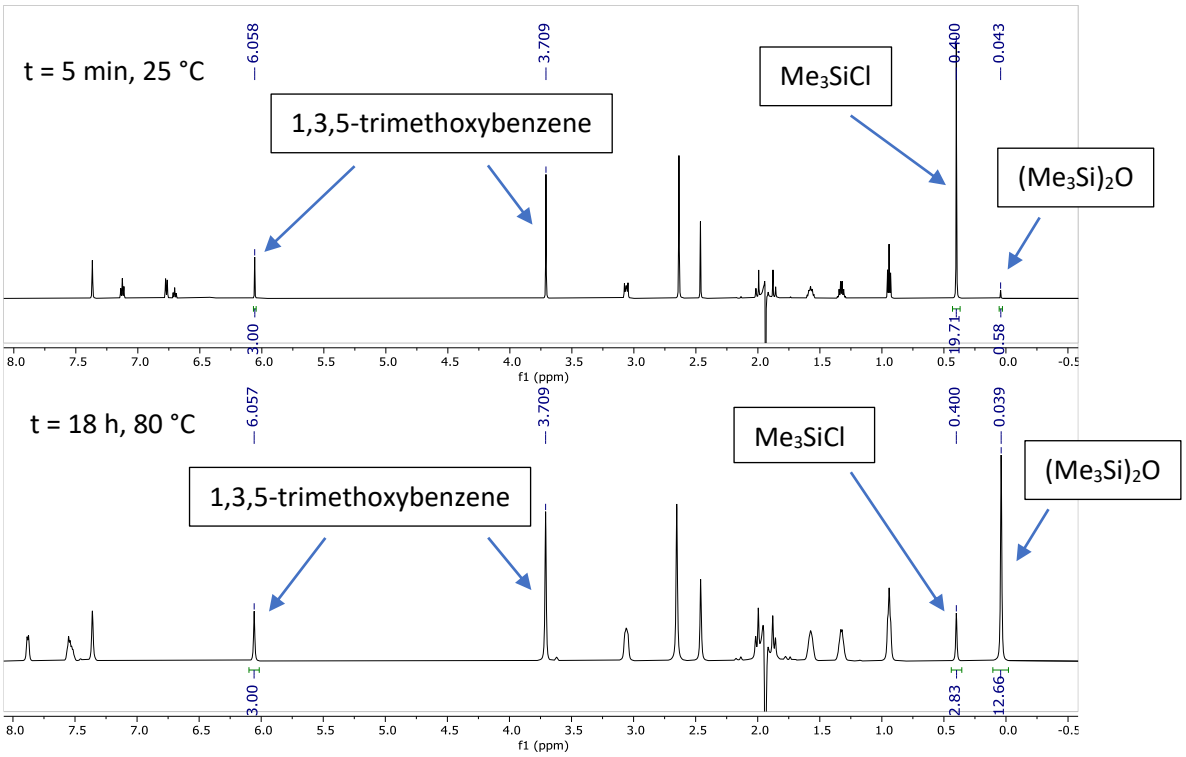

Supplementary Figure 87: Stacked ^{1}H q-NMR spectrum (600 MHz, MeCN, 25 °C) of separate crude reaction mixtures at 5 min and 18 h timepoints.

Procedure for H_2O Quantification for Photochemical Catalytic Reaction using HEH_2: Inside a glove box, two 10 mL Teflon-capped Schlenk tubes were charged with $[Bu_4N][NO_3]$ (12.2 mg, 0.04 mmol, 1.0 equiv.), HEH_2 (40.6 mg, 0.16 mmol, 4.0 equiv.), [Col] (15.9 µL, 0.12 mmol, 3.0 equiv.), [ColH][OTf] (32.6 mg, 0.12 mmol, 3.0 equiv.), and catalyst **I-OTf** (0.9 mg, 0.001 mmol) in 1.2 mL THF (experiment corresponding to Table 2, entry 3 in the main text). To one of them, Me_3SiCl (25.4 µL, 0.2 mmol, 5.0 equiv.) was added and ^{1}H q-NMR of the crude reaction mixture was taken using 1,3,5-trimethoxybenzene (10.1 mg, 0.06 mmol) as internal standard (no. of scans = 8, relaxation delay = 30 sec, pulse width = 90, ^{13}C decoupling ON). The other tube was heated in a pre-heated oil bath at 80 °C outside the glove box. After 18 h, the reaction was stopped and cooled to room temperature. Me_3SiCl (25.4 µL, 0.2 mmol, 5.0 equiv.) was added to this reaction mixture. ^{1}H q-NMR of the crude reaction mixture was taken using 1,3,5-trimethoxybenzene (26.9 mg, 0.16 mmol) as internal standard (no. of scans = 8, relaxation delay = 30 sec, pulse width = 90, ^{13}C decoupling ON). The difference in the amount of $(Me_3Si)_2O$ observed between the two timepoints showed an increment in the formation of $(Me_3Si)_2O$ after reaction which is known to form from a reaction between Me_3SiCl and H_2O. Therefore, we concluded the generation of H_2O in the catalytic reaction medium.

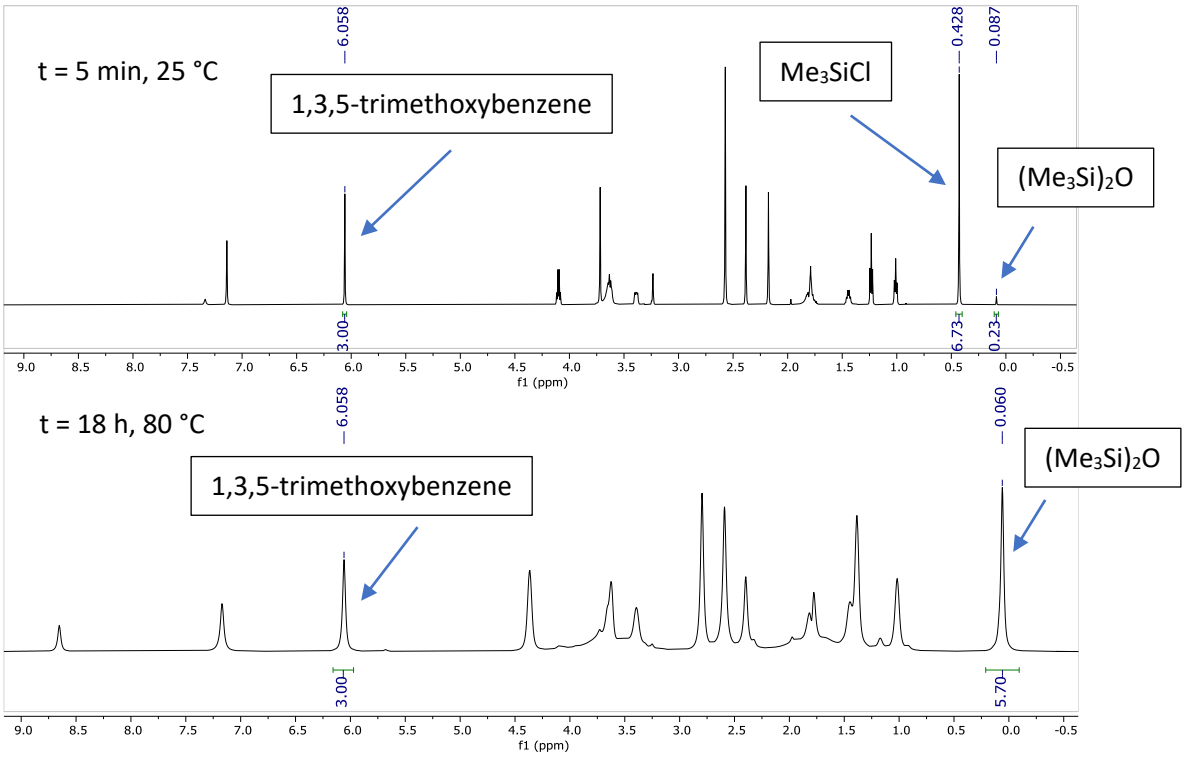

Supplementary Figure 88: Stacked ^{1}H q-NMR spectrum (600 MHz, THF, 25 °C) of separate crude reaction mixtures at 5 min and 18 h timepoints.

NO_3^- Quantification Studies

^{15}N NMR parameters: Unless otherwise stated, all ^{15}N NMR spectra were acquired using 64 scans, 30 second relaxation delay, 45° pulse width, ^{1}H decoupling, receiver gain set to 60, and subtraction of nuclear Overhauser effect; absolute integrals were calculated using VnmrJ software using the maximum integral normalization scale (ins) of 8190. Nitromethane ($MeNO_2$) was used as an external reference.

Procedure for NO_3^- Quantification for Thermal Catalytic Reaction using $Ph_2N_2H_2$: Inside a glove box, a J-young NMR tube was charged with $[Bu_4N][^{15}NO_3]$ (12.2 mg, 0.04 mmol, 1.0 equiv.), $Ph_2N_2H_2$ (11.1 mg, 0.06 mmol, 1.5 equiv.), [ColH][OTf] (32.6 mg, 0.12 mmol, 3.0 equiv), and catalyst **I-OTf** (0.4 mg, 0.0004 mmol, 1 mol%) in 1 mL MeCN (experiment corresponding to Table 1, entry 2 in the main text). A second reaction was prepared analogously in the absence of **I-OTf** (Table 1, entry 5 in the main text). ^{15}N NMR spectra of both reactions were acquired immediately (denoted as t = 18 h timepoint). The tubes were then heated in a pre-heated NMR tube heating block at 80 °C outside the glove box. After 18 h, the reactions were stopped and cooled to room temperature. The reaction mixtures were then transferred to separate vials after passing through a 2.5 cm of silica gel pad in a glass pipette, which was then eluted with MeCN (2 x 1 mL). Solvent was removed *in vacuo*, and the residues were taken back up in 1 mL MeCN. ^{15}N NMR spectra were then acquired again (denoted as t = 18 h timepoint).

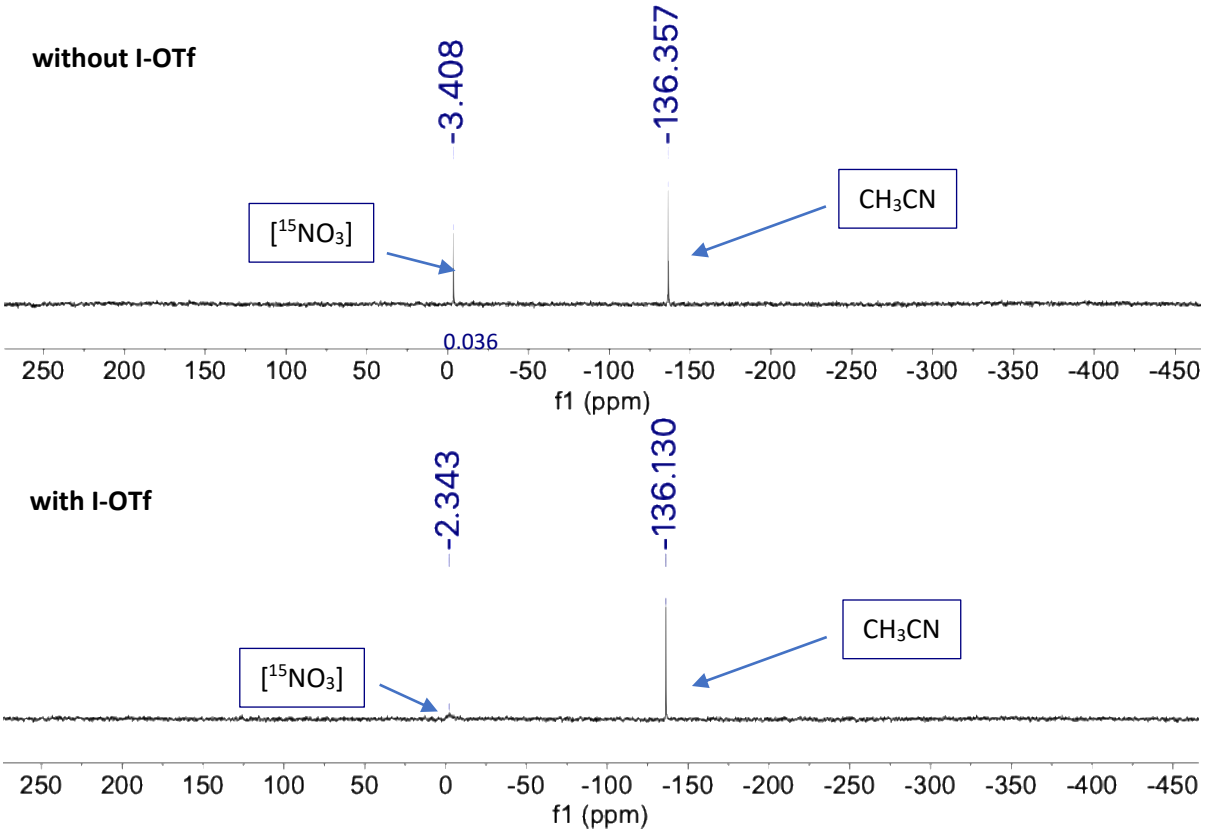

Supplementary Figure 89: Stacked ^{15}N NMR spectrum (700 MHz, MeCN, 25 °C) of crude reaction mixtures using $Ph_2N_2H_2$ as an HAT source with and without **I-OTf** catalyst at 5 min timepoint.

We propose that the low intensity of the ^{15}N signal for [$^{15}NO_3$] in the reaction with **I-OTf** (bottom spectra) due to binding interactions with the paramagnetic Fe-center.

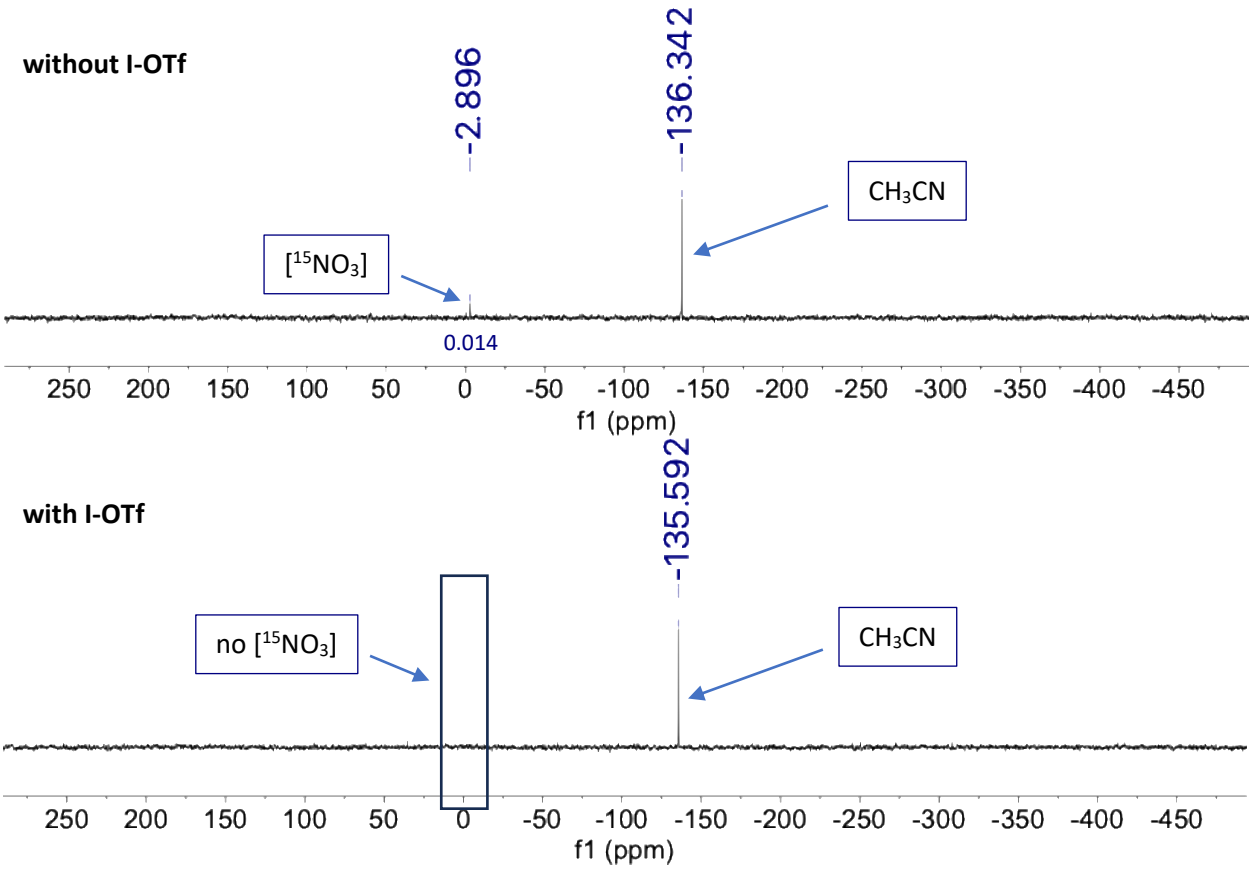

Supplementary Figure 90: Stacked ^{15}N NMR spectrum (700 MHz, MeCN, 25 °C) of crude reaction mixtures using $Ph_2N_2H_2$ as an HAT source with and without **I-OTf** catalyst at 18 h timepoint post silica gel filtration.

We propose that the decrease in intensity of the ^{15}N signal for [$^{15}NO_3$] due to loss in [NO_3] during post reaction silica gel filtration operation.

Following the silica workup, the [$^{15}NO_3$] absolute integral of the no-catalyst reaction mixture decreased (top spectra), indicating that [$^{15}NO_3$] is not quantitatively recovered during the workup; meanwhile, no signal was observed in the catalytic reaction mixture (bottom spectra) under exact similar operations, indicating a much lower concentration of [$^{15}NO_3$] prior to workup relative to the control, which showed minimal conversion. *This result is consistent with consumption of [$^{15}NO_3$] in the presence of catalyst.*

Procedure for NO_3^- Quantification for Photochemical Catalytic Reaction using HEH_2: Inside a glove box, a J-young NMR tube was charged with [Bu_4N][$^{15}NO_3$] (12.2 mg, 0.04 mmol, 1.0 equiv.), HEH_2 (40.6 mg, 0.16 mmol, 4.0 equiv.), [Col] (15.9 µL, 0.12 mmol, 3.0 equiv.), [ColH][OTf] (32.6 mg, 0.12 mmol, 3.0 equiv.), and catalyst **I-OTf** (0.9 mg, 0.001 mmol, 2.5 mol%) in 1.2 mL THF (experiment corresponding to Table 2, entry 3 in the main text). A second reaction was prepared analogously in the absence of **I-OTf** (experiment corresponding to Table 2, entry 4 in the main text). ^{15}N NMR spectra of both reactions were immediately acquired (denoted as t = 5 min timepoint). The tubes were then kept standing in a pre-set oil bath stirring at 25 °C, and the NMR tubes were irradiated with a 427 nm Kessil LED lamp at ~4-5 cm distance from the tube. After 18 h, the reactions were stopped, and ^{15}N NMR spectra were acquired again (denoted as t = 18 h timepoint).

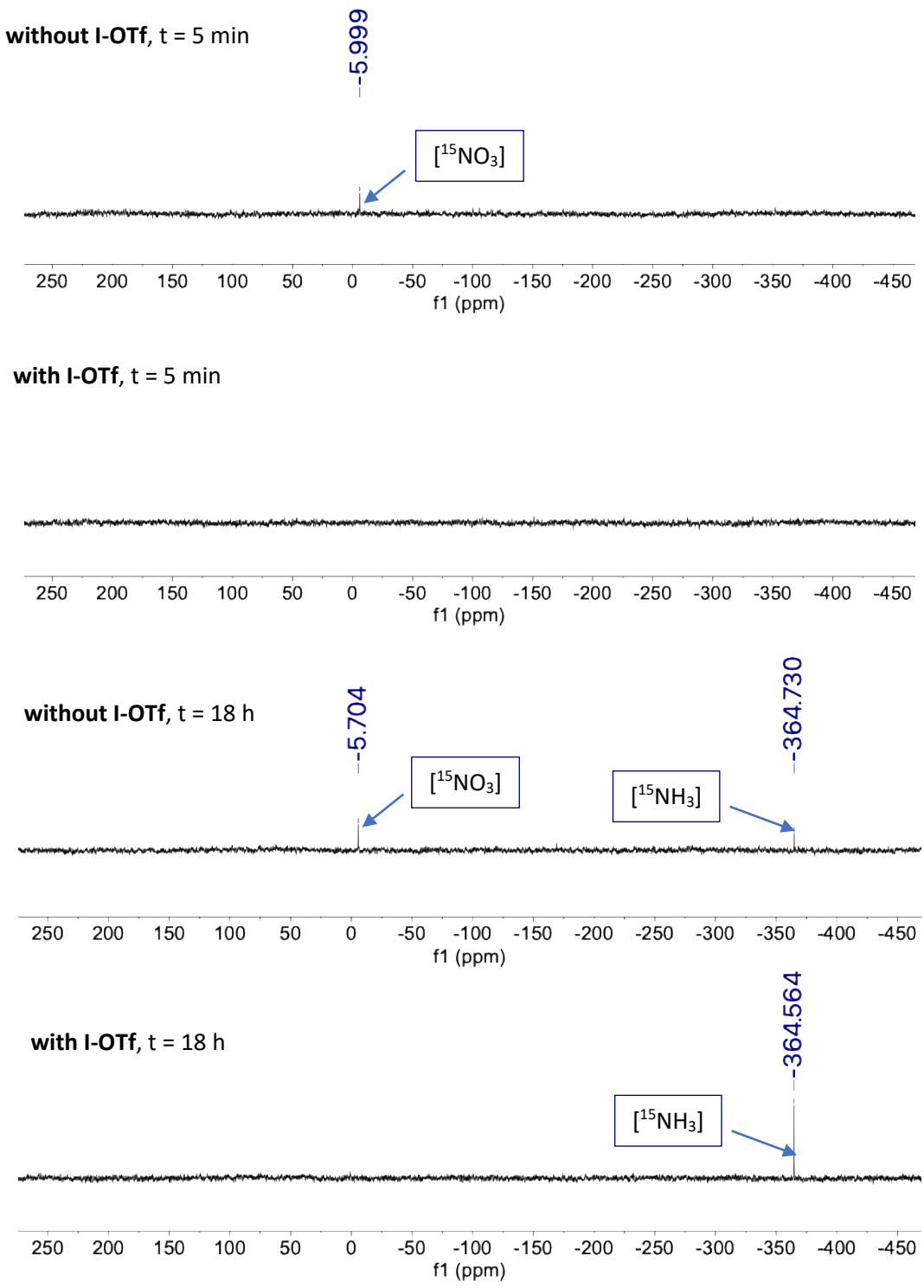

Supplementary Figure 91: Stacked ^{15}N NMR spectrum (700 MHz, THF, 25 °C) of crude reaction mixtures using HEH_2 as an HAT source with and without **I-OTf** catalyst at 5 min and 18 h timepoints.

We propose that the low intensity of the ^{15}N signal for [$^{15}NO_3$] in both the reactions at 5 min timepoint due to two possible reasons: a) poor solubility of HEH_2 in THF leading to heterogeneous reaction mixture

at the start of the reaction. b) binding interactions with the paramagnetic Fe-center (for the reaction with **I-OTf**).

We note that in both the reactions, a new peak grows in at -364 ppm resonance, with greater intensity in the reaction mixture with **I-OTf**. To confirm the identity of the spectroscopically observed nitrogenous product, the contents of the NMR tubes were frozen in liquid nitrogen and acidified with excess HCl in Et_2O (2 M, 0.5 mL, 1 mmol). The NMR tubes were then thawed and allowed to mix, resulting in solid precipitates. The contents of the NMR tubes were then extracted using THF (2 x 1 mL) into separate vials, the solvent removed under *vacuo*, and the residues taken up in DMSO-d_6. ^{1}H and ^{15}N (512 scans, 0.1 s relaxation delay, 45° pulse width, no ^{1}H decoupling) NMR spectra were then recorded for each.

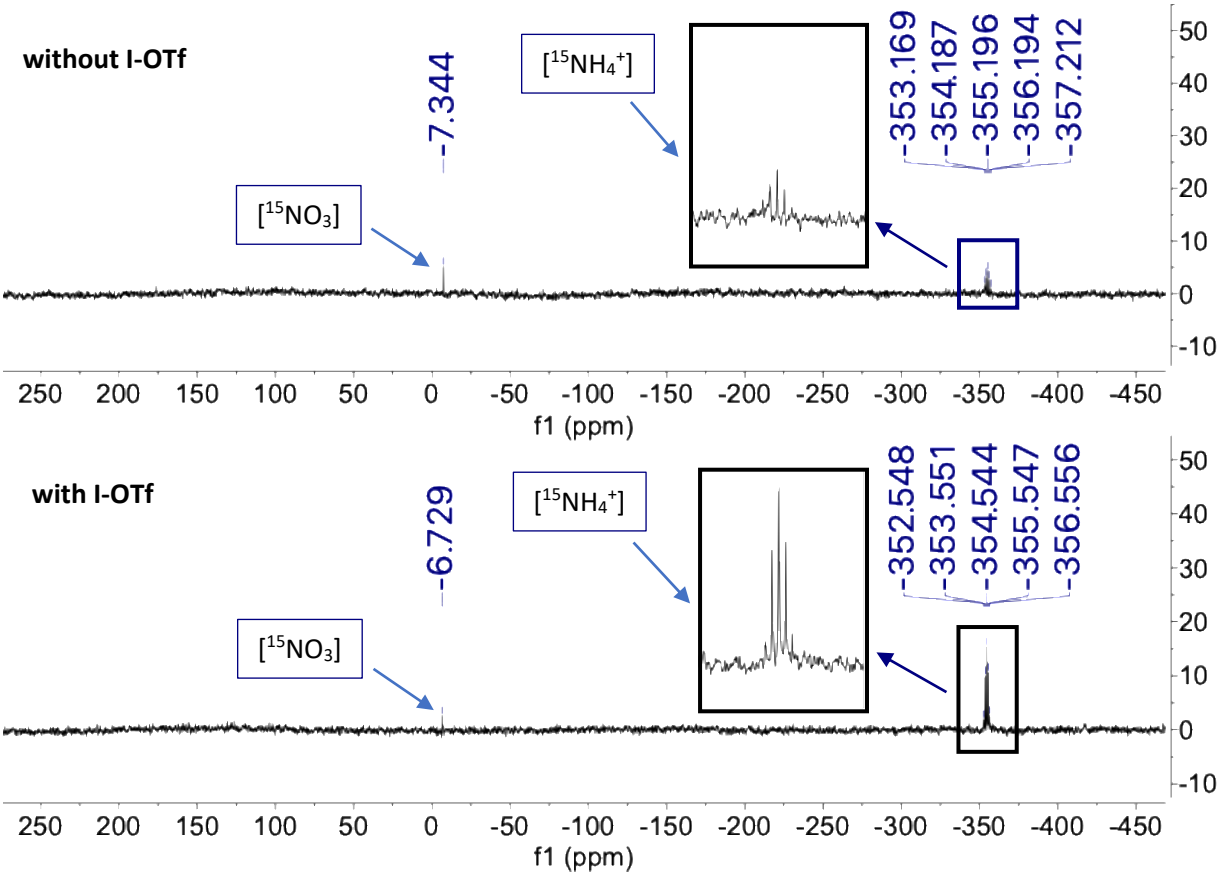

Supplementary Figure 92: Stacked ^{15}N NMR spectrum (700 MHz, DMSO-d_6, 25 °C) of the crude reaction mixtures post acidification workup with and without **I-OTf** catalyst. Insets are zoom-ins of the [$^{15}NH_4^+$] signal, with vertical scales kept consistent between insets.

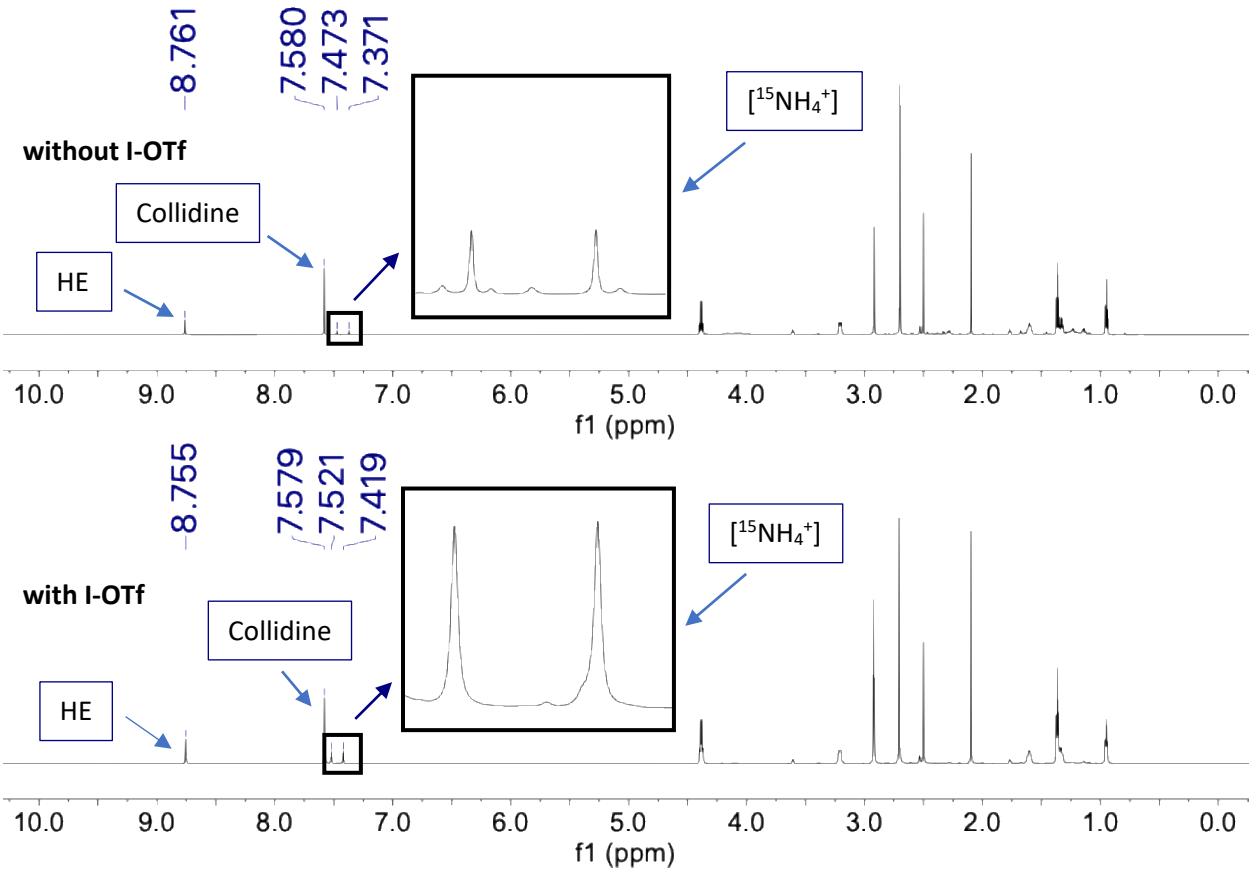

Supplementary Figure 93: Stacked ^{1}H NMR spectrum (700 MHz, DMSO-d_6, 25 °C) of the crude reaction mixtures post acidification workup with and without **I-OTf** catalyst. Insets are zoom-ins of the [$^{15}NH_4^+$] signal, with vertical scales kept consistent between insets.

Upon acidification, both ^{1}H spectrum exhibited a characteristic doublet peak centered around 7.4 ppm (J = 71 Hz), and both ^{15}N spectra exhibited characteristic quintets centered around -355 ppm (J = 71 Hz). Together, we conclude that these data are consistent with the formation of $^{15}NH_4^+$, with increased yields in the presence of **I-OTf**. Based on these observations, we propose that the formation of $^{15}NH_4^+$goes in tandem with the consumption of [$^{15}NO_3$].

Kinetic Studies of the Thermal Catalytic NO_3^- Reduction

Procedure: Inside a glovebox, a 20 mL scintillation vial was charged with [Bu_4N][NO_3] (12.2 mg, 0.040 mmol, 1.0 equiv), $Ph_2N_2H_2$ (10.9 mg, 0.060 mmol, 1.5 equiv), and [ColH][OTf] (32.6 mg, 0.120 mmol, 3.0 equiv). To the vial was added a portion of **I-OTf** stock solution (0.16 mL, 0.040 mmol, 1 mol%). The mixture was then diluted to 2.96 mL with MeCN and transferred to a modified UV/Vis cuvette containing a Teflon-coated stir bar. The cuvette was then stoppered, taken out of the glovebox, and placed in the spectrophotometer with its cryostat pre-heated to 80°C. Spectra were collected every 5 minutes for 2 h. Initial rates (k_{obs}) were determined by tracking the band growing in centered at 441 nm associated with Ph_2N_2.

Supplementary Table 7: Tabulated k_{obs} data from kinetic experiments

Entry	Modification from standard condition	k_{obs} (10^{-7} M/s)
1*	none	2.48 ± 0.19
2	60°C instead of 80°C	0.347
3	90°C instead of 80°C	4.66
4	100°C instead of 80°C	17.4
5*	0.50 mol% of **I-OTf** instead of 1 mol%	0.948 ± 0.066
6*	0.25 mol% of **I-OTf** instead of 1 mol%	0.376 ± 0.043
7	**I^{CF3}-OTf** used instead of **I-OTf**	3.71
*average rates (with standard deviation) after triplicate results.		

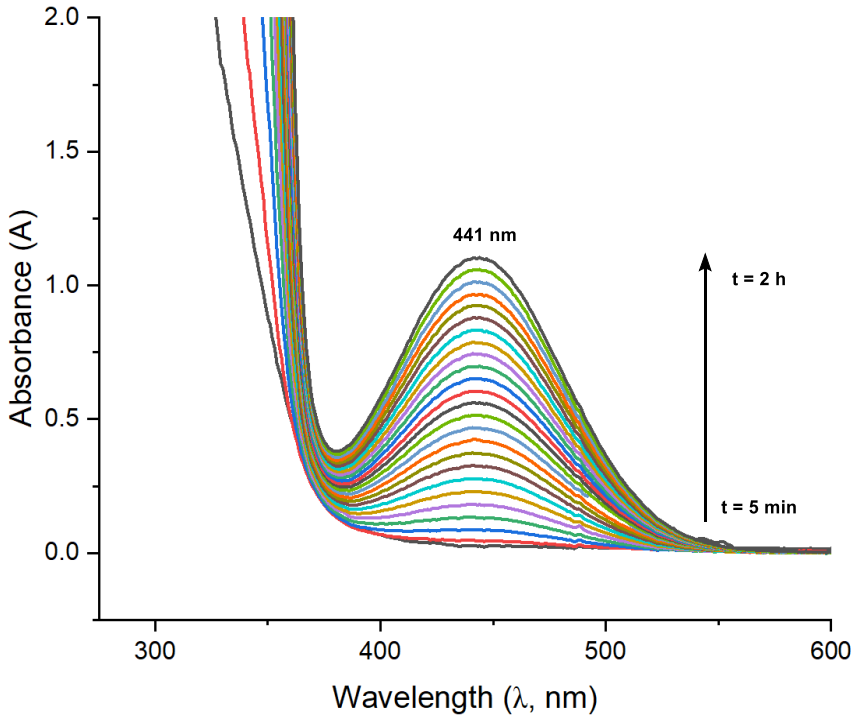

Supplementary Figure 94: Representative UV-Vis spectra for the kinetic analyses over a span of 2 h (Supplementary Table 7, entry 1).

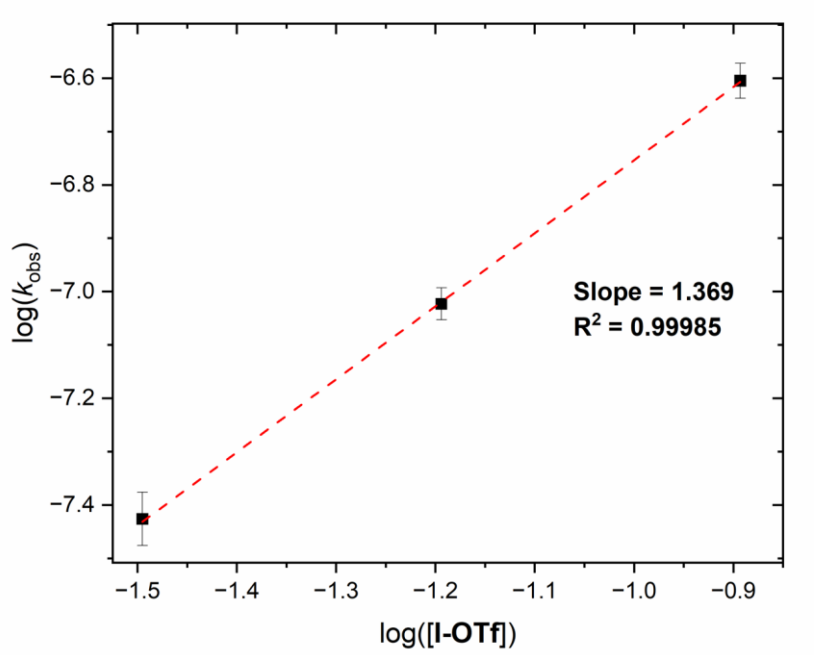

Supplementary Figure 95: Log-log plot determining reaction order in **I-OTf** (1.369).

(1.5 equiv. $Ph_2N_2H_2$, 1 equiv. $[Bu_4N][NO_3]$, using 1 mol%, 0.5 mol%, and 0.25 mol% **I-OTf**, reaction was run at 80 °C separately for 2 h).

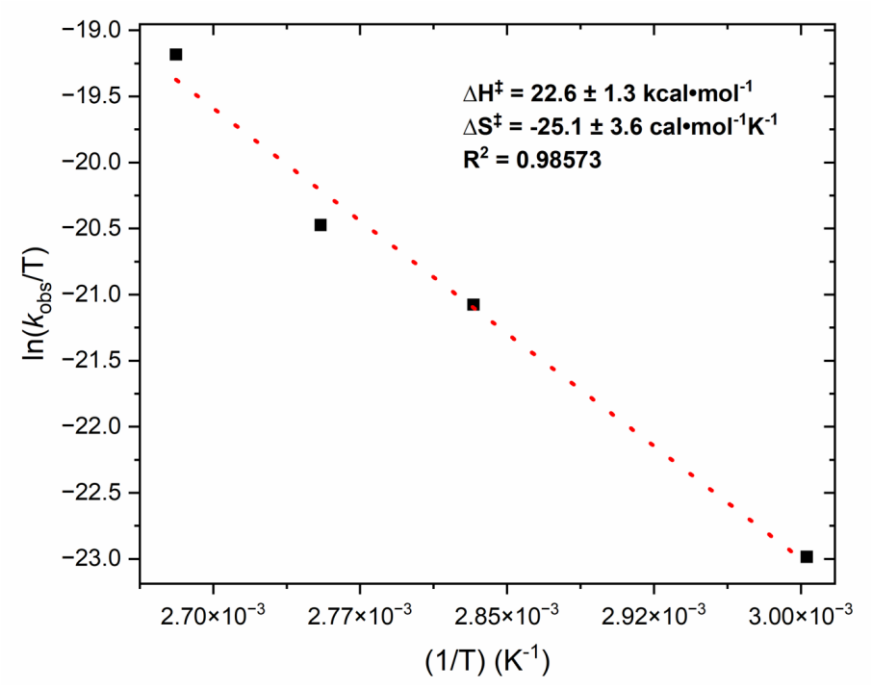

Supplementary Figure 96: Eyring analysis for reduction of NO_3^- to NO under optimized thermal catalytic conditions.

(1.5 equiv. $Ph_2N_2H_2$, 1 equiv. $[Bu_4N][NO_3]$, 1 mol% **I-OTf**, reaction was run at 60 °C, 80 °C, 90 °C, and 100 °C separately for 2 h).

Eyring equation:

$$ln\left(\frac{k}{T}\right) = \frac{-\Delta H^{\ddagger}}{R} \bullet \frac{1}{T} + ln\left(\frac{k_B}{h}\right) + \frac{\Delta S^{\ddagger}}{R}$$

Linear regression equation from Eyring analysis:

$$y = -11369.02x + 11.11$$

Derived thermodynamic parameters: $\Delta H^{\ddagger}$ = 22.6 ± 1.3 kcal•mol^{-1}, $\Delta S^{\ddagger}$ = -25.1 ± 3.6 cal•mol^{-1}K^{-1}

From concentration-dependent studies on the catalyst, **I-OTf**, the turnover limiting step is 1.37 order in **I-OTf**. Eyring analysis provided further insight into the turnover-limiting step: the activation parameters describe a high enthalpic barrier ($\Delta H^{\ddagger}$ = 22.6 ± 1.3 kcal•mol^{-1}) and an ordered transition state. $\Delta S^{\ddagger}$ = -25 ± 3.6 cal•mol^{-1}K^{-1}). These thermodynamic values and reaction orders are consistent with the monomeric N-O bond cleavage reaction as the slowest step in the catalytic cycle. We therefore propose the following detailed plausible mechanism, based on the above kinetic studies and the qualitative timeframes for the completion of interconversions between Fe-O(H) species.

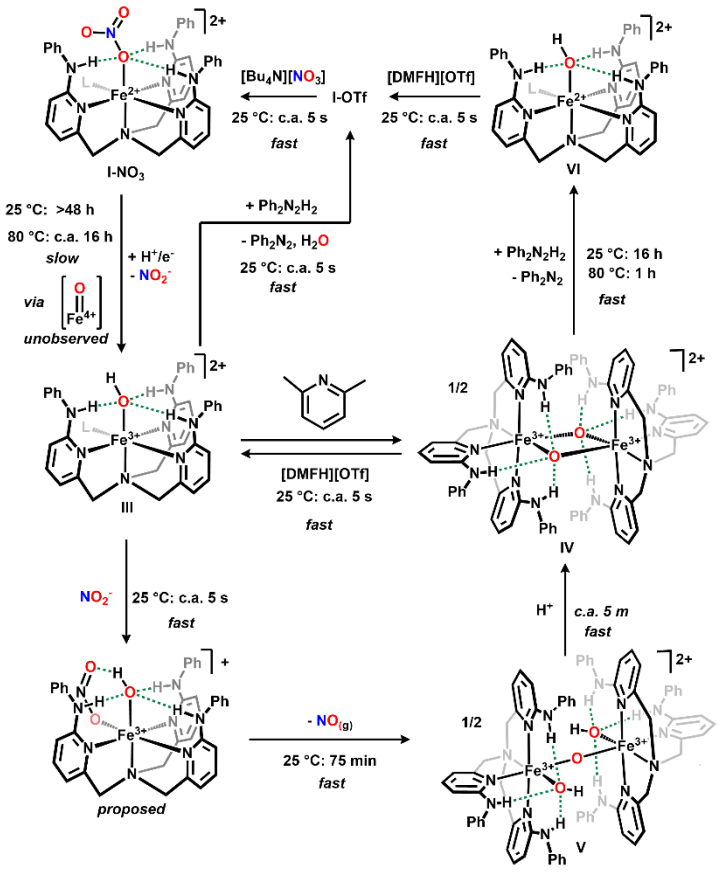

Supplementary Figure 97: Proposed catalytic cycle for NO_3^- reduction to NO(g) with **I-OTf** as the catalyst with approximate rate profiles of stoichiometric acid/base/reduction reactions.

We propose that the transformation of NO_3^- to NH_3 under photochemical conditions with HEH_2 as the reductant may proceed through analogous pathway to form NO, which then could subsequently proceed to NH_3 with or without a catalyst. Since the initial NO_3^- reduction step is the most challenging, the presence of **I-OTf** as a catalyst increases the rate of NO formation and therefore the production of NH_3.

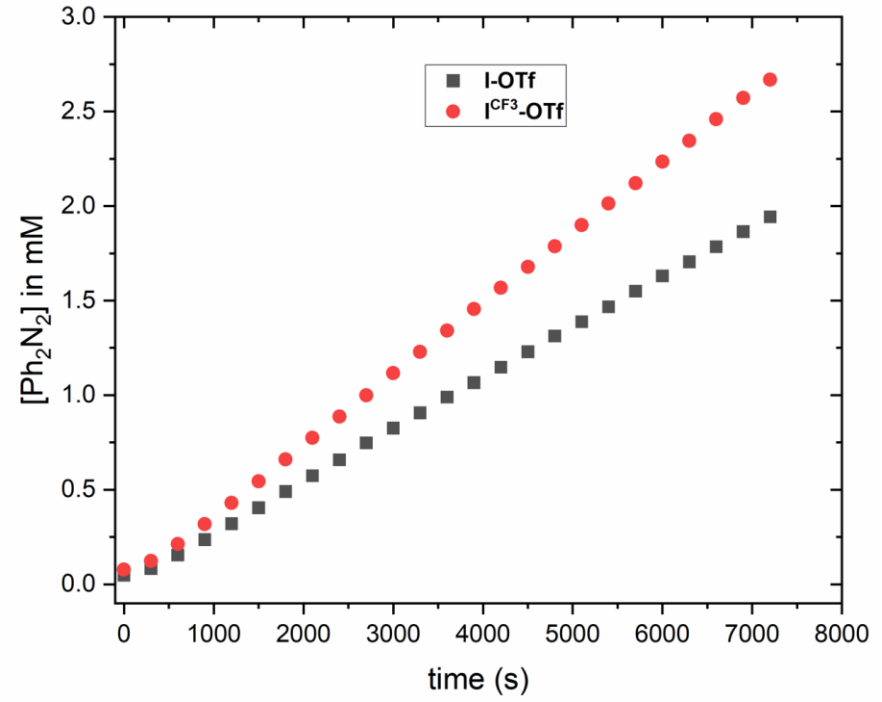

Supplementary Figure 98: Plot of the initial 10% growth of azobenzene (as an average of triplicate reactions for **I-OTf**) for reactions using **I-OTf** or **I^{CF3}-OTf**.

Supplementary Table 8: Calculated turnover frequencies (TOF) for **I-OTf** and **I^{CF3}-OTf**

Entry	Catalyst	k_{obs} (10^{-7} M/s)	TOF (s^{-1})
1*	**I-OTf**	2.48 ± 0.19	14
2	**I^{CF3}-OTf**	3.71	20
*data collected in triplicate, errors are standard deviations			

Computational Studies of Zn-NO_3 Adducts

Supplementary Table 9: Functional-dependent N_1-O_1 distances of **I-Zn$(NO_3)_2$**

Functional	N_1-O_1 bond, calc.	Δ(calc-exp)
TPSSh	1.3304	0.0074
TPSS0	1.3121	-0.0109
TPSS	1.3366	0.1066

Supplementary Table 10: Optimized structures of **I-Zn**, **II-Zn**, their 1:1 and 1:2 adducts with NO_3^- or OTf^-, and ΔG°_{soln} values (Ha)

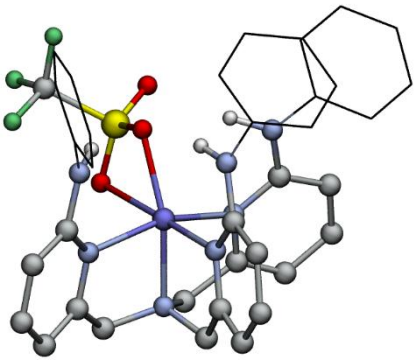

I-Zn(OTf)
ΔG = - -4516.502078 Ha

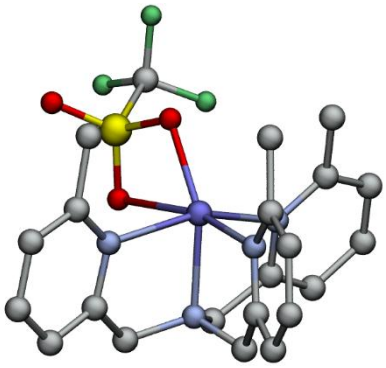

II-Zn(OTf)
ΔG =-3775.025298 Ha

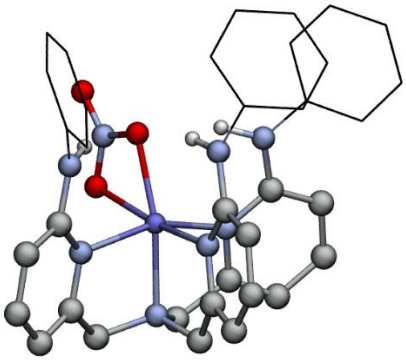

I-Zn(NO_3)
ΔG = -3835.160339Ha

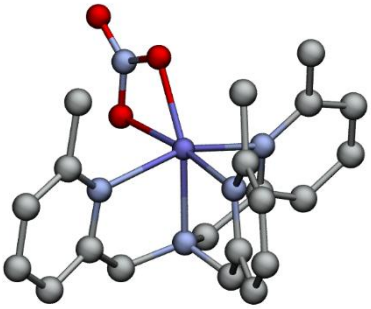

II-Zn(NO_3)
ΔG = -3093.683446 Ha

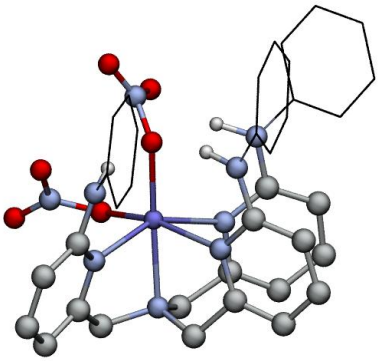

I-Zn(NO_3)$_2$
ΔG = -4115.752361 Ha

NO_3^-
ΔG = -280.5977113 Ha

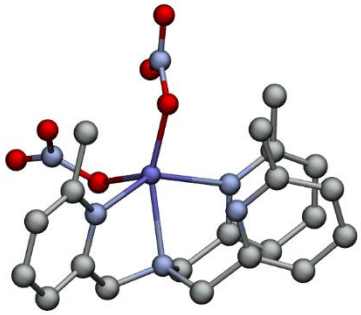

II-Zn(NO_3)$_2$
ΔG = -3374.258752 Ha

OTf^-
ΔG = -961.9499386 Ha

The ΔG for each species was corrected by -1.89 kcal/mol to convert from gas phase to solution-phase at 1 M and 298 K.

Supplementary Table 11: Comparison of experimental and computed bond lengths of **I-Zn(NO$_3$)$_2$** and **II-Zn(NO$_3$)**

I-Zn(NO$_3$)$_2$	N_1-O_1	N_1-O_2	N_1-O_3	Zn-O_1	N_2-O_1	N_3-O_1	N_4-O_2
Experimental	1.323	1.231	1.228	2.112	2.911	2.794	3.075
Calculated	1.2936	1.2126	1.2004	2.0717	2.7908	2.7051	2.9737
Δ	0.0294	0.0184	0.0276	0.0403	0.1202	0.0889	0.1013
II-Zn(NO$_3$)	N_1-O_1	N_1-O_2	N_1-O_3	Zn-O_1	Zn-O_2		
Experimental	1.301	1.245	1.223	2.042	2.447		
Calculated	1.2935	1.2450	1.2274	2.0671	2.5257		
Δ	0.0075	0	-0.0044	-0.0251	-0.0787		

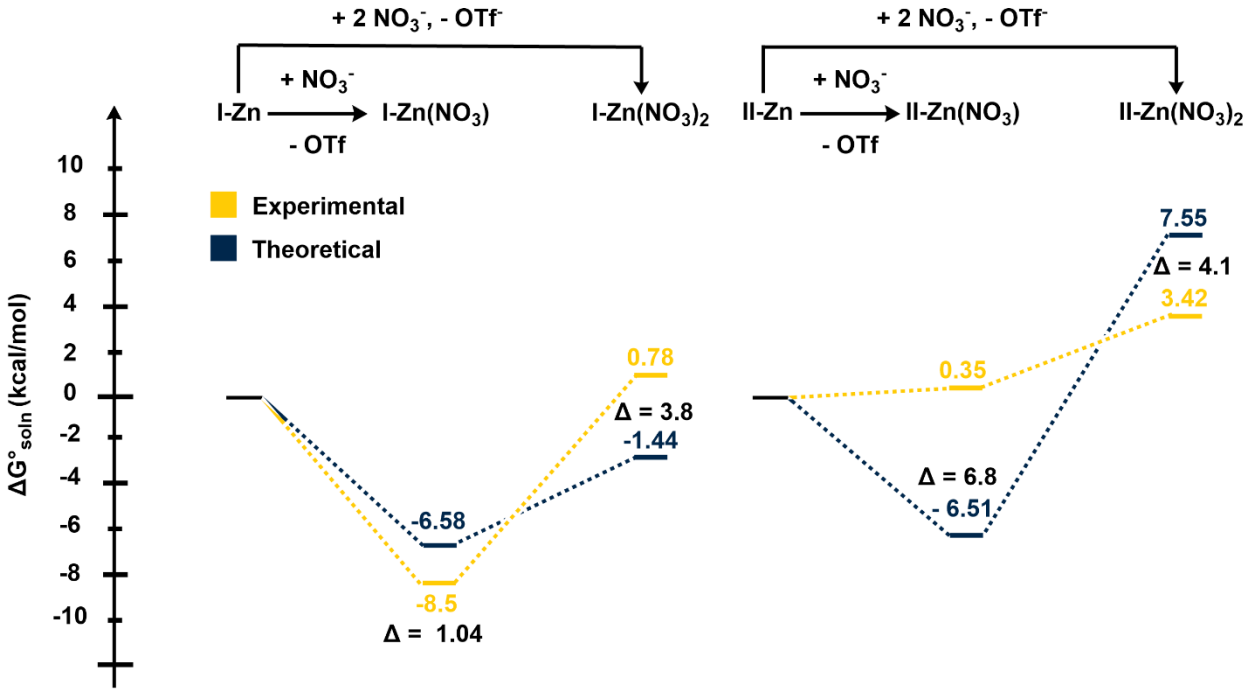

Supplementary Figure 99: Free energy diagram comparing experimental (maize) and theoretical (blue) and ΔG°$_{1:2}$ values for NO_3^- binding to **I-Zn** and **II-Zn**. Δ = |experimental - theoretical|.

The reaction scheme above the diagram represents the thermochemical reaction scheme used to calculate ΔG° values. A standard 1.89 kcal/mol correction was applied to convert each ΔG°$_{gas}$ to ΔG°$_{soln}$.

The theoretical and experimental ΔG°$_{soln}$ values were determined to be within 1-7 kcal/mol, validating the computational methods.[27] We propose the large discrepancy for ΔG°$_{1:1}$ within II-Zn is because DFT may not accurately represent solution state structure or dynamics for weakly interacting systems in coordinating solvent environments.

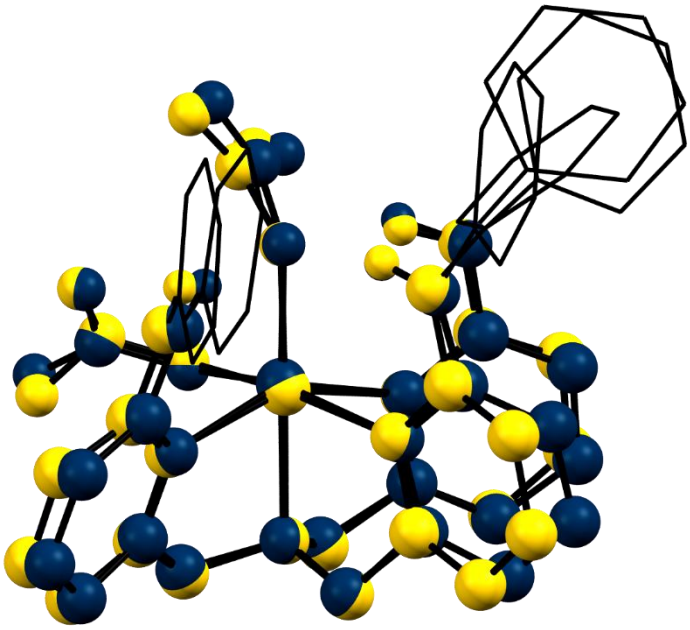

Supplementary Figure 100: Overlay of the crystal (maize) and optimized (blue) structures of **I-Zn(NO$_3$)$_2$** (RMS = 0.075).

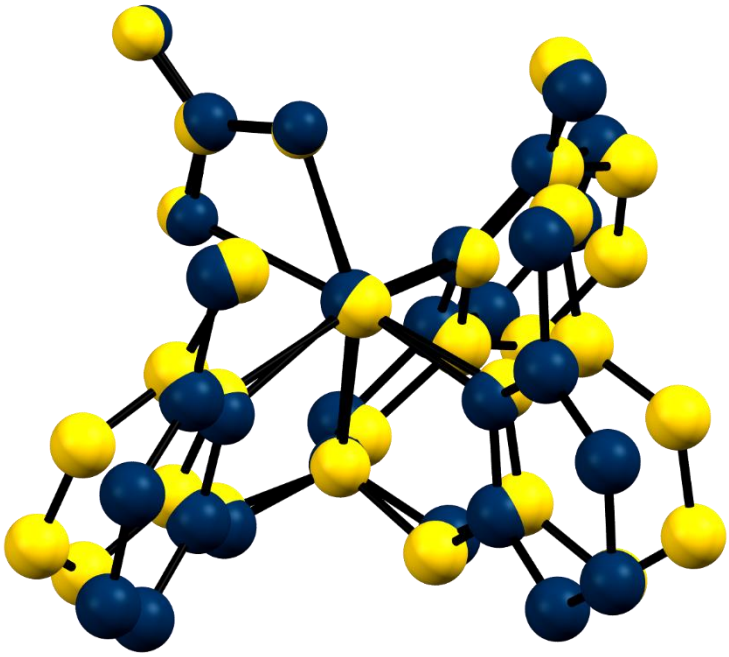

Supplementary Figure 101: Overlay of the crystal (maize) and optimized (blue) structures of **II-Zn(NO$_3$)** (RMS = 0.06).

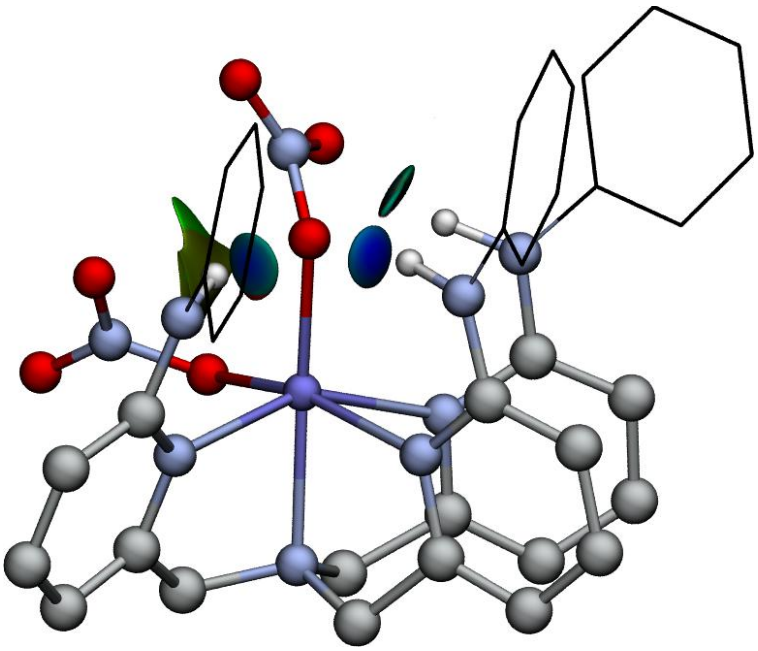

Supplementary Figure 102: NCI isosurfaces of the relevant regions of **I-Zn(NO$_3$)$_2$** (isovalue = 0.45 a.u.).

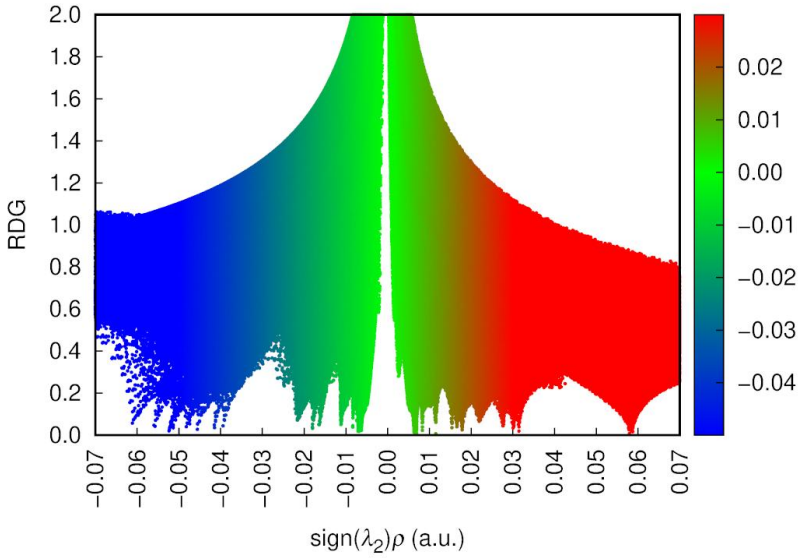

Supplementary Figure 103: Scatter plot of reduced density gradient (RDG) versus (sign(λ^2))ρ for **I-Zn(NO$_3$)$_2$**.

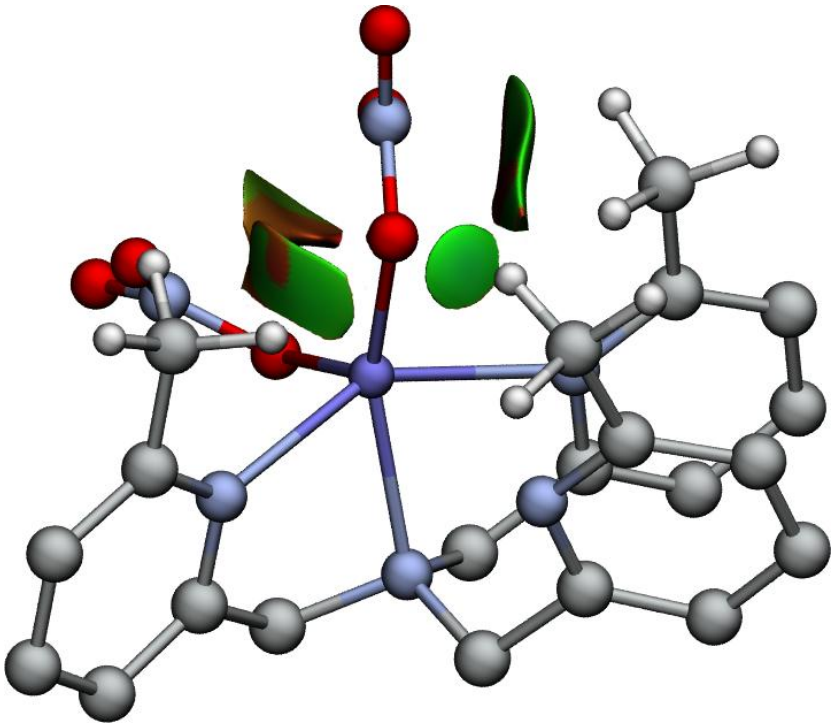

Supplementary Figure 104: NCI isosurfaces of the relevant regions of **II-Zn(NO$_3$)$_2$** (isovalue = 0.45 a.u.).

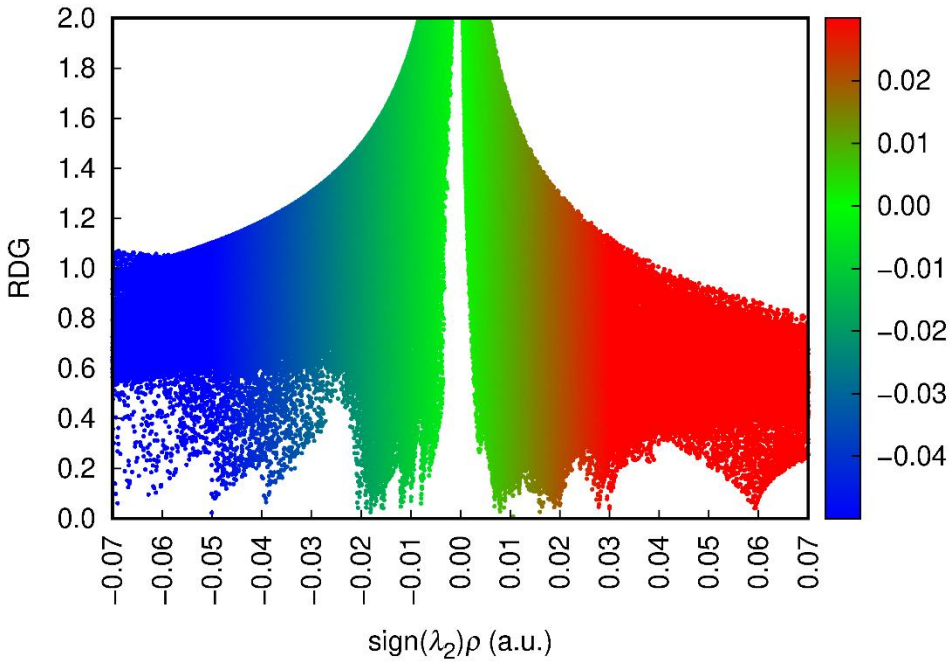

Supplementary Figure 105: Scatter plot of reduced density gradient (RDG) versus (sign(λ^2))ρ for **II-Zn(NO$_3$)$_2$**.

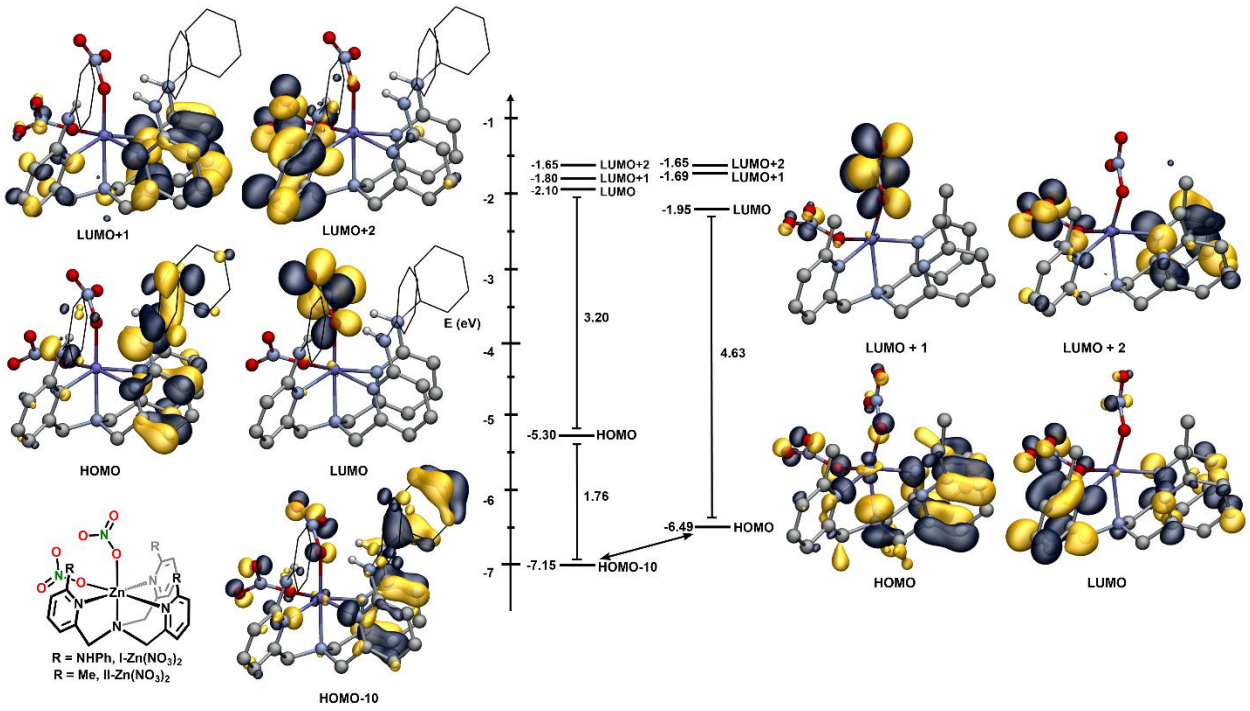

Supplementary Figure 106: Frontier molecular orbitals of **I-Zn(NO$_3$)$_2$** (left) and **II-Zn(NO$_3$)$_2$** and a qualitative MO diagram (middle) (isovalue = 0.05 on all).

Supplementary Scheme 2: Atom numbering for the charge parameters and bond metrics in Supplementary **Error! Reference source not found.** and Supplementary

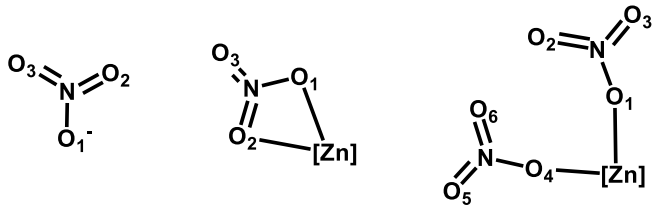

Supplementary Table 12: Natural charges and Loewdin charges of the NO_3^- ligands in the studied compounds

Natural charges	**N_1**	**O_1**	**O_2**	**O_3**	**N_2**	**O_4**	**O_5**	**O_6**
NO_3^-	0.643	-0.630	-0.507	-0.507	--	--	--	--
I-Zn(NO$_3$)	0.675	-0.685	-0.483	-0.365	--	--	--	--
I-Zn(NO$_3$)$_2$	0.696	-0.711	-0.440	-0.398	0.670	-0.670	-0.459	-0.461
II-Zn(NO$_3$)	-0.188	-0.211	-0.058	-0.022	--	--	--	--
II-Zn(NO$_3$)$_2$	0.674	-0.681	-0.442	-0.451	0.675	-0.680	-0.448	-0.462
Loewdin charges	**N_1**	**O_1**	**O_2**	**O_3**	**N_2**	**O_4**	**O_5**	**O_6**
NO_3^-	-0.237	-0.364	-0.199	-0.199	--	--	--	--
I-Zn(NO$_3$)	-0.188	-0.211	-0.589	-0.022	--	--	--	--
I-Zn(NO$_3$)$_2$	-0.219	-0.217	-0.107	-0.063	-0.222	-0.170	-0.119	-0.102

II-Zn(NO_3)	-0.192	-0.173	-0.097	-0.043	--	--	--	--
II-Zn($NO3)_2$	-0.241	-0.208	-0.101	-0.101	-0.213	-0.177	-0.104	-0.106

Supplementary Table 13: Wiberg bond indices (WBI) within the NO_3^- ligands in each Zn adduct and unbound NO_3^-

Compound	N_1-O_1	N_1-O_2	N_1-O_3	N_2-O_4	N_2-O_5	N_2-O_6
NO_3^-	1.1452	1.4533	1.4282	-	-	-
I-Zn(NO_3)	1.1235	1.3684	1.5314	-	-	-
I-Zn($NO_3)_2$	1.1006	1.4197	1.4964	1.1642	1.4353	1.4252
II-Zn(NO_3)	1.1920	1.3243	1.5110	-	-	-
II-Zn($NO_3)_2$	1.1452	1.4533	1.4282	1.1613	1.4504	1.4166

Supplementary Table 14: Crystal data and structural refinement for **I-Zn(NO$_3$)$_2$**

CCDC number	2518192
Empirical formula	$C_{36}H_{33}N_9O_6Zn$
Formula weight	753.08
Temperature [K]	100.00(10)
Crystal system	monoclinic
Space group (number)	$P2_1/n$ (14)
a [Å]	10.15010(10)
b [Å]	24.2499(2)
c [Å]	13.70500(10)
α [°]	90
β [°]	98.0660(10)
γ [°]	90
Volume [Å^3]	3339.96(5)
Z	4
ρ_{calc} [gcm^{-3}]	1.498
μ [mm^{-1}]	1.548
F(000)	1560
Crystal size [mm^3]	0.11×0.15×0.22
Crystal colour	colourless
Crystal shape	block
Radiation	Cu K_α (λ=1.54184 Å)
2θ range [°]	7.29 to 151.61 (0.80 Å)
Index ranges	−12 ≤ h ≤ 9, −29 ≤ k ≤ 30, −16 ≤ l ≤ 16
Reflections collected	34241
Independent reflections	6824, R_{int} = 0.0208, R_{sigma} = 0.0145
Completeness to = 67.684°	99.7 %
Data / Restraints / Parameters	6824 / 15 / 521
Absorption correction T_{min}/T_{max} (method)	0.4890 / 1.0000 (gaussian)
Goodness-of-fit on F^2	1.057
Final *R* indexes [$I \geq 2\sigma(I)$]	R_1 = 0.0305 wR_2 = 0.0800
Final *R* indexes [all data]	R_1 = 0.0324 wR_2 = 0.0811
Largest peak/hole [eÅ^{-3}]	0.29/−0.30

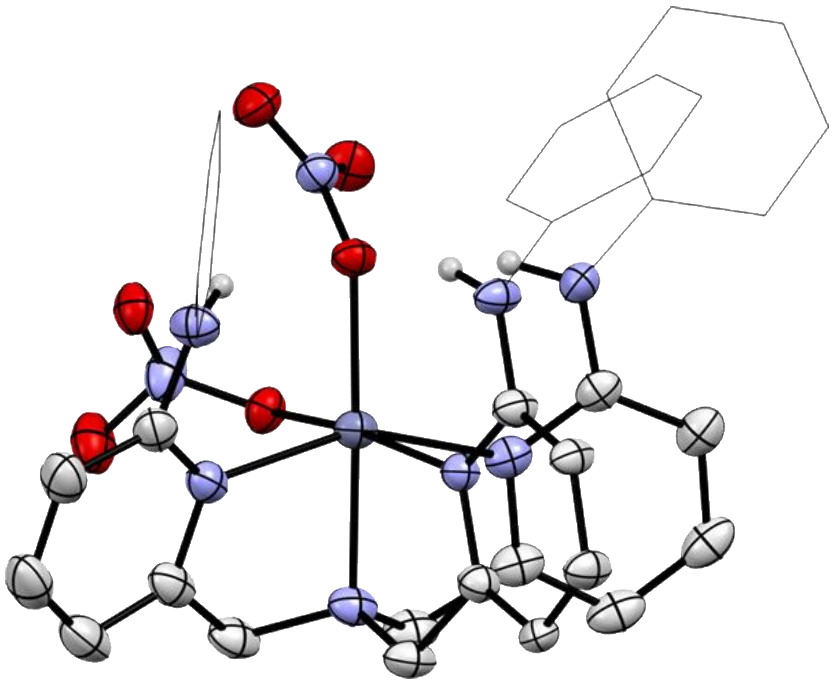

Supplementary Figure 107: Molecular structure of **I-Zn(NO_3)$_2$** (50% probability ellipsoids).

Minor disorder in the pyridine trans to the equatorial NO_3^- ligand was modelled with SIMU constraints. Phenyl rings are wireframed, disordered atoms and H-atoms on carbon atoms removed for clarity.

Supplementary Table 15: Crystal data and structure refinement for **II-Zn(NO_3)**

CCDC number	2518193
Empirical formula	$C_{23}H_{27}N_7O_6Zn$
Formula weight	562.88
Temperature [K]	100.00(10)
Crystal system	monoclinic
Space group (number)	$P2_1/c$ (14)
a [Å]	10.6974(2)
b [Å]	15.2419(3)
c [Å]	15.4507(3)
α [°]	90
β [°]	102.523(2)
γ [°]	90
Volume [Å^3]	2459.28(8)
Z	4
ρ_{calc} [gcm^{-3}]	1.520
μ [mm^{-1}]	1.856
F(000)	1168
Crystal size [mm^3]	0.035×0.054×0.099
Crystal colour	colourless
Crystal shape	prism
Radiation	Cu K_α (λ=1.54184 Å)
2θ range [°]	8.25 to 151.55 (0.80 Å)
Index ranges	−13 ≤ h ≤ 12 −17 ≤ k ≤ 18 −19 ≤ l ≤ 17
Reflections collected	17733
Independent reflections	4995 R_{int} = 0.0268 R_{sigma} = 0.0230
Completeness to θ = 67.684°	99.8 %
Data / Restraints / Parameters	4995 / 0 / 338
Absorption correction T_{min}/T_{max} (method)	0.9190 / 1.0000 (gaussian)
Goodness-of-fit on F^2	1.059
Final *R* indexes [$I \geq 2\sigma(I)$]	R_1 = 0.0516 wR_2 = 0.1481
Final *R* indexes [all data]	R_1 = 0.0552 wR_2 = 0.1515
Largest peak/hole [eÅ^{-3}]	1.76/−0.80

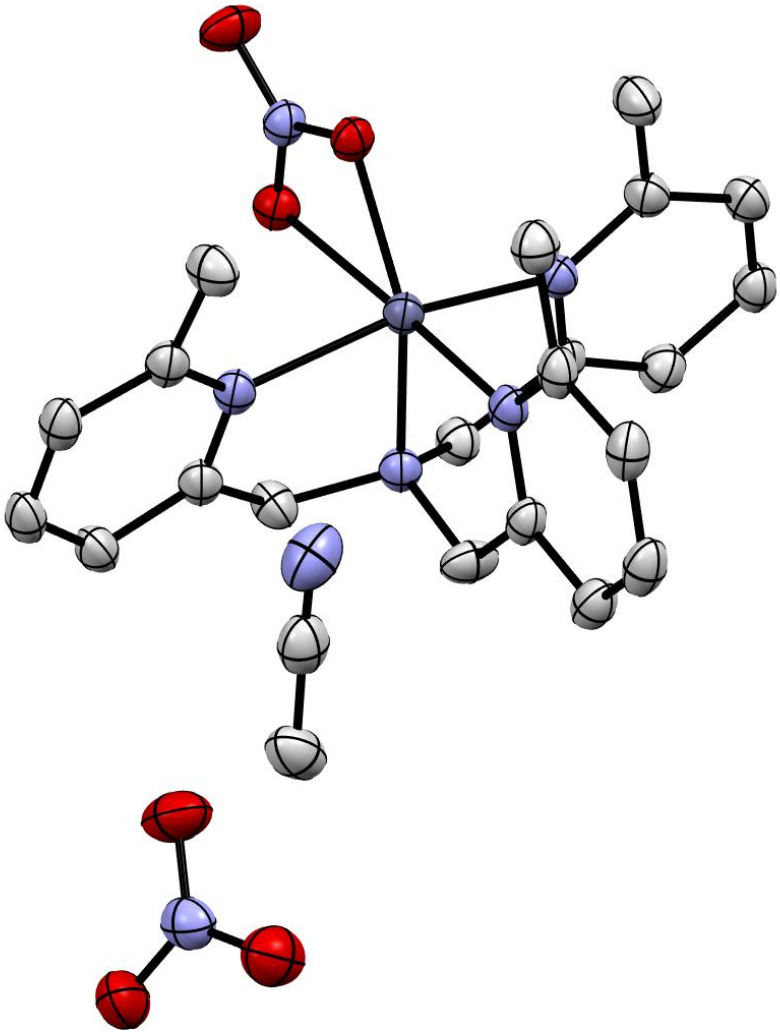

Supplementary Figure 108: Molecular structure of **II-Zn(NO_3)** (50% probability ellipsoids). Hydrogen atoms omitted for clarity.

Supplementary Table 16: Crystal data and refinement for **I-Zn(MeCNH)**

CCDC number	2518194
Empirical formula	$C_{40}H_{36}F_6N_8O_6S_2Zn$
Formula weight	968.26
Temperature [K]	293(2)
Crystal system	monoclinic
Space group (number)	$I2/a$ (15)
a [Å]	21.3747(2)
b [Å]	13.1097(2)
c [Å]	31.5641(4)
α [°]	90
β [°]	93.2140(10)
γ [°]	90
Volume [Å^3]	8830.85(19)
Z	8
ρ_{calc} [gcm^{-3}]	1.457
μ [mm^{-1}]	2.360
F(000)	3968
Crystal size [mm^3]	0.058×0.133×0.144
Crystal colour	colourless
Crystal shape	cube
Radiation	Cu K_α (λ=1.54184 Å)
2θ range [°]	5.61 to 138.64 (0.82 Å)
Index ranges	−25 ≤ h ≤ 25 −15 ≤ k ≤ 15 −35 ≤ l ≤ 38
Reflections collected	64473
Independent reflections	8101 R_{int} = 0.0357 R_{sigma} = 0.0177
Completeness to θ = 67.684°	98.9 %
Data / Restraints / Parameters	8101 / 0 / 574
Absorption correction T_{min}/T_{max} (method)	0.8297 / 1.0000 (multi-scan)
Goodness-of-fit on F^2	1.119
Final *R* indexes [I≥2σ(I)]	R_1 = 0.0424 wR_2 = 0.1050
Final *R* indexes [all data]	R_1 = 0.0434 wR_2 = 0.1068
Largest peak/hole [eÅ^{-3}]	0.63/−0.55
Extinction coefficient	0.000275(14)

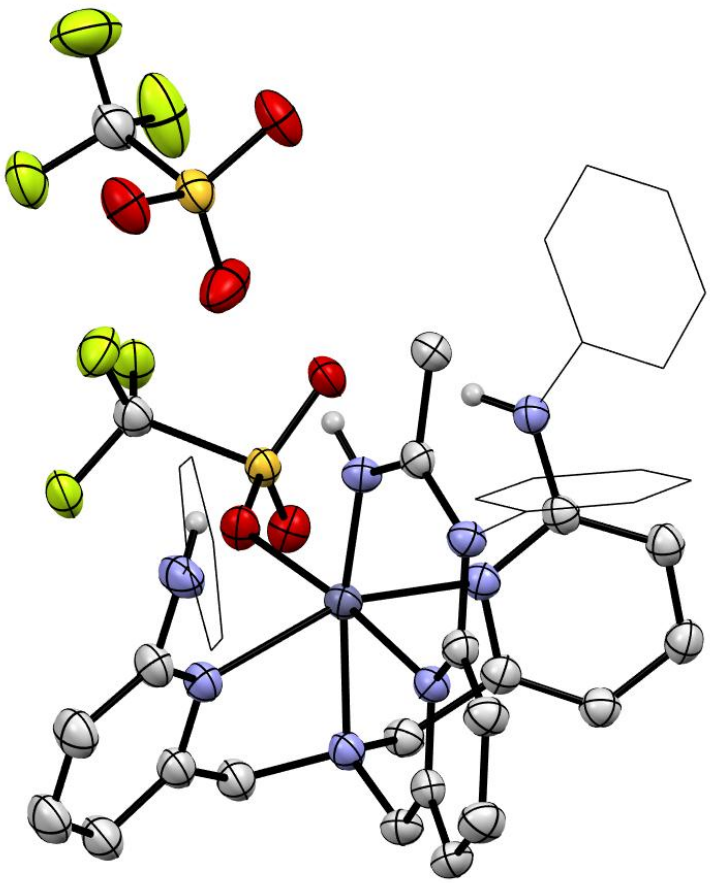

Supplementary Figure 109: Molecular structure of **I-Zn(MeCNH)** (50% probability ellipsoids). Phenyl rings wireframed and hydrogen atoms attached to carbons removed for clarity.

Supplementary Table 17: Crystal data and refinement of **V**

CCDC number	2518195
Empirical formula	$C_{74}H_{68}F_6Fe_2N_{14}O_9S_2$
Formula weight	1587.24
Temperature [K]	85
Crystal system	triclinic
Space group (number)	$P\overline{1}$ (2)
a [Å]	11.0150(4)
b [Å]	12.9556(5)
c [Å]	14.4489(4)
α [°]	91.082(3)
β [°]	107.876(3)
γ [°]	114.634(4)
Volume [Å^3]	1757.91(10)
Z	1
ρ_{calc} [gcm^{-3}]	1.499
μ [mm^{-1}]	4.595
F(000)	820
Crystal size [mm^3]	0.052×0.151×0.209
Crystal colour	orange
Crystal shape	plate
Radiation	Cu K_α (λ=1.54184 Å)
2θ range [°]	6.52 to 138.80 (0.82 Å)
Index ranges	−12 ≤ h ≤ 12 −15 ≤ k ≤ 15 −17 ≤ l ≤ 17
Reflections collected	27580
Independent reflections	6378 R_{int} = 0.0603 R_{sigma} = 0.0391
Completeness to θ = 69.2733°	96.4 %
Data / Restraints / Parameters	6378 / 0 / 620
Absorption correction T_{min}/T_{max} (method)	0.6495 / 1.0000 (multi-scan)
Goodness-of-fit on F^2	1.104
Final *R* indexes [I≥2σ(I)]	R_1 = 0.0389 wR_2 = 0.1061
Final *R* indexes [all data]	R_1 = 0.0405 wR_2 = 0.1117
Largest peak/hole [eÅ^{-3}]	0.34/−0.69

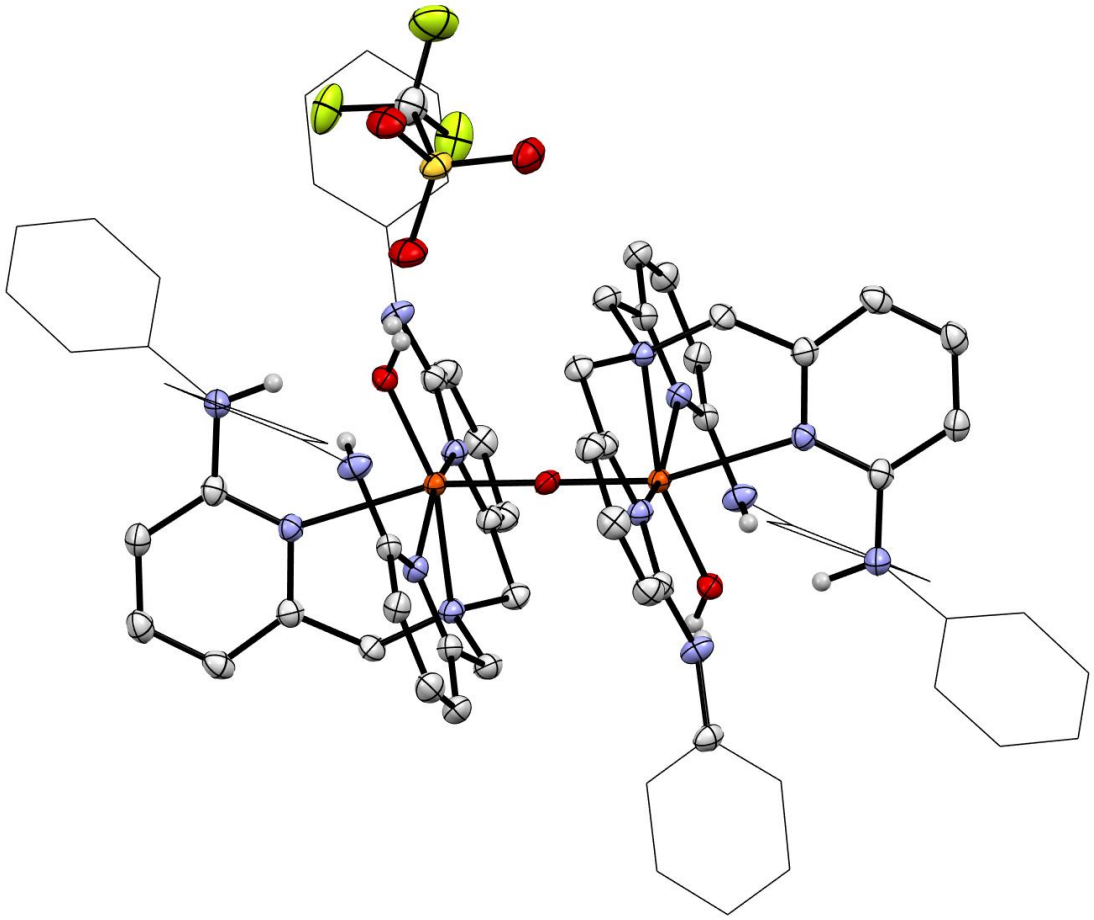

Supplementary Figure 110: Molecular structure of **V** (30% thermal ellipsoids).

Phenyl rings wireframed and hydrogen atoms attached to carbons removed for clarity.

Supplementary Table 18: Crystal data and refinement of **II-NO_3**

CCDC number	2555400
Empirical formula	$C_{11}H_{12}F_{1.50}Fe_{0.50}N_{2.50}O_3S_{0.50}$
Formula weight	299.69
Temperature [K]	100.00(10)
Crystal system	monoclinic
Space group (number)	$P2_1/c$ (14)
a [Å]	9.7019(2)
b [Å]	13.0958(3)
c [Å]	20.2626(4)
α [°]	90
β [°]	99.401(2)
γ [°]	90
Volume [Å^3]	2539.87(9)
Z	8
ρ_{calc} [gcm^{-3}]	1.567
μ [mm^{-1}]	6.165
F(000)	1232
Crystal size [mm^3]	0.06×0.07×0.1
Crystal colour	orange
Crystal shape	needle
Radiation	Cu K_α (λ=1.54184 Å)
2θ range [°]	8.07 to 151.49 (0.80 Å)
Index ranges	−10 ≤ h ≤ 12 −16 ≤ k ≤ 15 −24 ≤ l ≤ 25
Reflections collected	22344
Independent reflections	5174 R_{int} = 0.0330 R_{sigma} = 0.0294
Completeness to θ = 67.684°	99.9 %
Data / Restraints / Parameters	5174 / 341 / 419
Absorption correction T_{min}/T_{max} (method)	0.8250 / 1.0000 (gaussian)
Goodness-of-fit on F^2	1.069
Final *R* indexes [$I \geq 2\sigma(I)$]	R_1 = 0.0694 wR_2 = 0.1792
Final *R* indexes [all data]	R_1 = 0.0746 wR_2 = 0.1829
Largest peak/hole [eÅ^{-3}]	1.42/−0.50

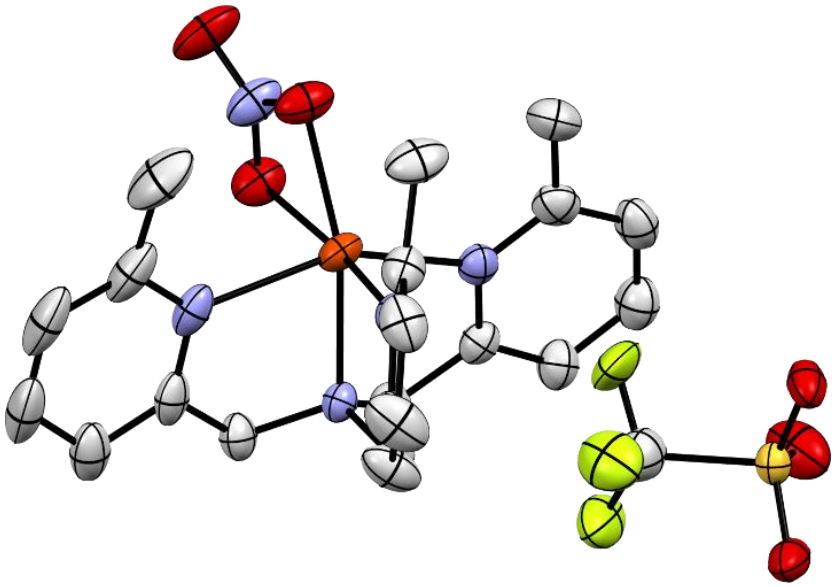

Supplementary Figure 111: Molecular structure of **II-NO_3** (50% thermal ellipsoids).

Hydrogen atoms attached to carbons and disorder in the outer-sphere OTf^- ion are omitted for clarity.

References

1 Favier, I. & Duñach, E. New protic salts of aprotic polar solvents. *Tetrahedron Letters* **45**, 3393-3395 (2004). https://doi.org/https://doi.org/10.1016/j.tetlet.2004.03.025

2 Wakasugi, K., Misaki, T., Yamada, K. & Tanabe, Y. Diphenylammonium triflate (DPAT): efficient catalyst for esterification of carboxylic acids and for transesterification of carboxylic esters with nearly equimolar amounts of alcohols. *Tetrahedron Letters* **41**, 5249-5252 (2000). https://doi.org/https://doi.org/10.1016/S0040-4039(00)00821-2

3 An, F. *et al.* Reactivities of allenic and olefinic Michael acceptors towards phosphines. *Chemical Communications* **58**, 3358-3361 (2022). https://doi.org/10.1039/D1CC06786A

4 Chalkley, M. J., Del Castillo, T. J., Matson, B. D. & Peters, J. C. Fe-Mediated Nitrogen Fixation with a Metallocene Mediator: Exploring pKa Effects and Demonstrating Electrocatalysis. *Journal of the American Chemical Society* **140**, 6122-6129 (2018). https://doi.org/10.1021/jacs.8b02335

5 Dahl, E. W., Dong, H. T. & Szymczak, N. K. Phenylamino derivatives of tris(2-pyridylmethyl)amine: hydrogen-bonded peroxodicopper complexes. *Chemical Communications* **54**, 892-895 (2018). https://doi.org/10.1039/C7CC08619A

6 Sarkar, W., LaDuca, A., Wilson, J. R. & Szymczak, N. K. Iron-Catalyzed C–H Oxygenation Using Perchlorate Enabled by Secondary Sphere Hydrogen Bonds. *Journal of the American Chemical Society* **146**, 10508-10516 (2024). https://doi.org/10.1021/jacs.3c14433

7 Beni, A., Dei, A., Laschi, S., Rizzitano, M. & Sorace, L. Tuning the Charge Distribution and Photoswitchable Properties of Cobalt–Dioxolene Complexes by Using Molecular Techniques. *Chemistry – A European Journal* **14**, 1804-1813 (2008). https://doi.org/https://doi.org/10.1002/chem.200701163

8 LaDuca, A. R., Wilson, J. R., Sarkar, W., Zeller, M. & Szymczak, N. K. Impact of Secondary Sphere Hydrogen Bonds on O2 Reactivity within a Nonheme Iron Complex. *Journal of the American Chemical Society* **147**, 5099-5105 (2025). https://doi.org/10.1021/jacs.4c15153

9 LaDuca, A. R., Gonder, J. E., Sarkar, W., Gilbertson, J. D. & Szymczak, N. K. Rapid nitrite reduction enabled by secondary sphere hydrogen bonds within non-heme iron complexes. *Chemical Science* **16**, 18364-18371 (2025). https://doi.org/10.1039/D5SC04153H

10 Huet, J., Gaudemer, A., Boucly-Goester, C. & Boucly, P. Structural studies of metalloporphyrins. 7. Proton NMR and electrochemical investigation of the (meso-5,10,15,20-tetraarylporphine)cobalt(III) complexes XCoIII(TPP-p-R). *Inorganic Chemistry* **21**, 3413-3419 (1982). https://doi.org/10.1021/ic00139a029

11 Kumar, A. *et al.* One-pot general synthesis of metalloporphyrins. *Tetrahedron Letters* **48**, 7287-7290 (2007). https://doi.org/https://doi.org/10.1016/j.tetlet.2007.08.046

12 Neese, F. The ORCA program system. *WIREs Computational Molecular Science* **2**, 73-78 (2012). https://doi.org/https://doi.org/10.1002/wcms.81

13 Neese, F., Wennmohs, F., Becker, U. & Riplinger, C. The ORCA quantum chemistry program package. *The Journal of Chemical Physics* **152**, 224108 (2020). https://doi.org/10.1063/5.0004608

14 Jensen, K. P. Bioinorganic Chemistry Modeled with the TPSSh Density Functional. *Inorganic Chemistry* **47**, 10357-10365 (2008). https://doi.org/10.1021/ic800841t

15 Staroverov, V. N., Scuseria, G. E., Tao, J. & Perdew, J. P. Comparative assessment of a new nonempirical density functional: Molecules and hydrogen-bonded complexes. *The Journal of Chemical Physics* **119**, 12129-12137 (2003). https://doi.org/10.1063/1.1626543

16 Weigend, F. & Ahlrichs, R. Balanced basis sets of split valence, triple zeta valence and quadruple zeta valence quality for H to Rn: Design and assessment of accuracy. *Physical Chemistry Chemical Physics* **7**, 3297-3305 (2005). https://doi.org/10.1039/B508541A

17 Grimme, S., Antony, J., Ehrlich, S. & Krieg, H. A consistent and accurate ab initio parametrization of density functional dispersion correction (DFT-D) for the 94 elements H-Pu. *The Journal of Chemical Physics* **132**, 154104 (2010). https://doi.org/10.1063/1.3382344
18 Johnson, E. R. & Becke, A. D. A post-Hartree–Fock model of intermolecular interactions. *The Journal of Chemical Physics* **123**, 024101 (2005). https://doi.org/10.1063/1.1949201
19 Neese, F. An improvement of the resolution of the identity approximation for the formation of the Coulomb matrix. *Journal of Computational Chemistry* **24**, 1740-1747 (2003). https://doi.org/https://doi.org/10.1002/jcc.10318
20 NBO 7.0 (Theoretical Chemistry Institute, University of Wisconsin, Madison, WI, 2018).
21 Lu, T. & Chen, F. Multiwfn: A multifunctional wavefunction analyzer. *Journal of Computational Chemistry* **33**, 580-592 (2012). https://doi.org/https://doi.org/10.1002/jcc.22885
22 Humphrey, W., Dalke, A. & Schulten, K. VMD: Visual molecular dynamics. *Journal of Molecular Graphics* **14**, 33-38 (1996). https://doi.org/https://doi.org/10.1016/0263-7855(96)00018-5
23 Hübler, C. SupraFit – An Open Source Qt Based Fitting Application to Determine Stability Constants from Titration Experiments. *Chemistry–Methods* **2**, e202200006 (2022). https://doi.org/https://doi.org/10.1002/cmtd.202200006
24 Hübler, C. (2020).
25 Hübler, C. Analysing binding stoichiometries in NMR titration experiments using Monte Carlo simulation and resampling techniques. *PeerJ Anal. Chem* **4,** (2022). https://doi.org/https://doi.org/10.7717/peerj-achem.23
26 Holland, R. F., Vasquez, M. C., Beattie, W. H. & McDowell, R. S. Absorptivity of nitric oxide in the fundamental vibrational band. *Journal of Quantitative Spectroscopy and Radiative Transfer* **29**, 435-438 (1983). https://doi.org/https://doi.org/10.1016/0022-4073(83)90117-6
27 Grimme, S. Supramolecular Binding Thermodynamics by Dispersion-Corrected Density Functional Theory. *Chemistry – A European Journal* **18**, 9955-9964 (2012). https://doi.org/https://doi.org/10.1002/chem.201200497